UNIVERSITY OF OKLAHOMA

GRADUATE COLLEGE

COMPUTATIONAL INVESTIGATION OF THE BEHAVIOR OF NANOPARTICLES AND SURFACTANTS AT THE OIL-WATER INTERFACE

A DISSERTATION

SUBMITTED TO THE GRADUATE FACULTY

in partial fulfillment of the requirements for the

Degree of

DOCTOR OF PHILOSOPHY

By

TUAN VIET VU
Norman, Oklahoma
2021

COMPUTATIONAL INVESTIGATION OF THE BEHAVIOR OF NANOPARTICLES AND SURFACTANTS AT THE OIL-WATER INTERFACE

A DISSERTATION APPROVED FOR THE

SCHOOL OF CHEMICAL, BIOLOGICAL AND MATERIALS ENGINEERING

BY THE COMMITTEE CONSISTING OF

Dr. Dimitrios V. Papavassiliou, Chair

Dr. Jeffrey H. Harwell

Dr. Edgar A. O'Rear III

Dr. Bin Wang

Dr. Prakash Vedula

This work is dedicated to my parents, my wife, and my little son Albert

Acknowledgements

I would like to acknowledge my advisor, Dr. Dimitrios Papavassiliou, for his support, and understanding during my Ph.D life. I will never forget his guidance, patience, and encouragement, especially during the hard time of the COVID 19 pandemic. I also want to thank the members of my committee, including Dr. Jeffrey H. Harwell, Dr. Edgar A. O'Rear III, Dr. Bin Wang, and Dr. Prakash Vedula for their time and helpful suggestions. I am thankful to Dr. Sepideh Razavi for her helpful discussions.

I gratefully appreciate the financial support from the National Science Foundation (Grant No CBET- 1934513) and the American Chemical Society Petroleum Research Fund (Grant No PRF # 58518-ND9). In addition, I acknowledge the use of computing facilities at the University of Oklahoma Supercomputing Center for Education and Research (OSCER) and at XSEDE (under allocation CTS-090025).

I am grateful to my colleagues and friends for the useful discussions and the fun that we had together. Lastly, I am thankful to my family for always supporting me.

Table of Contents

List of Tables

List of Figures

Abstract

Surfactants and nanoparticles (NPs) are commonly used to stabilize emulsions, which have found applications in different areas. The fundamental understanding of the behavior of surfactants and NPs adsorbed at the oil-water interface at different conditions is necessary for their applications. In this thesis, dissipative particle dynamics (DPD) simulation method was used to investigate computationally the individual and synergistic effects of surfactants and NPs at the oil-water interface. First, a systematic protocol to parameterize DPD models containing anionic surfactant (sodium dodecyl sulfate - SDS) or nonionic surfactant (octaethylene glycol monododecyl ether – C12E8) at the oil-water interface was constructed. It is important to place the theoretically calculated number of surfactant molecules at the interface at the critical micelle concentration. Based on this approach, the molecular description of surfactants and the effects of various interactions parameters on the interfacial tension were investigated. When adsorbing surfactants on the shape-anisotropic NPs such as carbon nanotubes (CNT), it was found that the adsorption capacities of SDS and C12E8 were 2.62 and 2.43 molecules/nm^2, respectively. When the surfactant-adsorbed-CNTs reached the oil-water interface, the surfactant molecules quickly desorbed from the CNTs and distributed at the interface, leading to the reduction of the oil-water interfacial tension (IFT). At low surfactant concentration, the CNT remained at the interface, resulting in a further reduction of the IFT. When the surfactant interfacial concentration was high enough (at the value corresponding to the bulk critical micelle concentration (CMC)), the CNT was pushed into the oil phase, which did not have effects on the IFT. The synergistic effect of surfactants and various types of NPs on the oil-water interfacial tension was also investigated. It was found that at constant surfactant concentration, adding NPs reduced the IFT; while with the absence of surfactant, NPs expressed no effect on the IFT. Among different types of NPs, the most

effective ones were those that maximized their footprint at the interface; thus, reducing the interfacial area available to surfactants. The interactions of the NPs with the surfactant molecules determined exactly which pattern of heterogeneity was most favorable. Based on these results, we formulated suggestions for designing NPs for maximum synergistic effects with surfactants. The stability of oil-in-water emulsion with the presence of SDS surfactants and Janus nanoparticles was also studied. Two oil droplets with different Janus particle surface coverages and surfactant surface concentrations were pushed towards each other for coalescing. The coalescence progressed by moving the Janus particles away from the point of drop contact, followed by the diffusion of surfactant from the contact area to allow the direct oil-oil contact. The emulsion stability was quantified using the difference of free energy between the final and the initial state of coalescence. At particle coverage of less than 70% of the drop surface, Janus particles alone could not thermodynamically stabilize the emulsion. However, when combined with surfactants, Janus particles would improve emulsion stability by increasing the effective surfactant concentration on the emulsion surface. Finally, the behavior of C12E8 surfactant and Janus nanoparticles at the oil-water interface under compression was investigated. Compression of the interface with only surfactants resulted in the expulsion of surfactant molecules to the water phase once the interfacial concentration of surfactant molecules reached the CMC value. Compression of a Janus particle-laden interface past the closed-packing point led to a buckled interface so that the total interfacial area remained constant upon further compression. When both surfactants and JPs were present at the interface, JPs still caused buckling, which helped retain the surfactant molecules at the interface. The interface exhibited a higher level of deformation in presence of surfactants. When the surfactant concentration was high, under compression, the surfactants were partitioned into the water phase, but the buckling of the interface persisted.

Chapter 1. Introduction

The interface of two immiscible liquids such as oil and water has been an important research topic. At the interface, the different molecules in each phase are in contact with each other. The potential energies of molecules at the interface are greater than those in the bulk phases, which only interact with molecules of the same types in all directions. To bring a molecule from one phase to the interface, an amount of work equal to this potential energy difference must be applied. The interfacial free energy per unit area, or interfacial tension (IFT), is a measure of this work [1].

One of the important behaviors of the oil-water interface is the formation of emulsions, which have found applications in different areas such as food processing [2], pharmaceuticals [3], material synthesis [4], oil recovery [5], drug delivery [6], etc. Because of the high interfacial tension between oil and water emulsions are not stable and tend to form separate phases of oil and water. Emulsions, therefore, need to be stabilized by emulsifiers. The ability of emulsifiers to stabilize emulsions is due to their natural tendency to remain at the oil-water interface, and consequently reduce the interfacial free energy.

1.1. Surfactant

Surfactants are the most common emulsifiers. Surfactant (surface-active agent) is a special type of molecule that possesses two distinct sides: one is hydrophilic (water-like), one is hydrophobic (water-dislike). When added to the oil-water interface, it will orient itself with the hydrophobic side facing the oil, and the hydrophilic side toward the water. The interactions between oil-water molecules are altered by the interactions of oil molecules with the hydrophobic group, and water molecules with the hydrophilic group, which are more attractive. Thus, the IFT is significantly reduced, and the emulsions are stabilized by the presence of surfactant. Research on the behavior of surfactants in the bulk phase and at the interface has been active for several decades [1, 7]. In

the bulk phase, surfactant molecules stay as separated monomers at low concentrations. When the surfactant concentration exceeds a critical value, which is called critical micelle concentration (CMC), additional surfactant molecules start to assemble into micelles, while the surfactant monomer concentration stays constant [1]. The formation and shape of micelles depend on the type of surfactant, solvent, temperature, and electrolyte concentration [8-12]. The structure and behavior of surfactants at the oil-water interface have also been studied extensively [13-16].

1.2. Nanoparticle

Nanoparticles (NPs) have also been used in stabilizing emulsions, which are called Pickering emulsions [17, 18]. Among different types of anisotropic nanoparticles, amphiphilic particles (i.e., Janus particles) are unique. Janus particles (JPs) are anisotropic since their surface has areas of distinct wettability, where one particle side is hydrophilic and the other side is hydrophobic [19, 20]. Emulsion stabilization mechanisms with NPs are still debatable [21-23]. It is widely accepted that the emulsions are kinetically stabilized by NPs [23, 24]. Kinetic stability refers to the delay of emulsion breakage by the presence of NPs. The ability to prevent emulsion breakage depends on the NP's desorption energy and the interaction between NPs. Desorption energy is the energy required to desorb an NP from the interface. For a spherical NP, it is calculated as [23, 25]

$$\Delta E = \pi R^2 \gamma (1 \pm cos\theta) \tag{1.1}$$

where R is the radius of the NP, γ is the oil-water IFT, and θ is the contact angle of NP at the interface. The sign in the bracket is plus (minus) for $\theta \geq 90^o$ ($\theta < 90^o$). Although a larger NP possesses higher desorption energy, a smaller NP can pack more efficiently at the interface, resulting in more stable emulsions [26, 27]. However, an NP that is too small cannot bind strongly to the interface due to a small desorption energy. Thus, the size of NPs should be in a range from a few nm to μm [27, 28]. The particle contact angle also determines its desorption energy. NPs

with contact angles in the range of 30^o to 150^o are suitable at stabilizing emulsions as the desorption energies are high [28]. Due to the adsorption of NPs at the oil-water interface, the interactions between two emulsions depend on the interactions between the NPs. NPs can prevent emulsion breakage by their steric effect or repulsive interactions [25, 29]. Although NPs are believed to stabilize emulsions kinetically, there are reports demonstrating that thermodynamically stable emulsions can be achieved using NPs [30, 31]. The stability of Pickering emulsions depends on the surface chemistry of the NPs [28, 32], their shape [33-36], their concentration [36, 37], and on the electrolyte [38, 39].

1.3. Surfactants and nanoparticles as co-emulsifiers

The co-existence of surfactants and NPs at the oil-water interface is expected to show more complex behavior than when either surfactants or nanoparticles are at the interface on their own. Reports on the effects of the presence of nanoparticles and surfactants on the oil-water interfacial behavior have been conflicting. Ranatunga *et al.*[40] found a synergistic effect of nanoparticles and non-ionic surfactants at the oil-water interface, in which nanoparticles reduced the oil-water IFT further than the surfactants alone. While several laboratory and simulation studies supported this observation, [41, 42] in other cases an increase in the IFT was observed as nanoparticles with surfactants were added to the oil-water interface.[43-45] Studies have also appeared reporting no effect [46, 47]. The explanation for such differences is based on the relative interactions between nanoparticle-surfactant and nanoparticle-ambient fluid. Increased IFT relative to the surfactant only case occurred when surfactant molecules were strongly adsorbed on the nanoparticle surface, which resulted in low surfactant concentration at the interface. The IFT decreased by the presence of nanoparticles when the particles stayed at the oil-water interface. In this case, the interfacial area that remained available to the surfactant molecules was smaller, making them appear more

active. When the nanoparticles settled in either the oil or water phase, they did not affect the oil-water IFT.

Furthermore, the interparticle interactions can be tuned in presence of surfactants. Rahman et al. demonstrated that the microstructure of the polystyrene particle-laden air-water interface can be altered by the addition of Tween 80 or sodium dodecyl sulfate (SDS) surfactants [48]. Three distinct interfacial microstructures were identified corresponding to the different ratios of the attractive to repulsive interparticle interactions controlled by the surfactant concentration. While the synergistic effect of homogeneous NPs and surfactants on the oil-water interfacial tension and emulsion stability has been examined in the literature [40, 49-52], several studies have also reported on the competitive interfacial behavior in these mixed systems. For example, Smits et al. reported that adding octadecylamine surfactant molecules could lead to the desorption of aminated silica particles from the decane-water interface due to displacement by surfactants [53]. A recent study by the same group demonstrated that the charges of NPs and surfactants determine whether their combination would lead to synergistic or competitive adsorption. Negatively charged silica NPs could only adsorb to the oil-water interface if it was covered with an oil-soluble cationic surfactant (octadecyl amine). In contrast, increasing the cationic surfactant concentration resulted in reversible desorption of positively charged NPs that were already adsorbed at the interface [54].

1.4. Surfactants and nanoparticles at oil-water interface under stress

In many applications, the emulsions encounter extreme deformation due to applied compressions or because of submission to shear stresses. The stabilization of the emulsions then depends strongly on the response of the stabilizers under these conditions. Surfactant molecules can be exchanged easily between the interface and the bulk phase; thus, the surfactant concentration in the bulk impacts the surface rheology [55]. In contrast, NPs have different response mechanisms to

deformation due to their stronger adsorption onto the oil-water interface (i.e., desorption energy on the order of thousands k_BT per particle in comparison to several k_BT per surfactant molecule) [56]. Previous studies for the particle-laden air-water interface subjected to compression have shown that the surface wettability of the NPs dictates the interfacial response. Under compression, hydrophilic NPs were irreversibly expulsed to the bulk aqueous phase, while the more hydrophobic NPs formed a solid monolayer at the air-water interface that collapsed by buckling and folding [57-61]. Other factors that contribute to the response of NPs to compression are the particle surface charge and presence of an electrolyte, particle shape and softness, and the pH of the suspension [57, 62-64]. A comprehensive review of factors influencing the interfacial rheological behavior of particle-laden interfaces can be found in a recent review article [65].

Despite their high potential for applications, few studies have been dedicated to the response of JPs to applied stresses. Razavi et al. showed that the amphiphilicity of the JPs controlled their collapse behavior on air-water interfaces [66]. Under applied compressions, JPs with low degrees of amphiphilicity formed a porous multi-layer particle film at the interface, while JPs with higher amphiphilicity resulted in a buckled monolayer at the interface similar to that of hydrophobic NPs [57]. Yin and coworkers also reported that Janus nanosheets exhibit a wrinkling and folding collapse mode. In addition, the oil-water interface covered by Janus nanosheets displayed a larger deformation compared to the bare interface under an applied vertical stress [67]. Compression of the interface containing both NPs and surfactants shows interesting effects. In a recent study, Yazhgure et al. observed that changing cetrimonium bromide (CTAB) surfactant concentration could alter the collapse mechanism of silica NPs on the air-water interface [45]. At low CTAB concentrations (1×10^{-6} to 4×10^{-5} M), the adsorbed NPs formed a solid-like monolayer, while at higher concentrations, the NP layer was more fragile and formed aggregates when collapsing. Due

to the observed increase in the interfacial tension with the addition of NPs, it was concluded that surfactants modify the hydrophobicity of the NPs, which resulted in the change of collapse mechanism.

1.5. Research Objectives

Understanding the mechanism for stabilizing emulsions using surfactants, NPs, or both of them is crucial to design suitable emulsifiers and operating conditions tuned for a particular application. From the previous reports, the combined effects of surfactant and NP at the oil-water interface are still debatable due to the complicated interactions of systems containing four different components: oil, water, surfactant, NP. In this thesis, we would like to address several problems:

(i) Investigate the adsorption of surfactants on shape-anisotropic NPs, and specifically carbon nanotubes (CNTs). The behavior of surfactant-adsorbed-CNTs in the vicinity of the oil-water interface is then studied.

(ii) Study the synergisms of surfactants and different types of NPs at the oil-water interface.

(iii) Investigate effects of surfactants and Janus particles on the coalescence of oil-in-water emulsions.

(iv) Reveal the individual and combined behaviors of surfactants and Janus particles at the oil-water interface under compression.

We used dissipative particle dynamics (DPD) simulation methods in our study. The principles of DPD simulation were described in chapter 2. In chapter 3, we build and validate models that can accurately describe the change of oil-water IFT with surfactant concentrations. The adsorption of surfactants on CNTs and the behavior of surfactant-adsorbed-CNTs at the oil-water interface were studied in chapter 4. This study confirmed the feasibility of using NPs to transport surfactants for enhanced oil recovery. In chapter 5, we studied the synergistic effects of surfactants and NPs on

the oil-water IFT. We revealed the mechanism for the synergism and provide guidelines on designing efficient NPs and surfactants for emulsion stabilization. The behaviors of Janus particles and surfactants on the oil droplets during coalescence were studied in chapter 6. We constructed a statistical model to predict emulsions stability as a function of surfactant and JP concentrations. In chapter 7, we analyzed the behaviors of surfactants and JPs individually and together at the oil-water interface under compression. The summary of findings and suggestions for future research were provided in chapter 8.

Chapter 2. Dissipative Particle Dynamics

Molecular dynamics (MD) simulation is normally used to investigate computationally the equilibrium and dynamic behavior of a system at the molecular level, especially when the number of atoms is small. For large, complex systems such as the ones considered in our work, MD is too computationally expensive. Thus, we employed dissipative particle dynamics (DPD) in our study. DPD is a coarse-grained molecular dynamics simulation method, where a *bead* is used to represent several molecules [68]. Depending on the level of coarse-graining, the number of calculations can be significantly reduced compared to MD. Although some detailed atomistic behaviors cannot be captured using DPD, the macroscopic properties can be calculated in a much faster simulation time. DPD was first developed by Hoogerbrugge and Koelman in 1992 [68], and it has been improved since then. DPD has been employed for the modeling of oil-water with the presence of surfactants or NPs in numerous reports [69-72]. The time evolution of the system is governed by Newton's equation of motion:

$$\frac{d\mathbf{r}_i}{dt} = \mathbf{v}_i \,, \tag{2.1}$$

$$m_i \frac{d\mathbf{v}_i}{dt} = \mathbf{f}_i = \sum\nolimits_{j \neq i} (\boldsymbol{F}_{ij}^C + \boldsymbol{F}_{ij}^D + \boldsymbol{F}_{ij}^R), \tag{2.2}$$

where $\mathbf{r}_i$, and $\mathbf{v}_i$ are the position and velocity vectors of bead *i* at time t, m_i is the mass of bead *i*, and $\mathbf{f}_i$ is the inter-particle force vector acting on particle *i*. In DPD, the total force consists of three forces: the conservative ($\boldsymbol{F}_{ij}^C$), dissipative ($\boldsymbol{F}_{ij}^D$) and random ($\boldsymbol{F}_{ij}^R$) forces [73]. Those forces are pairwise additive and are of the form

$$\boldsymbol{F}_{ij}^C = \begin{cases} a_{ij}\left(1 - \frac{\mathrm{r}_{ij}}{\mathrm{r}_c}\right)\hat{\mathbf{r}}_{ij} & if\ \mathrm{r}_{ij} < \mathrm{r}_c \\ 0 & if\ \mathrm{r}_{ij} \geq \mathrm{r}_c \end{cases}, \tag{2.3}$$

$$\boldsymbol{F}_{ij}^{D} = -\gamma_D w^D(\mathrm{r}_{ij})(\hat{\mathbf{r}}_{ij} \,.\, \mathbf{v}_{ij})\hat{\mathbf{r}}_{ij} \ , \tag{2.4}$$

$$\boldsymbol{F}_{ij}^{R} = \sigma w^R(\mathrm{r}_{ij})\theta_{ij}\hat{\mathbf{r}}_{ij} \ , \tag{2.5}$$

where $\mathbf{r}_{ij} = \mathbf{r}_i - \mathbf{r}_j$, $\mathrm{r}_{ij} = |\mathbf{r}_{ij}|$, $\hat{\mathbf{r}}_{ij}$=$\mathbf{r}_{ij}/|\mathbf{r}_{ij}|$, $\mathbf{v}_{ij} = \mathbf{v}_i - \mathbf{v}_j$, a_{ij} is the maximum repulsion between beads *i* and *j*, r_c is the cut-off radius, w^D and w^R are *r*-dependent weight functions vanishing for $r_{ij} > \mathrm{r}_c$, γ_D is the friction coefficient parameter, and σ is the noise amplitude [73]. The quantity $\theta_{ij}(t)$ is a randomly fluctuating variable with Gaussian statistics: $\langle\theta_{ij}(t)\theta_{kl}(t')\rangle = (\delta_{ik}\delta_{jl} + \delta_{il}\delta_{jk})\delta(t-t')$, where δ_{ij} is the Kronecker delta and $\delta(t-t')$ is the Dirac delta function. Espanol and Warren [74] showed that when one of the two weight functions w^D and w^R is arbitrarily selected, then the other can be determined as follows:

$$w^D(\mathrm{r}) = [w^R(\mathrm{r})]^2 \ . \tag{2.6}$$

In addition, the noise parameter is related to the friction parameter as

$$\sigma^2 = 2\gamma_D k_B T \ , \tag{2.7}$$

where k_B is the Boltzmann constant and T is the system temperature. As recommended by Groot et al., [73] the weight function is typically chosen as:

$$w^D(r_{ij}) = \begin{cases} (1-\mathrm{r}_{ij})^2 \ , & \text{for } \mathrm{r}_{ij} < \mathrm{r}_c \\ 0, & \text{for } \mathrm{r}_{ij} \geq \mathrm{r}_c \end{cases} \tag{2.8}$$

The noise amplitude σ and friction coefficient γ_D (in Eqn. 2.7) were maintained at 3, and 4.5, respectively [73]. The evolution of a simulated system depends on the repulsion parameters a_{ij}, which were constructed and validated with experimental data, as described in detail in the following chapters.

All simulations were conducted using the open-source Large-scale Atomic/Molecular Massively Parallel Simulator (LAMMPS) software package [75]. The visual molecular dynamics (VMD) software was used to visualize the simulated systems [76]. The computations with DPD were conducted using dimensionless DPD quantities and the time-step for all simulations was 0.02 in DPD units.

Chapter 3. Protocol to Determine Interaction Parameters for Systems of Surfactants at Oil-Water Interfaces

Abstract[*]

In order to investigate the interfacial region between oil and water with the presence of surfactants using coarse-grained computations, the interactions between different components of the system and the number of surfactant molecules present at the interface play an important role. However, in many prior studies, the number of surfactants used was chosen rather arbitrarily. In this work, a systematic approach to develop coarse-grained models for anionic surfactants (such as sodium dodecyl sulfate) and nonionic surfactants (such as octaethylene glycol monododecyl ether) in oil-water interfaces is presented. The key is to place the theoretically calculated number of surfactant molecules at the interface at the critical micelle concentration. Based on this approach, the molecular description of surfactants and the effects of various interactions parameters on the interfacial tension were investigated. The results indicate that the interfacial tension is affected mostly by the head-water and tail-oil interactions parameters. Even though the procedure presented herein is used with dissipative particle dynamics models, it can be applied for other coarse-grained methods to obtain the appropriate set of parameters (or force fields) to describe the surfactant behavior at the oil-water interface.

3.1. Introduction

Surfactants are molecules that have both hydrophilic (water-favoring) and hydrophobic (water-repelling) properties.[1] Due to this unique feature, they have been used extensively in a variety of commercial products (e.g., detergents, shampoos, personal hygiene products, etc.) [1, 77, 78].

[*] Material in this chapter has been published in T.V. Vu, D.V. Papavassiliou, The Journal of Chemical Physics 148(20) (2018) 204704.

In the oil exploration and production industry, surfactants have been used for enhanced oil recovery (EOR) to mobilize oil trapped in hydrocarbon reservoirs by reducing the oil-water interfacial tension (IFT) and boosting the production of oil [5, 79]. When present in oil-water mixtures, surfactants tend to move to the oil-water interface by aligning the hydrophilic part of the molecule toward the water phase and the hydrophobic part of the molecule toward the oil phase. The polar hydrophilic side of the surfactant is commonly referred to as the *head* and the hydrophobic, nonpolar part of the molecule as the *tail*. This phenomenon helps to reduce the IFT by altering the interfacial free energy of the oil-water interface [1].

The behavior of surfactants at oil-water interfaces has been investigated by both experimental [80-82] and simulation approaches [83-87]. Molecular dynamics (MD) simulations are the most commonly used tools to investigate these systems with computations. They have been applied to study the effects of various parameters, such as surfactant concentration and temperature, on phenomena like the IFT change and the surfactant micellization process [84, 88-90]. As already discussed in the previous chapter, the length and time scales employed in MD are very small (typical lengths are on the order of Angstroms to nanometers, and typical time-steps are on the order of 10^{-15} s for simulations covering hundreds of nanosecond at most). It is troublesome to simulate a system in scales that encompass several macromolecules, comparable to experiments. Thus, the development and use of suitable coarse-grained simulations are necessary to investigate the water-surfactant-oil systems at larger scales. One such coarse-grained modeling technique is DPD simulations, which are an excellent tool for studying systems at the mesoscale level [73, 91, 92]. Several studies for surfactants at oil-water interfaces have been reported with DPD [71, 72, 93, 94].

In general, to describe water-surfactant-oil systems, two different approaches are normally used. The first is to insert surfactants in one phase and run the simulation until the system reaches equilibrium, while the second is to place the surfactant molecules at the interface.

In the first approach, the surfactant would gradually move to the interface as the simulation progresses. The advantage of this method is that it describes the actual phenomena taking place in a physical system. However, it takes a long computational time for the surfactant molecules to arrive at the interface, especially when the interface is close to saturation. Moreover, to prevent the formation of micelles, only very small amounts of surfactant should be allowed to enter the system in a step-by-step process, which makes the simulation even more cumbersome. To overcome this difficulty, Rekvig et al.[93] used a combination of DPD and Monte Carlo methods to investigate surfactant efficiency. The Monte Carlo simulation was used to create a bath to ensure that the surfactant concentration was constant in the system. They found that increasing the length of the molecular chains and using larger or more ionic head groups led to higher surfactant efficacy in terms of IFT reduction. Interfacial properties, such as density of the surfactant at the interface, IFT, and the shape of the interface were also investigated for different types of surfactants.

In the other approach, only the interface is investigated by placing a certain number of surfactant molecules on it, *i.e.*, the simulation is carried out after the surfactant has reached the interface [95]. This method is faster since the simulation does not have to run for a long time to allow surfactants to arrive at the interface. Duan et al. used this approach to adjust DPD parameters for the description of surfactant on the water-air interface, considering air as a hydrophobic phase [96]. Recently, Ndao et al. performed DPD with this approach to study the contribution of changing intermolecular interactions to the interfacial tension [97].

However, these models can only describe the interfacial region qualitatively. In detail, the number of surfactant molecules present at the interface (whether artificially placed or naturally arriving) was not matching the exact number expected in a real system. Thus, the simulations may have generated unphysical phenomena, such as the distortion of the interface because of unrealistically high surfactant density at the interface. Moreover, the reduction of IFT by surfactants was mostly reported in dimensionless DPD simulation units rather than actual units. In other words, the model parameters used to describe these systems were not chosen to depict realistic systems with quantitative accuracy. This is a disadvantage of DPD modeling since simulation results cannot be viewed as representative of real systems and often cannot be validated through experimental results. This is the issue addressed in the present work. An approach, where experiments are used to validate the selection of each model parameter in a step-by-step process is presented. This approach can become the backbone of a simulation protocol when calculations for specific systems are needed.

In this work, we used the second approach for placing the surfactant molecules in the computational system, as did most of the prior reports. However, the interfacial region was described by placing the correct number of surfactant molecules at the oil-water interface, as predicted by theoretical calculations. The contribution of this chapter is to (a) demonstrate a systematic methodology to obtain DPD parameters that are appropriate for ionic and non-anionic surfactants at oil-water interfaces that represent specific physical systems, (b) to quantify the effect of various DPD model parameters on IFT, and (c) to present clear criteria for the selection of these parameters. An important finding in this research is that not only the interaction parameters are necessary to describe the interfacial region, but the molecular structure of surfactants also plays a crucial role. The rest of this report is organized as follows: section 3.2 provides details of the

simulations. In section 3.3a, the modeling of the sodium dodecyl sulfate (SDS) surfactant at the oil-water interface is presented. SDS represents the case of a simple, short molecule ionic surfactant at the interface. It is shown that the ionic nature of surfactants can be accounted for indirectly by adjusting head-head and head-water interaction parameters. In section 3.3b, the description of a longer, more complicated nonionic surfactant (octaethylene glycol monododecyl ether, C12E8) is presented. In this case, accounting for the steric effect of the presence of large molecules at the interface requires the incorporation of intramolecular angles in the DPD model. Finally, the findings of the simulations are summarized in section 3.4.

3.2. Simulation Details

The schematic representation of each molecule in the model is shown in Figure 3.1. The oil phase was represented by n-Heptadecane ($C_{17}H_{36}$) molecules. Computations were carried out for two different surfactant molecules. Sodium dodecyl sulfate (SDS), which has been employed in simulations and experiments of surfactant systems quite often, [98-100] was selected as a representative anionic surfactant with a relatively short molecule. The nonionic, long-chain octaethylene glycol monododecyl ether (C12E8) was selected as the second surfactant. Water, oil, head, and tail beads were denoted as W, O, H, T respectively. The water bead mass, cut-off radius (r_c), and k_BT were chosen as the simulation units for mass, length, and energy, so $m = 1$, $r_c = 1$, and $k_BT = 1$. The number density was set to be 5 beads per unit volume. Thus, the mass and length (r_c) scales were calculated to be 1.496 x 10^{-25} kg and 0.9086 x 10^{-9} m, following Keaveny et al.[101] The time scale was determined [91] as $\tau = r_c\sqrt{m/k_BT}$ with the value 5.478 x 10^{-12} s.

In DPD, the selection of the part of a large molecule that would be grouped as one bead is made based on the principle that the simulation beads for all components should have the same volume [73]. In our simulation, one heptadecane molecule was represented by three oil beads connected

by harmonic bonds. Thus, an SDS molecule had to contain one head and two tail beads, while five water molecules were lumped together in one bead to represent water in the aqueous phase. Because of the structure of C12E8, it was reasonable to divide its molecule into 6 different beads: 2 tail and 4 head beads (see Figure 3.1). For C12E8, the harmonic bond and angle potentials were applied between beads. The equations for bond and angle potentials are as follows:

$$E = k_b(r - r_0)^2 \qquad \text{for bonding} \qquad (3.1)$$

$$E = k_\theta(\theta - \theta_0)^2 \qquad \text{for angle} \qquad (3.2)$$

where k_b, k_θ are bonding and angle potential coefficients, respectively, r, r_0 are the bond distance and the equilibrium bond distance, and θ, θ_0 are the angle and equilibrium values of the angle. The values for k_b, k_θ, θ_0 were 100 k_BT/r_c^2, 15 k_BT, and 130°, respectively. The equilibrium bond distances r_0 were calculated from the molecule length of SDS and C12E8 to be 1.14 r_c and 0.8 r_c, respectively.

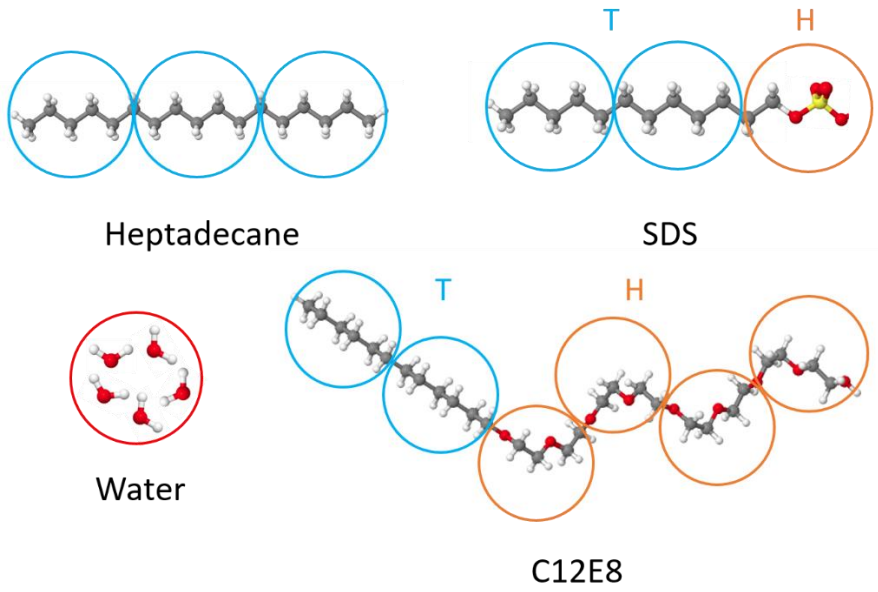

Figure 3.1. Schematic configuration of water, heptadecane, SDS, and C12E8 surfactant molecules in the DPD simulation. An SDS molecule consists of one head (H) and two tail (T) beads, while a C12E8 molecule consists of two T and four H beads. Note also that a water bead for the C12E8

simulations would be composed of 6 H_2O molecules. White, gray, red, yellow spheres represent hydrogen, carbon, oxygen, and sulfur molecules, respectively.

To maintain comparable volumes of beads in the same system, in the case of simulations with C12E8, one DPD bead in the aqueous phase was then equivalent to 6 water molecules. This different level of coarse-graining leads to different length and time scales. The suitable scales for C12E8 were calculated using the same approach as for the SDS case – the time and length scales for both cases are presented in Table 3.1. Note that the water number density was the number of water molecules in a water bead. The mass of a water bead was 1. The masses of SDS head and tail, C12E8 head and tail beads were calculated from their molecular weights as 1.32, 0.93, 0.85, and 0.78, respectively.

Table 3.1. Scaling factors for the simulations with SDS and C12E8 surfactants

Surfactant	**Water Number density**	**Number of water molecules in a bead**	**Mass scale (kg)**	**Length scale (m)**	**Temperature scale (K)**	**Time scale (s)**
SDS	5	5	1.5×10^{-25}	9.09×10^{-10}	298	5.48×10^{-12}
C12E8	5	6	1.8×10^{-25}	9.66×10^{-10}	298	6.38×10^{-12}

The difficulty of describing an oil-water–surfactant system is that even when the oil-water interface is saturated with the surfactant, the concentration of surfactant in the bulk phase is very small; meanwhile, the interfacial region is too small in comparison to the whole volume of the system. To represent such systems, the simulation box needs to be infinitely long, which is not feasible. To overcome that obstacle, the present simulations were focused on the interfacial region by placing the theoretically expected number of surfactant molecules at the interface at the critical micelle concentration (CMC). This number was calculated by the Gibbs adsorption equation as follows: [1]

$$d\gamma = -\sum_i \Gamma_i d\mu_i \ , \tag{3.3}$$

where $d\gamma$ is the change in interfacial tension of the solvent, $d\mu_i$ is the change in chemical potential of any component i of the system, and Γ_i is the surface excess concentration of any component of the system. The surface excess concentration is the excess amount, per unit area of the interface, of the component over its concentration in the bulk phase. With surfactants, the difference between their amount at the interface and in the bulk phase is large; hence, Γ_i can be considered as interface concentration without significant error [1].

Equation (3.3) for the case of nonionic and ionic surfactant yields the following equations:

$$d\gamma = -2.303\ RT\ \Gamma_i\ \mathrm{d}logC_1 \ , \qquad \text{for nonionic surfactants} \tag{3.4}$$

$$d\gamma = -4.606\ RT\ \Gamma_i\ \mathrm{d}logC_1 \ , \qquad \text{for ionic surfactants} \tag{3.5}$$

where C_1 is the molar concentration of surfactant in solution and R is the ideal gas constant.

By plotting the dependence of interfacial tension to surfactant concentration, γ vs $logC_1$, the surface excess concentration can be calculated. In a typical γ vs $logC_1$ plot, for the region of concentrations below (but near) the CMC, the slope of the curve is essentially constant, following Equations (3.4) and (3.5). The reason is that in this range, the interface is considered to be saturated with surfactant [102] and the continued reduction in the interfacial tension is due mainly to the increased activity of the surfactant in the bulk phase rather than at the interface. Thus, the excess concentration can be determined from the slope of γ vs $logC_1$ plot. In this study, the two surfactants were chosen due to the availability of experimental data for γ vs $logC_1$ plot, as well as surface excess concentration. With SDS on water-heptadecane interface, $\Gamma_i = 3.3 \times 10^{-10}$ [mol/cm^2] [103], which is equivalent to 1.61 SDS surfactant molecules per 1 r_c^2 area in DPD units.

Similarly, in the case of C12E8 on a water-heptadecane interface, $\Gamma_i = 2.64 \times 10^{-10}$ [mol/cm^2] [104]. In DPD units, it is equal to 1.47 C12E8 molecules per 1 r_c^2 area. In fact, with C12E8, the data is only available for water-heptane (2.62×10^{-10} [mol/cm^2]) and water-hexadecane (2.64×10^{-10} [mol/cm^2]), but since the values are close enough, it was assumed that the same values can be applied for the case of water-heptadecane without significant errors.

In all simulations, the box size was L_x x L_y x L_z = 10 x 10 x 30 r_c^3. The initial positions of oil and water molecules were distributed in three continuous regions as water-oil-water. Because of the periodic boundary conditions in all directions, there were two interfaces. Based on the calculations above, the numbers of surfactant molecules placed at one interface for SDS and C12E8 were 161 and 147, corresponding to 483 and 882 surfactant beads, respectively. The number of oil beads was 4500, which fixed the numbers of water beads in the cases of SDS and C12E8 as 9534 and 8736, respectively, to maintain the number density of the simulation box as 5. All DPD simulations were carried out at constant NVT conditions, i.e., constant number of beads, and constant volume and temperature. All the simulations were carried out for 10^6 steps with a time-step of 0.02 in DPD units, which is equivalent to 1.1×10^{-13} s and 1.28×10^{-13} s in the case of SDS and C12E8 surfactants, respectively. After every 1000 time-steps, the state of the system was recorded for further analysis.

Since the interfacial regions arranged along the z-direction, the interfacial tension was calculated as [105]

$$\gamma = \langle P_{zz} - \frac{P_{xx} + P_{yy}}{2} \rangle \frac{L_z}{2} \tag{3.6}$$

where P_{ij} is the ij element of the stress tensor, L_z is the length of the simulation box in the z-direction, and the brackets represent the ensemble average. The interfacial tension values were calculated at each time step of the simulation and then were averaged for 1000 steps. Further

averaging of those values gave the final IFT. It is seen later that with the short-molecule surfactants, like SDS, the interfacial tension can be matched by simply adjusting the interaction parameter of the DPD model; meanwhile, to describe the interfacial region correctly, the steric effect needs to be accounted by the implementation of appropriate molecular angles.

3.3. Results and Discussion

Looking at Equations (2.3) to (2.8) that describe the DPD model, it is apparent that to model oil-water-surfactant systems we need to obtain the interaction parameters for oil-water, oil-surfactant (both oil-heat and oil-tail), and water-surfactant (both water-head and water-oil). This process is sequential, as described in this section. The first parameter to be determined was the oil-water interaction parameter. It was adjusted to fit the interfacial tension value of water-heptadecane (53.2 mN/m) [103] and a_{WO} was determined to be 90 for the SDS case and 100 for C12E8. The difference in the value of a_{WO} is because of different levels of coarse-graining.

The steps taken for the system with SDS and with C12E8 are described in the next two sections, along with findings of the effect of the interaction parameters on the stability of the oil-water interface and the IFT.

a. Oil-water System with Anionic Surfactant (SDS)

The focus is first on obtaining the interaction parameters for head, tail, and water beads. For number density $\rho = 5$, Groot and Warren [73] showed that the like interaction parameter is $a_{ii} = 15$. For the head-head interaction parameter ($a_{H\text{-}H}$), the electrostatic interactions were accounted by choosing it as 20, a value higher than the value of a_{ii} for the other components [96, 106]. Groot and Warren[73] also demonstrated that the repulsion parameters of beads of different molecules depend on their solubility parameter as follows:

$$\chi_{ij} \approx 0.689\left(a_{ij} - a_{ii}\right) \tag{3.7}$$

$$\chi_{ij} \approx \frac{V_b}{k_B T}\left(\delta_i - \delta_j\right)^2 \tag{3.8}$$

where δ_i is the solubility parameter of component i, χ_{ij} is the Flory-Huggins parameter and V_b is the volume of one DPD bead. Using Equations (3.7) and (3.8) with the solubility parameter obtained from Barton,[107] (14.9 $MPa^{-1/2}$ and 47.9 $MPa^{-1/2}$ for n-hexane and water, respectively) the repulsion parameter for tail-water is calculated to be 54. Note that one tail and oil beads are comparable to one n-hexane molecule.

For the remaining interaction parameters of H, T, W, the strategy described by Mai et al. [108] was applied by matching the micelles aggregation number (N_{ag}), which is defined as the number of surfactant molecules in one micelle. The interaction parameters were adjusted to get N_{ag} = 64 [109]. In short, it was observed that there was a trend of increasing N_{ag} by enhancing a_{HW}, a_{WT}, or reducing a_{HT}, as was discussed in Mai et al. The formation of micelles is driven by the increase of water entropy as the water molecules are orderly arranged around the surfactant tails. By forming micelles, these water molecules become as randomly ordered as the other water, contributing an entropy increase to the system. Furthermore, it was found here that increasing the head-head interaction leads to decreasing N_{ag}. This observation can be explained by considering that with a high repulsion between head beads, they tend to be away from each other, leading to fewer surfactant molecules that can get into micelles. All the parameters for interactions between head, tail, and water beads are listed in Table 3.2. The final interaction parameters between oil beads and the others are also presented.

When introducing the oil phase, there are three more parameters that are necessary to describe the interfacial region: head-oil (a_{HO}), water-oil (a_{WO}), tail-oil (a_{TO}). In fact, the IFT is also affected by the parameters determined earlier in this section, but to keep N_{ag} in agreement with the experimental value, those should not be changed.

The effects of a_{HO}, a_{TO}, a_{HW} on IFT were then examined. The values of a_{HW} were also tested to show its effect, but its value should be kept at 10 to ensure that N_{ag} remains at 64. Figure 3.2 is a typical snapshot of the SDS surfactant morphology in the simulations. It can be seen that all the surfactant molecules are located at the interfaces with the heads (red beads) oriented toward the water phase, and the tails (blue beads) directed to the oil phase.

Table 3.2. Set of repulsion parameters used in the simulations. H and T represent the head and tail of SDS surfactant, while W and O denote water and oil, respectively.

	H	**T**	**W**	**O**
H	20	42	10	54
T		15	54	12
W			15	90
O				15

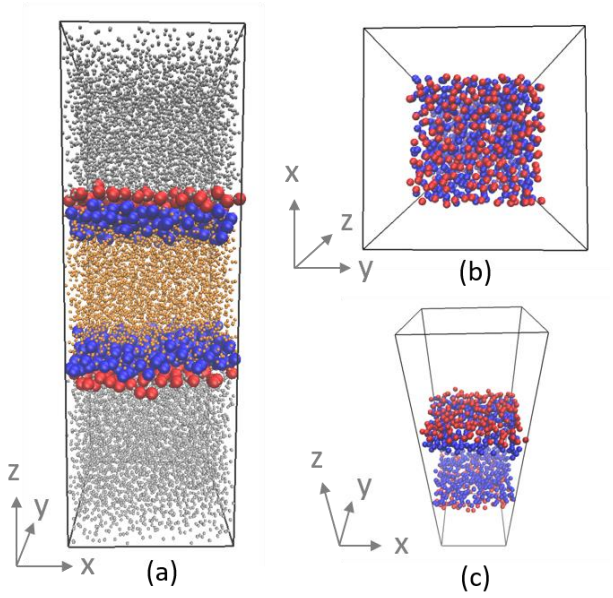

Figure 3.2. Snapshot of SDS surfactants at the oil-water interface from different perspectives. The snapshots were taken after 100000 time-steps. Water, oil, surfactant head, and tail beads are represented by silver, orange, red and blue respectively; in (b) and (c) water and oil beads are not shown for clarity.

When the concentration of the surfactant reaches the CMC, the interface is covered by surfactant molecules. Because of their hydro- and lipophilicity, the heads and tails are tailored into the water and oil phases, respectively. Most of the direct interactions between oil and water are altered by the interactions between head-water and tail-oil. Thus, the interaction between them would determine the reduction of IFT by the presence of the surfactant. It can be seen in Figure 3.3 that IFT increases with a_{TO} and a_{HW}. When a_{HW} is fixed to be 10, as a_{TO} increases from 10 to 15, IFT rises from 5.49 to 23.78 mN/m. The linear dependence of IFT to H-W, and T-O parameters can be explained based on the formula for calculating the IFT when the interaction forces between the beads are known. This equation, which is used in LAMMPS to obtain the IFT, is as follows:[105]

$$\gamma_{12} = \frac{1}{A}\left[\sum_{ij} F_{ijz} r_{ijz} - \frac{1}{2}\left(F_{ijx} r_{ijx} + F_{ijy} r_{ijy}\right)\right] \tag{3.9}$$

where A is the interfacial area, F_{ijx}, F_{ijy}, F_{ijz} and r_{ijx}, r_{ijy}, r_{ijz} are the x, y, z components of the total force and distance vectors between beads *i* and *j*. The summation is carried out over all particle pairs. The first term denotes the normal stress tensor in the direction perpendicular to the interface (z-direction), while the second term represents the tangential stress tensor (in x- and y-direction). By plotting the difference between normal and tangential stress tensor elements along the *z*-direction, Ndao et al. [97] showed that only the interface region, in which most of the interactions are head-water and tail-oil, contributes to IFT. The force formulas are presented in Equations (2.3), (2.4), and (2.5), and indicate that the forces are linearly dependent on a_{ij}. Thus, IFT increases linearly with the increase of a_{HW} and a_{TO}, as expected.

The contribution of a_{TO} and a_{HW} in IFT was quantified as seen in Figure 3.3. The sensitivity of IFT to a_{TO} and a_{HW} is represented by the slopes of IFT vs. parameter lines. By linear fitting, the slopes are calculated to be 3.55 and 1.25 for the case of a_{TO} and a_{HW}, respectively. One can expect that IFT is more sensitive to the variation of a_{TO} than that of a_{HW}, since there are two tail beads in comparison to one head bead. It is noteworthy that the ratio of the slope values is 2.84, instead of 2 that is expected based on the number ratio of the tail over the head. In Eq. (3.9), there is another factor that affects the IFT value, namely r_{ij}. With the two tail beads, when increasing the repulsion parameters between them and oil, the oil bead tends to be pushed farther due to a higher total force acting on it. As a result, r_{ij} is higher than that in the case of increasing a_{HW}, leading to a ratio of slope values between a_{TO} and a_{HW} cases higher than 2. In summary, IFT increases linearly with the increment of a_{TO} and a_{HW}, and it is more sensitive to the changes of a_{TO} than a_{HW}.

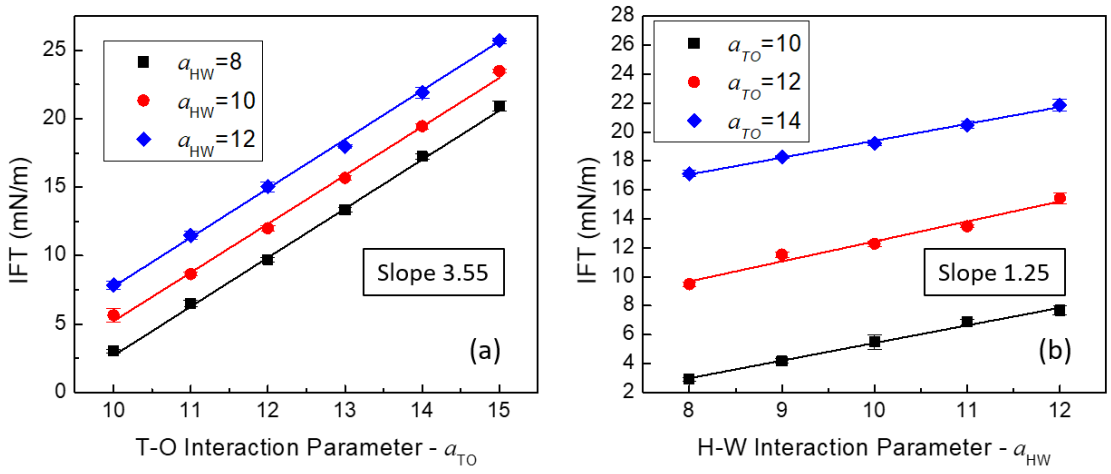

Figure 3.3. Dependence of IFT on tail-oil (a_{TO}), and head-water (a_{HW}) interaction parameters for the simulations using SDS surfactant. The error bars shown on the data points represent the standard deviation of the IFT values for each point for 5 different IFT calculations.

The influence of a_{HH} and a_{HO} on IFT is plotted in Figure 3.4a. It is seen that the IFT does not vary with the change of a_{HO}. The reason can be determined by looking at the snapshot of the interface at equilibrium in Figure 3.2a. In the interfacial region, it can be observed that there is a very small chance of oil beads being in contact with surfactant head beads, or water being in contact with tail beads. Therefore, their interaction parameters do not have a significant impact on IFT. Since there is not a significant contribution of a_{HO} to IFT, it is chosen to be 54 so that $a_{HO} = a_{TW}$ for simplicity.

Regarding changes of a_{HH}, it is seen in Figure 3.4a that the IFT decreases with increasing a_{HH}. This behavior can be explained by considering that stronger repulsive forces between head beads hinder the direct contact between oil and water beads, thus helping the reduction of IFT. Since the electrostatics interactions are not explicitly included in the DPD formalism (i.e., in Equations 2.1 to 2.8), the a_{HH} and a_{HW} indirectly represent the charges of the surfactant heads [96, 100, 106, 110]. The study of a_{HH} and a_{HW} here also helps to predict the impact of salt concentration on the IFT of oil-water with ionic surfactants. A higher concentration of counter ions (because of salt) in

the solution would reduce the charge of surfactant heads, which would lead to the decrease of a_{HH} and a_{HW}. The reduction of a_{HH} increases IFT, while the reduction of a_{HW} would produce the opposite effect. Depending on the magnitude of those effects, the IFT might increase or decrease with higher concentration of salt. This phenomenon is well described in the literature [1, 111]. Since the electrostatic forces are not directly implemented in DPD, the trends described here are only qualitatively correct for the effect of salt concentration. In other words, we are not sure exactly how the a_{HH} and a_{HW} would change with the presence of counter ions. However, the protocol developed here could also describe the oil-water-ionic surfactant systems in the presence of salt. In that case, one needs to simply adjust a_{HH} and a_{HW} to match the IFT and N_{ag} in the salt solution.

For the generalization of the model to use with other ionic surfactants without the presence of salt, the parameters that account for electrostatics, which are a_{HH} and a_{HW}, could be assumed to be the same as the parameters described here.

The effect of the bonding potential coefficient (k_b) to IFT is shown in Figure 3.4b. Deguillard et al. [112] showed that at high concentration, k_b has a negative effect on IFT. The same trend is observed here. Since the concentration of surfactant placed at the interface here corresponds to the concentration in an actual system, the explanation for the observation is quite straightforward. As stated above, at CMC, most of the direct water-oil interactions are replaced by water-surfactant and oil-surfactant interactions. With a fixed, more organized surfactant molecule (having a higher k_b), the surfactant molecule tends to stay close to the interface, meaning that there is less room for oil and water beads to be in contact. In other words, it prevents direct contact between oil-water better. Consequently, the IFT is lower, or one can say that the surfactant is more effective at the interface.

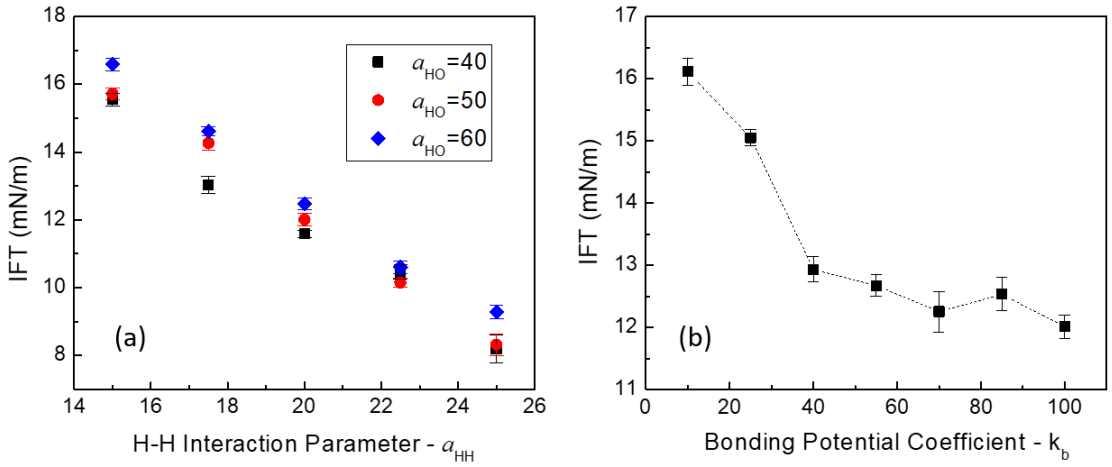

Figure 3.4. Dependence of IFT on tail-oil interaction parameter (a) and surfactant bonding potential coefficient (b) for the simulations of SDS surfactant. The error bars shown represent the standard deviation of the IFT values utilizing 5 different IFT calculations.

The dependence of IFT on the total concentration of surfactants in the simulation box is plotted in Figure 3.5. At concentrations lower than the CMC, all the surfactants were placed at the interface, while after CMC, the additional surfactant molecules were in the water phase. In this plot, there is no specification of the surfactant concentration as either surface or bulk concentration, it is the total number of surfactant molecules in the system. It is seen in the plot that although there is the formation of micelles after CMC, the IFT value does not change. This affirms that only the interface region contributes to the value of IFT. In terms of physical meaning, for concentrations higher than the CMC, the interface is saturated with surfactant; the additional surfactant molecules cannot reach the interface. Thus, the simulation process adopted herein can be well-fitted for the region of concentrations larger than the CMC. At concentrations less than the CMC, the IFT decreases linearly with the concentration of surfactant at the oil-water interface. One might note the difference between this plot and a typical plot of IFT vs. concentration based on experimental data. A typical plot would show a linear dependence of IFT with the logarithm of surfactant

concentration near the CMC, while in this plot (or any others from simulations [96]) one sees a linear correlation between the IFT and the concentration of the surfactant. The explanation is based on the setup of the simulation, in which all the surfactant molecules are placed at the interface. The typical plots from experiments follow Eqns. (3.42) and (3.5), where the bulk concentration is used. From those equations, the surface concentration can be estimated, while in the simulation, the surface concentration is used as an input. Thus, it can be said that the plots from the simulation indirectly imply the Gibbs adsorption equation by using surface concentration. In comparison to the plot by Ndao et al.,[97] the plot here is closer to a real system. The IFT at CMC in their plot is close to 0 mN/m, which is much different from the experimental value (~ 11.2 mN/m). We also carried out a simulation following the Ndao et al. procedure, in which the number of surfactants placed at the interface was more than the real amount at the CMC. However, the equilibrium configuration of the system depends strongly on the initial configuration of the simulation and the initial placement of the surfactant molecules. The configuration at equilibrium could be either a distorted interface or a configuration with micelles formed because of surfactants leaving the interface, as described in prior literature [90]. Because of that, the IFT vs. concentration plot does not always reach a plateau as expected. However, the procedure proposed herein can give more reliable information for the interfacial region.

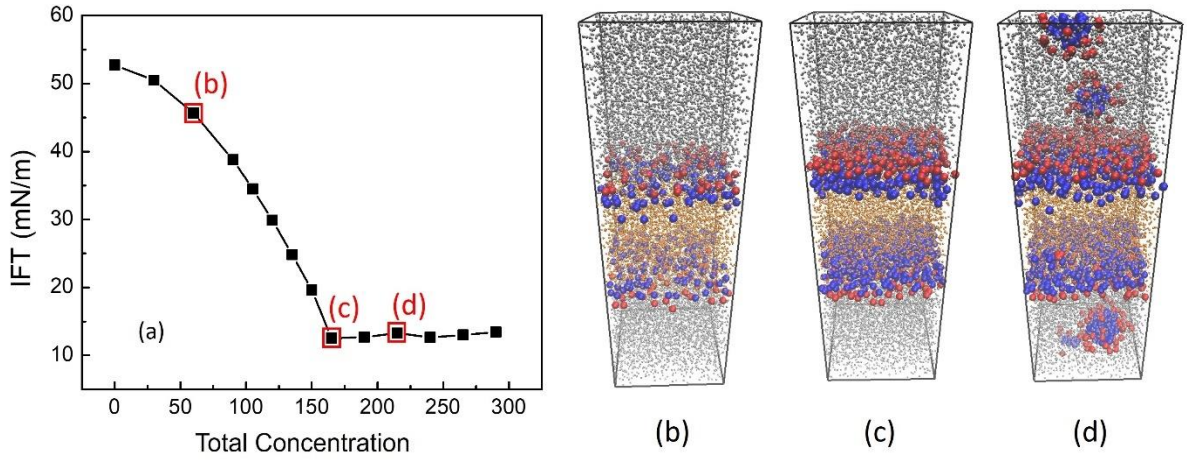

Figure 3.5. IFT as a function of the total concentration of SDS surfactant. The water and oil beads are shown as gray and orange, while surfactant tail beads are blue and head beads are red. Note that for concentrations lower than the CMC, all the surfactant molecules are at the interface. The error bars are smaller than the symbols – the maximum error value is 0.65 mN/m.

b. Oil-water System with Nonionic Surfactant (C12E8)

The description for SDS surfactant is quite simple, considering the SDS short molecular structure. When it comes to longer surfactants such as C12E8, the problem is much more complicated. One may expect that with a quite similar surface excess value (3.3 and 2.64 x 10^{-10} mol/cm^2 for SDS and C12E8, respectively), the number of surfactant beads at the interface for C12E8 will be roughly twice that of SDS, due to the double length of C12E8 in comparison to SDS. Placing all the surfactant beads of C12E8 at the interface creates an issue that can be seen in Figure 3.6a. Due to the high density of surfactant, the interface is distorted, and some surfactant molecules even leave the surface to create micelles in the water phase. This observation is common in previous reports [72, 90]. In those reports, because the surface concentration is chosen quite randomly, it is normally assumed that the concentration of surfactant at the interface is too high. However, here we placed at the interface the exact amount of surfactant that is enough to saturate the interface at CMC conditions in a real system; thus, this phenomenon is not physical. To overcome this

obstacle, the angle between three consecutive beads of the surfactant molecule should be considered in the model. Typically, the angles between segments connecting the center points of the surfactant beads are chosen to be 180° [97, 113]. Applying an angle of 180° in the simulation yields straight surfactant molecules and the configuration depicted in Figure 3.6d. In such a system, the surfactant molecules are well-arranged at the interface, and the interface is flat. However, the choice of an angle equal to 180° is not necessarily correct. When the surfactant molecules are straight, they turn into a perpendicular position relative to the interface and occupy a small space. In fact, one molecule could be counted as one bead in the *xy* plane since its axis is oriented along the *z*-direction. Consequently, there is enough space for more surfactants to be packed, which might violate the experimentally observed saturation concentration at the interface. Thus, the choice of a correct angle is crucial in the description of the interfacial region. The molecular structure of C12E8 is illustrated in Figure 3.1.[114, 115] Based on this structure, the Tail-Tail-Head angle was fixed as 180°. All the other angles were considered to be equal and were varied from 90 to 180° to conduct a parametric investigation. The goal was to determine the appropriate angle in the molecule to satisfy two criteria: (a) the interface is still flat, and (b) it is saturated with the surfactants. To quantify those criteria, we used the variance of the last head bead's position in the z-direction (Δ). Δ was calculated by the following equation:

$$\Delta = \frac{\sum_{i=1}^{n}(z_i - \overline{z})^2}{n} \tag{3.10}$$

where z_i is the *z*-component of the vector position of bead *i*, $\overline{z}$ is the average of z_i, and *n* is the total number of the last head beads of all the surfactant molecules. The summation is carried out over the *n* beads. One can see Δ as a representation of the stability of the interfacial region. High Δ implies a curved interface with various locations for the same kind of bead. The value of Δ is expected to be as small as possible for a stable interface.

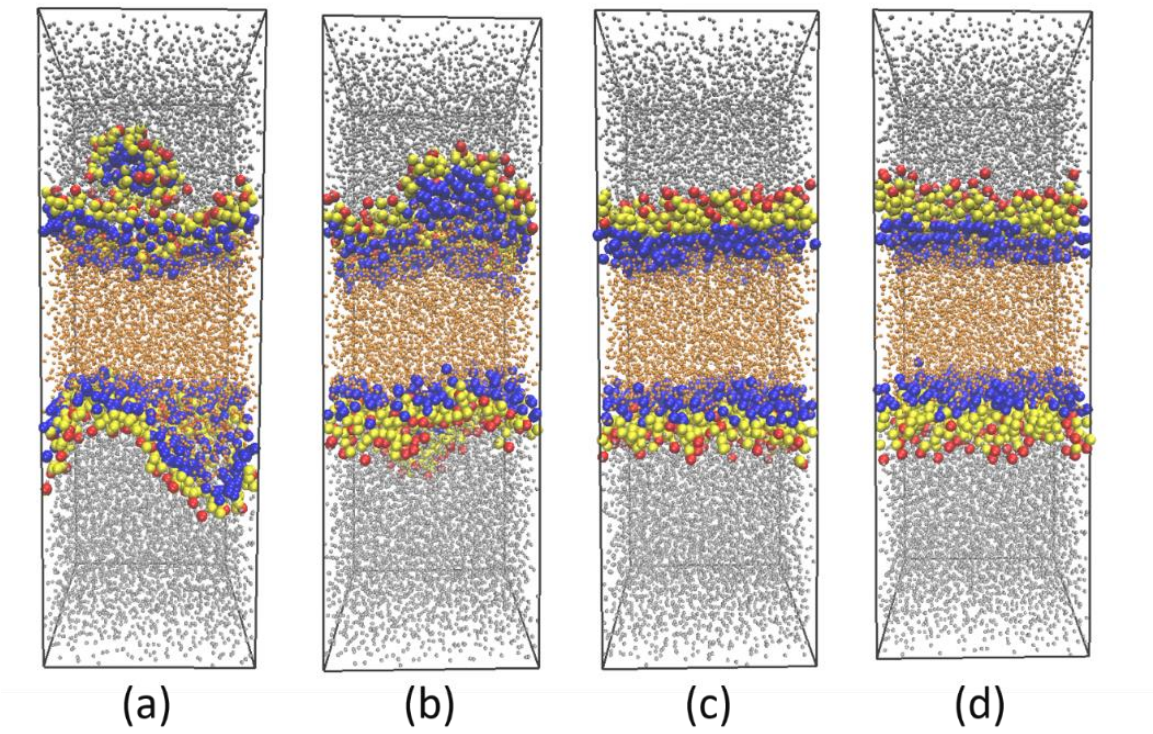

Figure 3.6. Snapshots of a water-C12E8-oil system in different molecule angles of surfactant (a) no angle, (b) 90º, (c) 130º, (d) 180º. The water and oil beads are shown as gray and orange, surfactant tails are blue, while red and yellow beads represent the surfactant head beads. The last surfactant heads are colored differently than other heads just for indicating the beads used in variance calculation.

Figure 3.7d is a plot of the dependence of Δ on the variation of surfactant intramolecular angle. From 90º to 130º, Δ decreases monotonically with the increase of this angle. It is understandable that at small angles the surfactant molecule takes up a larger space, pushing the other surfactant molecules away. Because the surfactant has a natural tendency to stay at the interface, the interface was forced to curve, to allow for enough space for all the surfactant molecules. Without considering the intramolecular angle, the interaction forces between surfactant beads were high enough to overpower the tendency of surfactants to be at the interface, leading to the breakup of the interface and the movement of surfactants to the water phase. As the angle increases, the space needed for each surfactant molecule decreases. Hence, the interface is less distorted, *i.e.*, it is more

stable. This observation also indicates that using angle potential is a good representation of the steric effect of a surfactant molecule. In the region from 130^o to 180^o, Δ does not change with the angle. The reason is that the interface is no longer saturated with surfactants. In this regime, the footprint of each surfactant molecule at the interface is small enough for all surfactants to fit into the interface without stretching it. The transitional point is at 130^o, which is the chosen value. This choice satisfies both selection criteria: it ensures that the number of surfactant molecules placed at the interface is enough for saturation and that the interface is still stable.

The number density profile of the system along the z-direction in case of not using the angle potential and using the angle potential for 180^o is plotted in Figures 3.7a and 3.7b. For clarification, Figure 3.7c shows only the density profile of surfactant at different angles. The two highest peaks in all cases identify the interfacial region, in which most of the surfactants are located. When there is no angle potential applied, there exist other peaks in the water region, indicating that the surfactants not only stay at the interface but also into the water phase. At angle 95^o, these peaks almost disappear, while the two main peaks are flattened out. When the angle increases, the peaks gradually sharpen, meaning that the surfactants are more concentrated at the interface. Comparing the peaks between angles 130^o and 180^o, their positions and shapes are quite similar, which shows that in both cases the surfactant molecules are well arranged on stable interfaces. The only difference is the intensity of the peaks: 4.14 and 3.86 in cases of 130^o and 180^o, respectively. In all the simulations, the number density is 5. Hence, the value closer to 5 indicates a more concentrated surfactant. With angle 130^o, the number densities of oil and water in the interfacial region are smaller than that in the case of angle 180^o, since higher surfactant density means lower oil and water density. In other words, oil and water have less of a chance to interact, which also means that the surfactants are more efficient with angle 130^o. This result confirms that

incorporating the intramolecular angle in computations is an appropriate implementation of the steric effects of surfactants.

After choosing the correct angle for beads inside the C12E8 molecule, we consider the effect of various parameters on the IFT. Similar to SDS, the surfactant and water beads interaction parameters were determined to match the aggregation number of C12E8 in micelles, which is 99 [116]. The final determined parameters are listed in Table 3.3.

Table 3.3. Interaction parameters for C12E8, water, oil. H, T represent the head and tail of C12E8 surfactant; W, O denote water and oil respectively.

	H	**T**	**W**	**O**
H	15	25	15	25
T		15	54	14.5
W			15	100
O				15

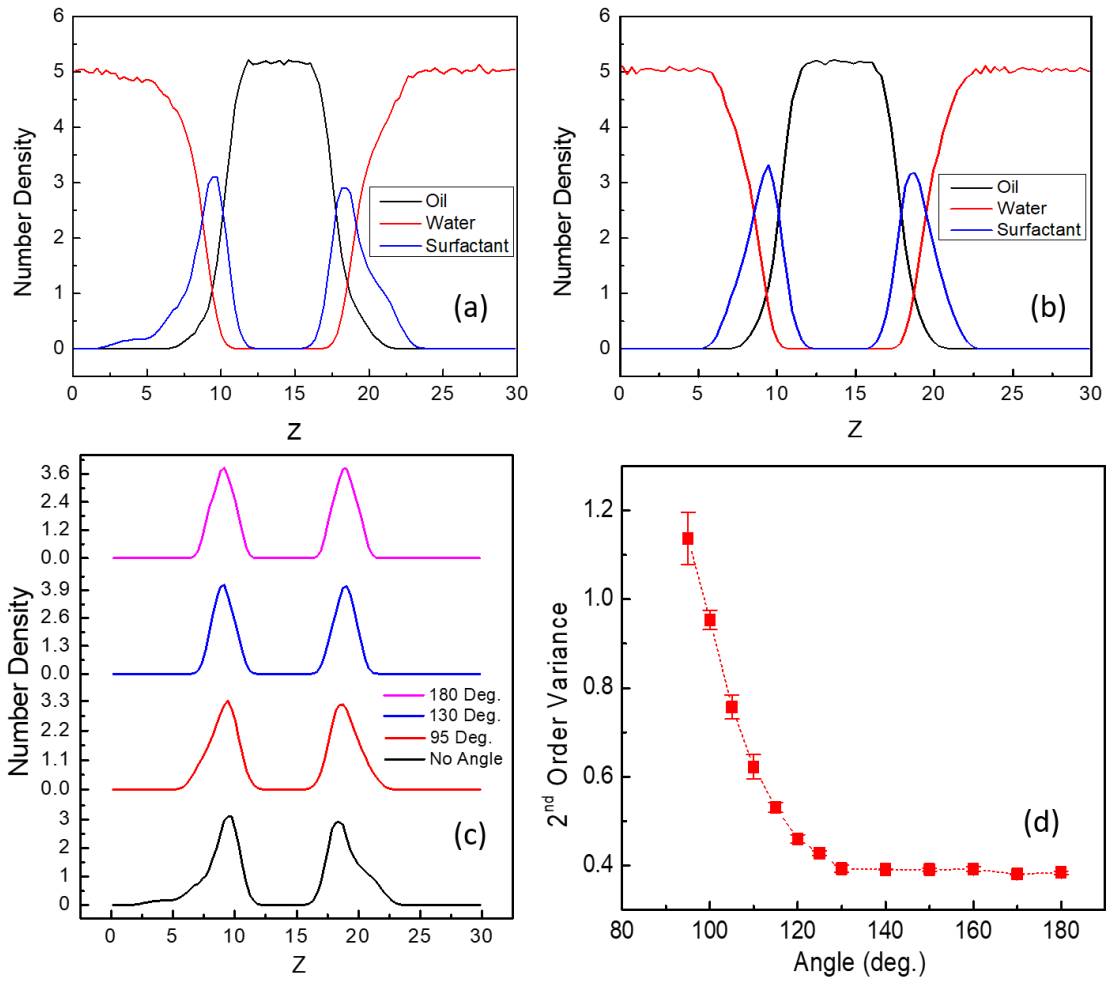

Figure 3.7. Density profile of the water-C12E8-oil system. (a) with no surfactant molecule angle; (b) 180^0 angle; (c) surfactant density profile at different angles. Panel (d) is a plot of the change of the variance of the head bead positions with surfactant molecule angles. The error bars shown represent the standard deviation utilizing 5 different calculations.

Figure 3.8a is a plot of the dependence of IFT on head-water and tail-oil interaction parameters. As expected, IFT increases linearly with both of these parameters as in the case of SDS. However, it is interesting to note that the slopes of the IFT with a_{TO} and a_{HW} are comparable: 3.19 with a_{TO} and 3.61 with a_{HW}. With the double number of head beads, one would expect that the slope of a_{HW} will be approximately two times that of a_{TO}. The reason for these phenomena is different from the case of SDS. Here we employed the intramolecular angles in the description of the surfactant

molecules. The rigid body of C12E8 prevents the surfactant beads from spreading out on a single layer. Without angle, the two tails of SDS can lay on the same xy plane and can be considered as two different beads. In contrast, the four tail beads of C12E8 with angle 130^o are projected as approximately 2 beads on the xy plane. This can be seen by looking at the molecular structure of C12E8 along the horizontal direction in Figure 3.1. Thus, it can be concluded that using a surfactant molecule with angles between the beads reduces the sensitivity of IFT on a_{TO} and a_{HW}. The most appropriate set of interaction parameters for water-C12E8-oil is presented in Table 3.3.

The effect of k_θ on IFT has not been investigated thoroughly in the literature. In Figure 3.8b, we present the change of IFT corresponding to the angle potential coefficient (k_θ). In the range of 5 to 15, IFT increases with k_θ. From 15 to 25, IFT does not change much with k_θ. Here, we propose an explanation for the observed trend. When the angle is quite loose ($5 \leq k_\theta \leq 15$), the surfactant beads are free to move. When k_θ is low, surfactant beads can cover the interface efficiently because the beads are free to move to their favored positions. Increasing k_θ leads to a more rigid body, and the surfactant beads are fixed to their positions in the molecules. Hence, they leave space for oil and water beads to be in contact, which increases IFT. In the range of 15 to 25, the body is rigid enough, further increment of k_θ does not reduce the degrees of freedom of surfactant beads significantly. Thus, IFT changes slightly with k_θ. The angle potential coefficient, therefore, is chosen to be 15 to ensure the body is hard enough, and the coefficient is not too high to create non-physical dynamics in the simulation.

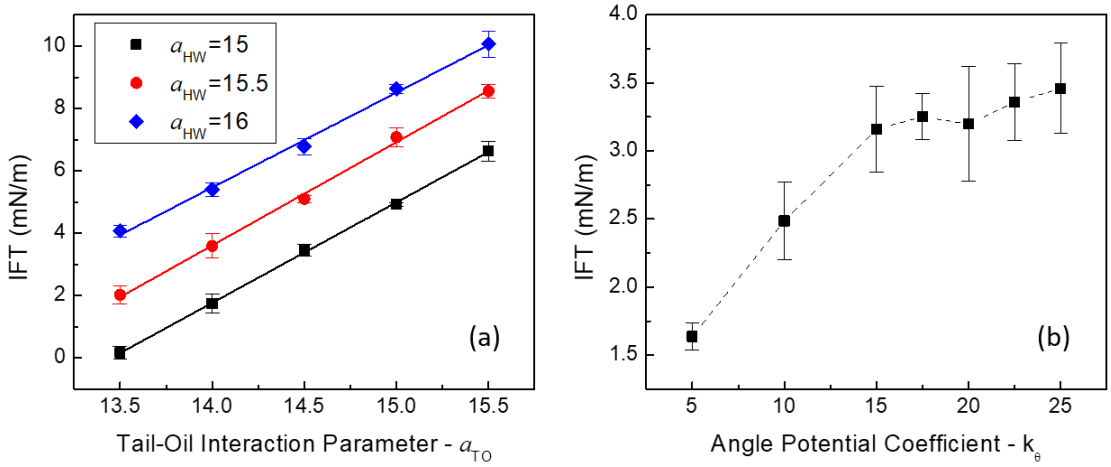

Figure 3.8. (a) Dependence of IFT on head-water and tail-oil interaction parameters; (b) dependence of IFT on the angle potential for the simulations of C12E8 surfactant. The error bars shown represent the standard deviation of the IFT values utilizing 5 different IFT calculations.

Figure 3.9 is a plot of the variation of IFT as a function of the concentration of C12E8. Similar to SDS at concentrations lower than the CMC, IFT decreases linearly with surfactant surface concentration. This observation is consistent with the Gibbs adsorption equation. After the CMC, all the inserted surfactant exists in the water phase forming micelles, as can be seen in Figure 3.9d. As a result, the IFT does not change with increasing the amount of surfactant, which is shown as the plateau of the plot in Fig. 3.9a. The formation of micelles in the water phase also confirms the saturation of the interface with surfactant. The plot is a validation of the suitability of the model to describe C12E8 at the oil-water interface.

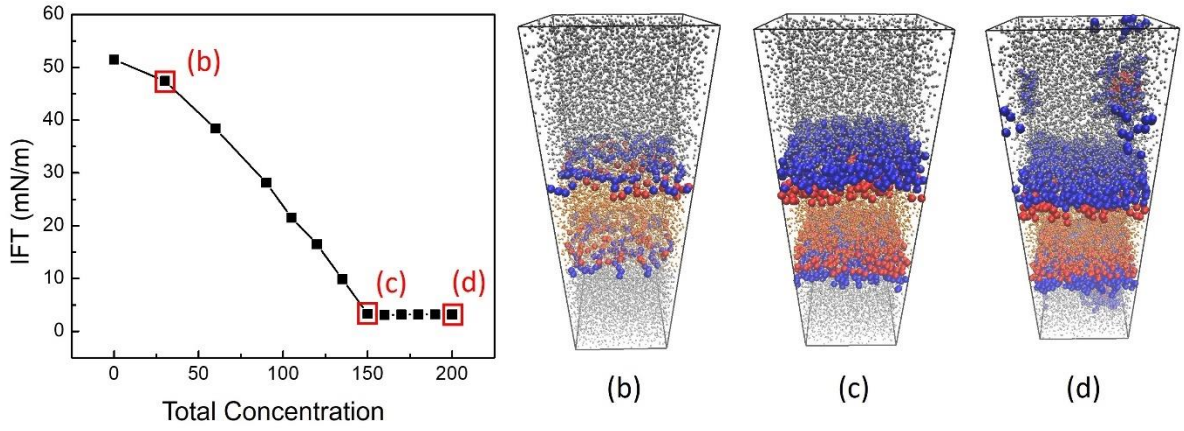

Figure 3.9. IFT as a function of C12E8 total concentration. The water and oil beads are shown as gray and orange, surfactant tail beads are blue, head beads are red. Note that at the region before CMC, all the surfactant molecules are at the interface. The error bars, with a maximum value of 0.45 mN/m, are smaller than the symbols.

3.4. Conclusions

The DPD simulation method was applied to investigate the interaction of surfactants at the oil-water interface. The procedure to describe the interfacial regions is summarized as follows: The exact number of surfactant molecules to be placed at the interface at the CMC for the simulation was calculated from the Gibbs adsorption equations. The surfactant molecules were then described to satisfy the two criteria: (a) the interface is saturated with the number of placed surfactants, and (b) the interface is flat, stable. Finally, the conservative interaction parameters were varied to match the IFT of the oil-water-surfactant system at CMC.

It was demonstrated that with a short surfactant like SDS, the model can be validated easily by adjusting the interaction parameters to get the experimentally obtained IFT values. The number of surfactant beads is small enough to keep the interface stable. The ionic nature of surfactant can be captured by using higher head-head and lower head-water interaction parameters. Whereas, in the case of long molecule surfactants like C12E8, the molecule needs to be carefully constructed to

satisfy the above criteria. The angles between surfactant beads should be used to account for the steric effect of long molecule surfactants. In all cases, IFT increased linearly with the increase of a_{HW} and a_{TO}, and decreased with increasing $a_{HH,}$, while the value of a_{HO} did not appear to have a significant impact on IFT. The reason is that at the interface, most of the direct contacts between oil and water were altered by the interactions between head-water and oil-tail. Hence, the strengths of these interactions determine IFT.

The impact of using bonding and angle potential and the coefficients k_b and k_θ on IFT were also studied. Increasing k_b showed a negative effect while increasing k_θ expressed a positive effect on IFT. The explanation comes from the ability to stay fixed at the interface of surfactants. A high value of k_b helps to keep surfactant beads close together and reduces direct oil-water contact, while a high k_θ reduces the degrees of freedom of surfactant beads on the *xy* plane, leading to more space for oil-water interaction.

The plot of IFT vs surfactant concentration showed the feasibility of the proposed procedure. It indirectly implied the use of the Gibbs adsorption equation in our model. In addition, the plateau reached at concentrations larger than the CMC demonstrated that only the interfacial region contributed to IFT values. The plateau value for each surfactant matches the corresponding experimental data.

The model was developed for the coarse-grained level of 5 or 6 water molecules in one bead. However, the protocol for selecting DPD parameters can be applied for different levels of coarse-graining, as well as different simulation methods to get the correct parameters for the description of surfactants at oil-water interfaces.

Chapter 4. Surfactant-Adsorbed Carbon Nanotubes at the Oil-Water Interfaces

Abstract[†]

In this research, simulation results for using carbon nanotubes (CNTs) to deliver surfactants to an oil-water interface are reported. Two different surfactants were considered, the anionic sodium dodecyl sulfate (SDS) and the nonionic octaethylene glycol monododecyl ether (C12E8). The surfactants were first allowed to adsorb on the CNT surface in an aqueous environment. It was found that the capacities of SDS and C12E8 to adsorb on the CNT were 2.62 and 2.43 molecules/nm^2, respectively. The electrostatic effect of the anionic surfactant and the steric effect of the nonionic surfactant negatively affected the adsorption process. At the oil-water interface, the surfactant molecules quickly desorbed from the CNT to distribute at the interface, leading to the reduction of the oil-water interfacial tension. At low surfactant concentration, the CNT also remained at the interface, reducing further the interfacial tension. When the surfactant interfacial concentration reached the value corresponding to the bulk critical micelle concentration, the CNT was forced to migrate into the oil phase. These results suggest that carbon nanotubes, or other hydrophobic nanoparticles, can be good candidates for delivering surfactants for applications like enhanced oil recovery.

4.1. Introduction

Oil-water interfaces, their behavior, and stability are important for many technical applications with significant industrial, environmental, and economic impacts [1, 117, 118]. The interfacial tension (IFT) at the oil-water interface affects critically industrial separation processes, consumer product manufacturing, the treatment of wastewater, and the production of oil using tertiary oil

[†] Material in this chapter has been published in T.V. Vu, D.V. Papavassiliou, The Journal of Physical Chemistry C 122(48) (2018) 27734-27744.

recovery techniques, such as chemical flooding [1, 5]. Modification of the interface can lead to the generation of oil-in-water or water-in-oil suspensions with the use of surfactants,[5, 119] and/or nanoparticles [18, 120-122]. Surfactants and nanoparticles tend to stay at the oil-water interface. The driving force for both surfactant and nanoparticles to remain at the interface is the reduction of excess free energy (free energy is given as $G = \gamma . A$, [40, 123] where γ is the oil-water interfacial tension and A is the interfacial contact area of oil and water). The mechanism by which surfactants and nanoparticles reduce this free energy is different: surfactants lower the interfacial tension, while nanoparticles reduce the contact area. An oil-water system containing both nanoparticles and surfactants is expected to exhibit a more complicated behavior.

Reports on the effects of the presence of nanoparticles and surfactants on the oil-water interfacial behavior have been conflicting. Ranatunga et al. [40] found a synergistic effect of nanoparticles and non-ionic surfactants at the oil-water interface, in which nanoparticles reduced the oil-water IFT further than the surfactants alone. While several laboratory and simulation studies supported this observation,[41, 42] in other cases an increase in the IFT was observed as nanoparticles with surfactants were added to the oil-water interface [43-45]. Studies have also appeared reporting no effect [46, 47]. The explanation for such differences is based on the relative interactions between nanoparticle-surfactant and nanoparticle-ambient fluid. Increased IFT relative to the surfactant only case occurred when surfactant molecules were strongly adsorbed on the nanoparticle surface, which resulted in low surfactant concentration at the interface. The IFT decreased by the presence of nanoparticles when the particles stayed at the oil-water interface. In this case, the interfacial area that remained available to the surfactant molecules was smaller, making them appear more active. When the nanoparticles settled in either the oil or water phase, they had no effect on the oil-water IFT.

In most of the prior computational research, the surfactant molecules and the nanoparticles were placed at the oil-water interface separately. In this study, however, we investigate the behavior of surfactant-adsorbed-carbon nanotubes in the vicinity of oil-water interfaces and the resulting changes in the IFT. We observe the desorption process of surfactants from the carbon nanotube surface to distribute at the oil-water interface. This behavior has not been described in detail in prior reports. The observed phenomena are important in different applications, but the emphasis here is on enhanced oil recovery (EOR). A commonly used technique in EOR is chemical flooding, where a suspension of chemicals (most often surfactants) is injected into an oil reservoir to mobilize the oil trapped after primary oil recovery. The role of the surfactant is to reduce the oil-water IFT [124]. However, the loss of surfactants due to adsorption on the formation rocks can dramatically increase the operation cost of the process [79, 125]. Nanotechnology has recently been used in an attempt to overcome this obstacle. Neves Libório De Avila et al. [126] used crosslinked polystyrene nanoparticles as surfactant carriers by trapping surfactant molecules within the nanoparticle structures. When reaching the oil phase, the surfactants were released as the nanoparticles swelled. Chen et al. [127] reported experimental results for using carbonaceous nanoparticles as surfactant carriers. The idea was to provide an alternative surface for the surfactant adsorption, e.g., carbon nanotubes (CNT) or carbon black particles, before injecting them into an oil reservoir. The surfactants helped to stabilize the CNTs in an aqueous solution, while being adsorbed on the CNTs reduced the loss of surfactant molecules by adsorption on the rock surface. Indeed, they observed a reduction of surfactant adsorption on sand surface in the case of using carriers, compared to the case of injecting only surfactants. When in contact with the oil, the surfactants carried by the nanoparticles reduced the interfacial tension of oil-water to a value that was comparable to the case of surfactant-only solution.

The process of carrying surfactants to the oil-water interface using CNTs as vehicles happens in three stages: (1) adsorption of surfactant molecules on the CNTs to create surfactant-adsorbed-CNTs (SACs);[106, 128] (2) propagation of SACs to the oil-water interface; and (3) release of surfactant molecules from the CNTs to the oil-water interface. Here it is assumed that the second stage can be achieved so that we focus on the first and third stages. The simulation results presented herein provide insights into the mechanism of this process.

The first stage was studied to determine the capability of CNTs to carry surfactants and to determine what might be the maximum capacity. Studying the third stage, the feasibility of the idea was examined, i.e., whether surfactant molecules would leave the CNT surface to adsorb at the oil-water interface and to modify the interfacial properties. The contribution of this chapter, thus, is (a) to present the application of dissipative particle dynamics (DPD) simulations and an appropriate model for SACs in oil-water systems; (b) to investigate the adsorption of anionic and nonionic surfactants on CNTs and the maximum capacity of CNTs to transport surfactants; (c) to elucidate the behavior of SACs in water and then at the oil-water interface.

4.2. Simulation Details

Figure 4.1a is a schematic representation of each molecule in the simulation. The prescription of water, oil, surfactants, CNT molecules followed the discussion in chapter 3 and previous publications [69, 106, 128]. In short, n-heptadecane ($C_{17}H_{36}$) was used as oil. The CNT had a length of 20 nm and a diameter of 4 nm (aspect ratio = 5). The diameter corresponds to a multi-walled CNT. The carbon beads comprising the CNT were arranged to form a matrix with the nearest distance between two beads of 0.3 r_c. Two different surfactants were modeled: sodium dodecyl sulfate (SDS) and octaethylene glycol monododecyl ether (C12E8) as representative

anionic and nonionic surfactants, respectively. The choice of these surfactants was based on the availability of experimental data for their behavior at the water-heptadecane interface [103, 104].

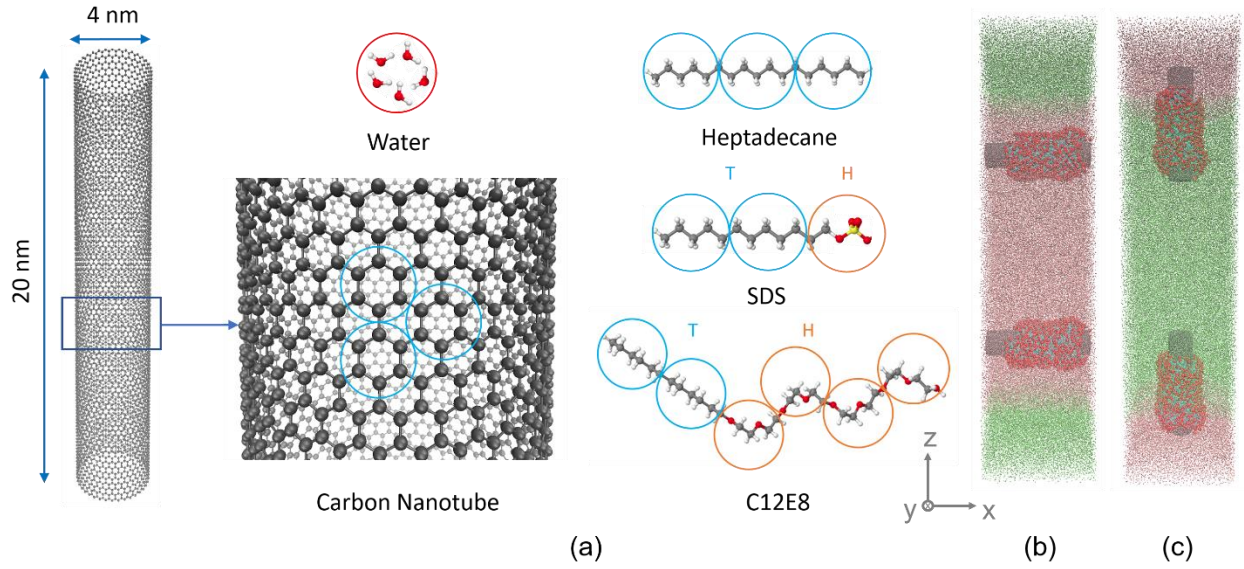

Figure 4.1. (a) Schematic configuration of CNT, water, heptadecane, SDS, and C12E8 surfactant molecules in the DPD simulation. A CNT bead is made up of six carbon molecules. An SDS molecule consists of one head (H) and two tail (T) beads, while a C12E8 molecule consists of two T and four H beads. White, gray, red, yellow spheres represent hydrogen, carbon, oxygen, and sulfur molecules, respectively. Simulation set up for behavior of surfactant-adsorbed-CNT in the water near oil-water interface (b), and at the interface (c). Surfactant head, tail, CNT, water, oil beads are shown in red, cyan, gray, pink, green, respectively.

The interaction parameters for water, oil, surfactant head and tail beads were determined based on careful validation of the DPD simulation results with experimental data, [69, 106, 128] and are listed in Table 4.1. The oil-water interaction parameters were determined using the IFT for a water-heptadecane system, the surfactant-water interaction parameters utilizing measurements of the surfactant micelle size, and the average number of molecules per micelle. The surfactant-oil parameters were determined based on the IFT of the oil-water interface with the presence of surfactant at concentrations equal to the CMC concentration. The remaining parameters between

the CNT beads and the other components were calculated based on the Flory-Huggins theory, as follows:[73]

$$\chi_{ij} \approx 0.689\left(a_{ij} - a_{ii}\right) \tag{4.1}$$

$$\chi_{ij} \approx \frac{V_b}{k_B T}\left(\delta_i - \delta_j\right)^2 \tag{4.2}$$

where χ_{ij} is the Flory-Huggins parameter, δ_i is the solubility parameter of component *i*, and V_b is the volume of one DPD bead. Using the solubility parameters obtained from Barton,[107] and Maiti[129] in Equations (4.1) and (4.2), the interaction parameters were computed to complete Table 4.1.

Table 4.1. Sets of repulsion parameters used in the simulations [a]

SDS						C12E8					
	H	T	W	O	CNT		H	T	W	O	CNT
H	20	42	10	54	35	H	15	25	15	25	30
T		15	54	12	15.5	T		15	54	14.5	15.5
W			15	90	60	W			15	100	60
O				15	15.5	O				15	15.5
CNT					15	CNT					15

[a] H and T represent the head and tail of surfactant, W, O, and CNT denote water, oil, and carbon nanotube beads, respectively. The parameters on the left and right are for simulations involving SDS and C12E8, respectively.

In all simulations, periodic boundary conditions were applied. For the adsorption of surfactants on CNT, the simulation box was 20 x 20 x 20 r_c^3. The interest of this study is focused on the adsorption of surfactants on the outer surface of the CNTs; thus, the CNT was considered as an infinitely

long, rigid cylinder for this simulation. The CNT was kept stationary in the center of the simulation box, with the axis of the CNT aligned with the *z*-direction of the box. Different concentrations of surfactants were used to investigate the adsorption isotherm and the morphology of the adsorbent on the CNT. The time-step was 0.02 for all simulations. Equilibrium was reached after $3x10^6$ time-steps for all cases. The system was considered to reach equilibrium when the number of surfactant molecules adsorbed stayed constant for $5x10^5$ time-steps. The simulations were conducted at 298K and 1 atm.

After equilibrium adsorption, the CNTs with different surfactant coverage (i.e., the SACs) were copied out of the simulation and placed in new simulation boxes to investigate their behavior in the vicinity of an oil-water interface. The setup for these simulations is seen in Figures 4b and 4c. The simulations were carried out for two different cases, where the SAC was placed in water or at the oil-water interface. The former situation is more likely to happen in a process such as the chemical flooding process, where a mixture of surfactants and oil is injected into an oil reservoir. Thus, it was investigated thoroughly in the present study. The latter case represents the situation where the SAC is forced to reach the interface by some disturbance. For the simulation of oil, water, CNT, and surfactant system, the computational box dimensions were 20 x 20 x 80 r_c^3. Because of the periodic boundary conditions in all directions, there exist two oil-water interfaces in the simulation box (as seen in Figures 4b and 4c). One SAC was placed in the vicinity of each interface, and the box was made large enough so that the behavior of each SAC was independent of the other. In this series of simulations, the CNTs were considered to be closed cylinders to avoid adsorption and desorption of surfactant inside the CNT, which is computationally time-consuming and not necessary for the present study. All simulations were carried out 3 times. The ensemble averages of the values were used for all the graphs.

Table 4.2. Simulation Conditions for the Adsorption of Surfactants on CNT

Surfactant	Concentration (mol/l)	Number of Surfactant Beads	Number of Water Beads
SDS	0.046	504	37976
	0.062	672	37808
	0.093	1008	37472
	0.124	1334	37136
	0.186	2016	36464
	0.221	2400	36080
	0.277	3000	35480
	0.332	3600	34880
C12E8	0.021	540	38110
	0.035	900	37750
	0.069	1800	36850
	0.111	2880	35770
	0.138	3600	35050
	0.166	4320	34330
	0.208	5400	33250
	0.277	7200	31450

As described in chapter 3, the maximum number of surfactant molecules that can be placed at the interface per area was determined from the Gibbs equation and was fixed for each surfactant. The size of the CNT was chosen so that at full coverage, the total number of surfactant molecules

adsorbed on the CNT surface did not exceed this maximum number. The purpose was to avoid the simulation of unrealistic systems, in which the interface was oversaturated with surfactant. All the simulations were carried out at constant number of beads, volume, and temperature conditions (similar to the NVT ensemble conditions). For the simulation of SAC near the oil-water interface, the system reached equilibrium after $5x10^5$ steps.

Table 4.3. Simulation Conditions for the Behavior of Surfactant-Adsorbed-CNT on the Vicinity of Oil-Water Interface

Surfactant		In Water		On Interface	
Number of Beads	Surfactant	Water	Oil	Water	Oil
SDS	1008	101947	54000	51004	104940
	1334	101611	54000	50668	104940
	2016	100939	54000	49996	104940
	2668	100267	54000	49324	104940
	3300	99655	54000	48712	104940
	4032	98923	54000	47980	104940
C12E8	1080	102220	54000	51280	104940
	1800	101500	54000	50560	104940
	3600	99700	54000	48760	104940
	5760	97540	54000	46600	104940
	7200	96100	54000	45160	104940

4.3. Results and Discussion

a. Adsorption of surfactant on CNT

The morphology of surfactants adsorbed on a CNT at different surfactant coverage is shown in Figure 4.2. In both anionic and nonionic surfactant cases, the adsorbed surfactants create ad-micelles at low concentration and cylindrical monolayers at higher coverages. As expected, the hydrophobic CNT surface attracts the hydrophobic part of the surfactant molecules, which adsorb on the CNT while their hydrophilic heads point towards the aqueous phase. The resulting particle (the surfactant-adsorbed-CNT, or SAC) with the surfactant heads pointing outside, thus, displays a hydrophilic character. In fact, the morphology of surfactant adsorption has been investigated in detail using DPD in earlier publications [106, 128, 130-132]. Here, we focus more on the adsorption capacity, since the CNT is considered as a vehicle to carry surfactant molecules to the oil-water interface. The higher the capacity of CNTs to adsorb surfactants, the more efficient the process will be. The amount of surfactants adsorbed was calculated by computing the distance between surfactant tails and the CNT surface. If the distance was less than the cut-off distance (r_c), the surfactant molecule would be considered as adsorbed.

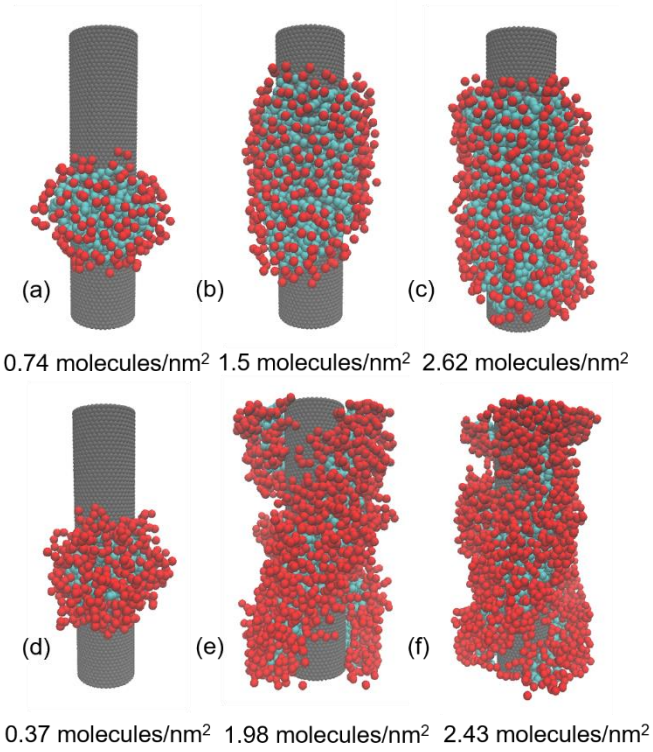

Figure 4.2. Morphology of surfactant adsorbed on CNT surface at different coverage. The top and bottom rows are displays of cases with SDS and C12E8 surfactant, respectively. The color codes are the same as in Figure 4.1.

The process of surfactant adsorption on CNT can be described as follows. The tails of surfactants are attracted to the CNT surface since the CNT surface is also hydrophobic. The adsorbed surfactant molecules then accumulate into a cluster to minimize the number of surfactant tails that are in contact with water, as can be seen in Figures 4.2a and 4.2d. The adsorption isotherms of SDS and C12E8 surfactant on CNT are seen in Figure 4.3. Initially, the adsorption increases with the surfactant concentration in the solution. The curve reaches a plateau at high concentrations, which represents the saturation of the adsorbed surfactant on the CNT. The explanation is that at lower CNT coverage, the CNT surface is still free. Thus, the surfactant can migrate from the aqueous phase to it relatively easily. As the CNT surface is covered, it becomes more difficult for the free surfactant molecules to reach the CNT. Moreover, the interactions between the tail of a

suspended surfactant molecule and the heads of the surfactant molecules that already partially cover the CNT repel the free surfactant and prevent it from coming too close to the CNT. These free surfactants then tend to aggregate and form micelles. The maximum coverage on CNT of SDS and C12E8 was found to be 2.62 and 2.43 molecules/nm^2, respectively. These values are in the range of surface density calculated from experiments,[127] and simulations [130, 131, 133]. With the bigger size of C12E8 (its molecule consists of 6 DPD beads with a molecular weight of 538.75, instead of 3 beads for SDS with a molecular weight of 288.32), one would expect the surface density of SDS to be higher than C12E8. However, the electrostatic interaction between SDS heads hinders their adsorption on the CNT. The heads do not like to be in contact with each other, since they have the same charge. Consequently, the number of surfactants adsorbed on the CNT reduces. In addition, there are only two tail beads in C12E8 molecules, which is similar to SDS. Thus, the comparable surface density of adsorption between two surfactants suggests that the steric effect created by the four heads of C12E8 has a similar influence as the electrostatic effect from the SDS head.

The determination of the maximum coverage of SDS and C12E8 leads to suggestions for the choice of surfactants in actual applications. To apply in EOR, a surfactant should be able to lower the oil-water IFT to 10^{-3}-10^{-2} mN/m [134, 135]. For higher adsorption capacity, short-molecule surfactants are preferable. With the long-molecule surfactants, those with short tails should be preferred for higher loading on CNT. In addition, non-ionic surfactants are more desirable since they do not have electrostatic repulsion between the heads. Finally, the straight-molecule surfactants are more suitable than branch-molecule ones because of the lower steric effect.

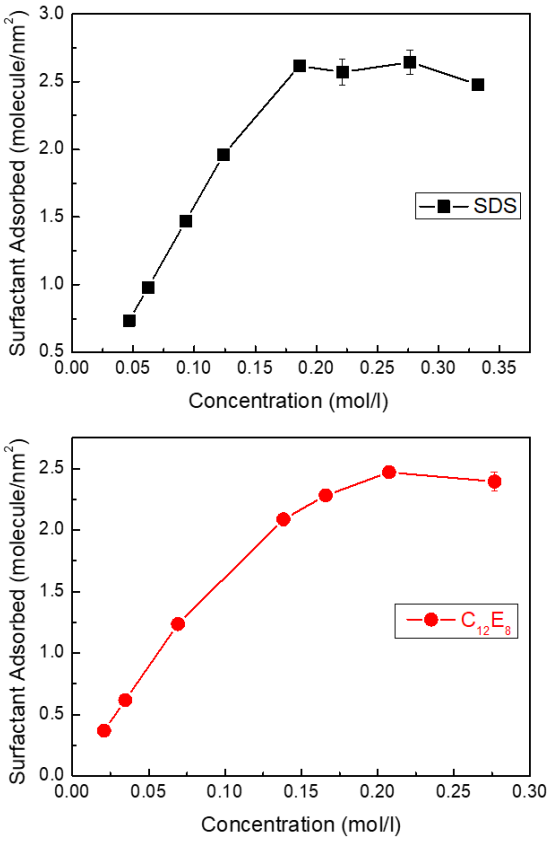

Figure 4.3. Adsorption isotherms of SDS (top panel) and C12E8 surfactants (bottom panel) on CNT. The error bars represent the standard deviation using 3 different simulations. In most cases, the error bars are smaller than the symbols.

b. Behavior of Surfactant-Adsorbed-CNT in Water near Oil-Water Interface

The feasibility of the whole process depends on whether surfactant molecules desorb from the CNT at the oil-water interface, given that their adsorption on the CNT and transportation of the SAC to the water-oil interface can be accomplished. The simulation conditions are shown in Table 4.3. The range of surfactant coverage on the CNT was 0.74 – 2.62 molecules/nm^2 for SDS and 0.37 – 2.43 molecules/nm^2 for C12E8.

The time-evolution of the interfacial system when a SAC approached the oil-water interface from the water phase is shown in Figure 4.4. The CNT dimensions were chosen so that the maximum

coverage of CNT is also the maximum concentration of surfactant that can saturate the oil-water interface. In both cases of anionic and nonionic surfactants, once the SAC reached the interface, surfactants started to desorb from the CNT and distribute at the interface. At the end of the process, all the surfactant molecules were at the interface, while the CNT migrated into the oil phase.

The physical mechanism for this process is as follows: in a SAC system, the CNT is covered by surfactant molecules with the tails on the CNT surface and the heads pointing outward. This turns a hydrophobic CNT into a hydrophilic SAC, which stabilizes CNTs in an aqueous solution.[136-138] Because of the repulsive interactions between the surfactant heads and the oil at the interface, the surfactant heads are pushed away by the oil, leaving space for oil-tail interaction. Due to the attraction between oil-tail, the surfactant molecules desorb from the CNT surface. The surfactant molecules then naturally accumulate at the oil-water interface, thanks to their amphiphilic characteristics. The hydrophobicity of the CNT also plays an important role in the whole process. The CNT is forced to go to the oil phase, while surfactant molecules stay at the interface, thus the desorption process is accelerated. As the CNT moves through the interface from the water to the oil phase, it is "stripped" of the adsorbed surfactant molecules and as it is stripped, it moves through the interface faster. The desorption process is quite similar between different morphologies formed by surfactants on the CNT.

It is noteworthy that the release of surfactant from the CNT to the interface occurred very quickly, in just a few nanoseconds. Meanwhile, it has been reported in the experimental study by Chen et al. [127] that equilibrium can be reached after 2 hours, which is significantly longer than the simulation results. From our simulation results, we speculate that in the study of Chen et al. the majority of the time was needed for the diffusion of the SACs through the water to the oil-water interface. Without an external disturbance, the SAC is expected to diffuse slowly based on its

bulky structure, which results in long diffusion times. In addition, as the SAC is considered hydrophilic, its preferred location is to be suspended in the water phase. Thus, it moves with random Brownian diffusion until it reaches the interface. This was confirmed by the simulations, where the time to reach equilibrium depended highly on the initial distance between the SAC and the interface. In some cases, the equilibrium could not be reached within the simulation time range of $2x10^6$ steps if the distance were too large, even though the length of the simulation box was just 80 r_c. Based on the simulation results, we have shown that the process happens almost instantaneously, and the time for diffusion of the SACs makes up the time for the system to reach equilibrium. There was no desorption of surfactant from the CNT to the water. Thus, it can be concluded that without exterior intervention, the desorption of surfactant from the CNT only occurs at the oil-water interface, i.e., CNTs can be good candidates as surfactant carriers from an aqueous suspension to the oil-water interface.

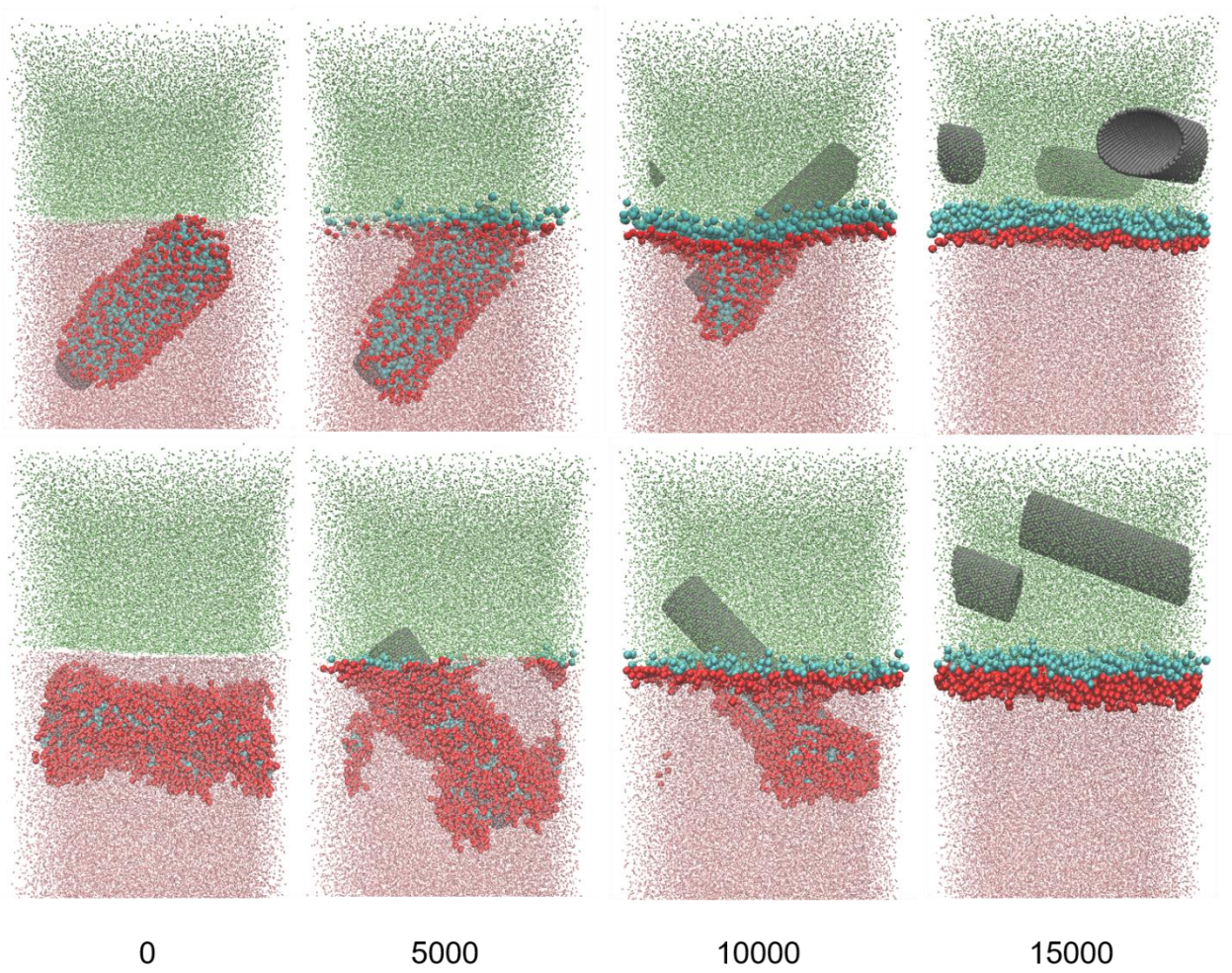

Figure 4.4. Time-evolution of the desorption process of surfactant from CNT surface to the oil-water interface. Time 0 corresponds to the instant when SAC reaches the interface. The whole process takes 15000 time-steps. The top and bottom rows show cases of SDS and C12E8, respectively. The color scheme is used as in Figure 4.1.

In Figure 4.5, the change of the oil-water interfacial tension during the process is seen, as it corresponds to the configuration of the CNT and the surfactant at different stages of the desorption process. Note here that the difference in time to reach equilibrium, which is indicated by the lowest value of IFT on the graph, does not show that either one of the surfactants reaches equilibrium faster. It is just a matter of chance for a SAC to reach the interface during the simulation; hence, the rate of the process could vary for the same type of surfactant. When SACs are still in the water

phase, the IFT has the same value as the oil-water IFT, which is 53.2 mN/m [103]. This is understandable since all the surface-active-agents are not at the interface and they do not have any impact on the IFT. In this case, the interface is basically a pure oil-water interface. During the transitional state, which appears at around time-step 75,000 and 120,000 for C12E8 and SDS, respectively, the IFT decreases dramatically from the oil-water IFT values to the IFT expected when the corresponding surfactants are at the critical micelle concentration (CMC). The transitional state is associated with the process of releasing the surfactant from the CNT to the interface, as seen in Figure 4.4. During the transitional state, surfactant molecules gradually desorb from the CNT and align themselves at the oil-water interface. The presence of surfactant at the interface reduces the IFT. As time progresses, all the surfactants are distributed at the interface. As has already been noted, the amount of surfactant used in this simulation was determined to be equal to the maximum amount that can potentially be placed at the interface. Therefore, if all surfactant molecules were desorbed and migrated to the interface, it would be saturated with surfactant. Indeed, at equilibrium, all the interface was covered by surfactants, leaving no space for the CNT. Consequently, the CNT migrated into the oil phase, and thus, it did not have any effect on the interfacial properties. This helps to explain the comparable values of IFT at equilibrium to the value of the IFT at CMC of the corresponding surfactants.

One might argue that the simulation results conflict with previous reports on the effect of CNT and surfactant on the oil-water IFT [138-140]. In most of those studies, the presence of CNT weakened the effect of surfactant at the interface. The reason is that surfactants were adsorbed on CNT to stabilize the CNT in water, leaving less surfactant than the CMC at the interface. We also observed higher IFT when the surfactants were still adsorbed on the CNT, which can be seen in Figure 4.6. However, once reaching the interface, all the surfactants were released leading to

maximum effect. The simulation results are thus not against the experiment data; in fact, they provide insights into the actual process and interpret the experimental findings based on the physical mechanism of the process. The experimental reports correspond to the cases where some surfactant molecules are still on the CNT, thus they have not reached equilibrium. As explained above, the time needed for the system to reach equilibrium depends on the diffusion time of SAC from water to the interface. In reality, other factors also hinder the transport of SAC. For example, the CNTs that are not fully covered by SDS might bundle up to create bigger particles, which have even lower diffusivity coefficients. These particles need longer times to move to the interface, resulting in longer times required for the system to reach equilibrium. In the simulation, we only used one SAC particle for one interface; hence, it is close to the ideal case. The equilibrium reached here also corresponds to the equilibrium of the ideal case in a real system. In conclusion, after desorption of all surfactant molecules, the IFT of the oil-water interface reached the value at CMC, which is the lowest value for a particular surfactant. At this maximum coverage, CNT is present in the oil phase and does not affect the interfacial properties.

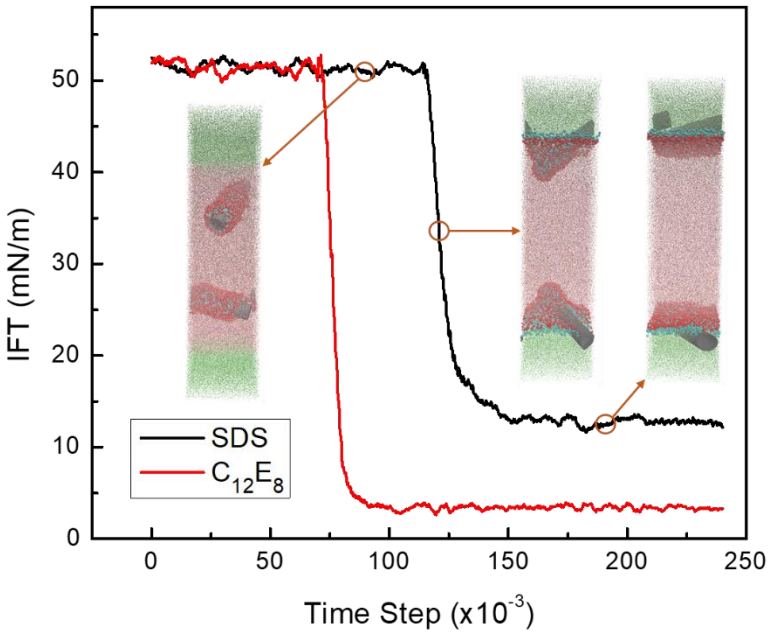

Figure 4.5. Change of oil-water interfacial tension as time progresses. The snapshots show the different stages of the system with SDS surfactant. The color scheme is that of Figure 4.1.

The discussion above is appropriate for the case where the surfactant concentrations were high enough to saturate the oil-water interface. However, this does not necessarily happen in a real system, since there are cases where a CNT might not be fully covered by surfactants, or where a small SAC particle reaches a large oil-water interface. To investigate those conditions, simulations of the effect of different coverage of surfactants at the interface along with CNT were performed.

In Figure 4.6, we show the structures and density profiles at the equilibrium of regions around interfaces for different interfacial concentrations of surfactant. The first and second rows of Figure 4.6 indicate that at surfactant concentration lower than the surface concentration at CMC, the CNT co-exists at the interface with surfactant. The reason is that the CNT-oil attraction is similar to the one between oil-tail, and the surfactants prefer to be at the interface. As the interfacial concentration of surfactant increases, the CNT is pushed farther into the oil phase. This trend can

be seen clearly in the second row of Figure 4.6. On this row, snapshots are shown that are perpendicular to the interface with only the surfactant tails presented. The footprint of the CNT at the interface is represented by the blank areas of these snapshots. The footprint is reduced with increasing surfactant interfacial concentration. Since the surfactant has a higher tendency of being at the interface than the CNT does, adding more surfactant molecules forces the CNT into the oil phase. The third row of Figure 4.6 is the density profile of the system near the interface. At lower surfactant concentrations, the positions of CNT and surfactants overlap, indicating that they both appear at the interface. From left to right, their relative positions move away from each other, meaning that the CNT shifts into the oil phase. Moreover, there are two sharp peaks of the CNT profile in Figures 4.6i and 4.6j. These peaks indicate the positions of CNT boundaries. They appear because the CNT is aligned along with the interface, which can be observed in Figures 4.6a and 4.6b. Increasing surfactant concentration results in the broadening of these two peaks, and finally, they merge into one peak at excess concentration, as seen in Figure 4.6l. The transition can be explained considering that at higher surfactant concentration the CNT is in the oil phase, where it no longer aligns to the interface. Since it is free to move in the oil phase, its density is more evenly distributed than when it is at the interface. In Figures 4.6k and 4.6l, there are dips in the oil density profile. They are related to the presence of the CNT in the oil phase. Because CNT is described as a hollow, closed cylinder, molecules of water, oil, and surfactant cannot get inside, creating the unoccupied space inside the liquid phase. Consequently, there appears a depression in the density of the liquid at that location. This phenomenon has also been described in previous reports on simulations with solid particles [40, 141].

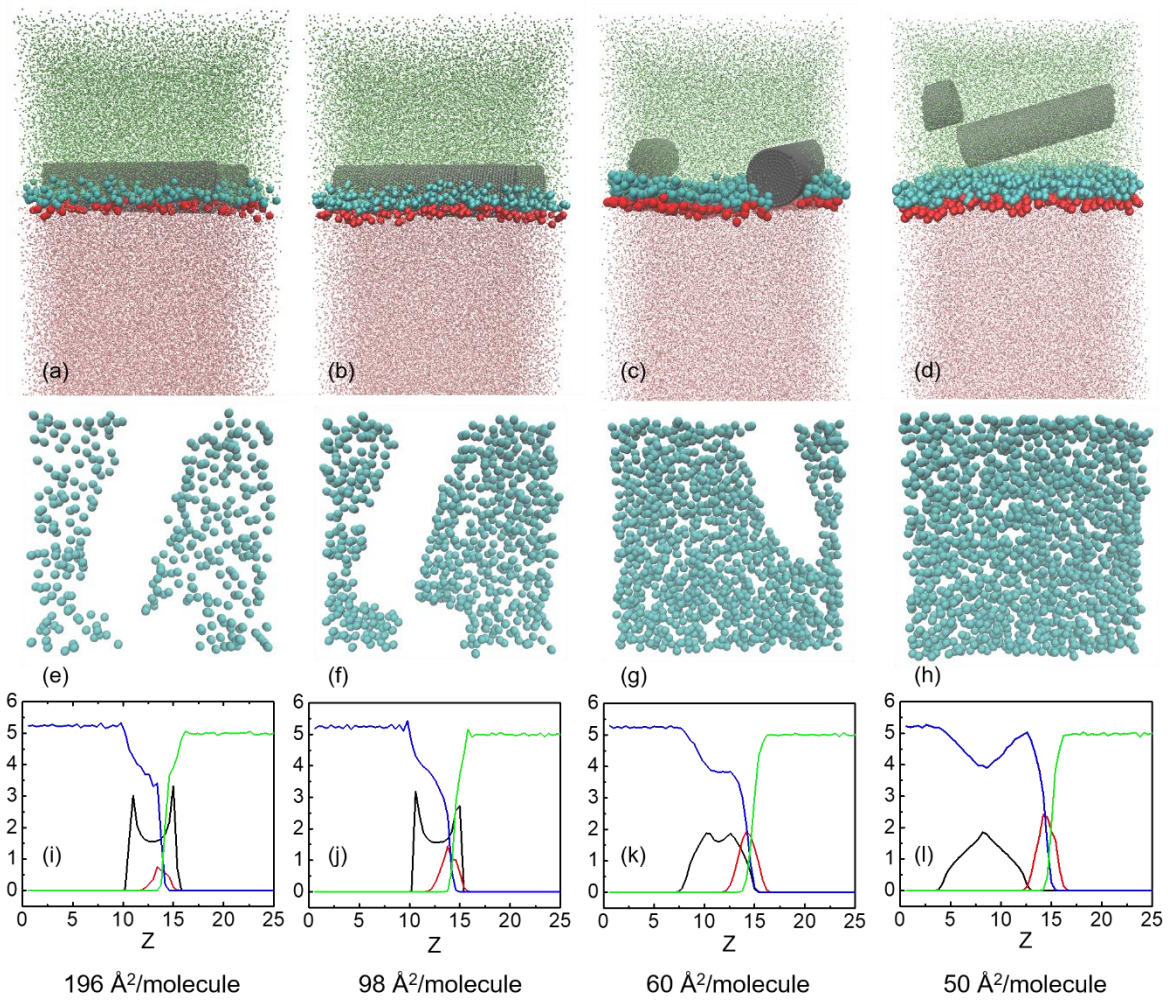

Figure 4.6. (a-h) Snapshots of oil-water interface with CNT, surfactant at different SDS concentrations, (i-l) density profile at the region near oil-water interface. The first and second rows show the top and side views of the interface, respectively. The color code is similar to Figure 4.1. For the density profiles in the third row, blue, green, black, and red lines represent oil, water, CNT, and surfactant density, respectively.

The dependence of IFT on the interfacial concentration of surfactant with and without the presence of a CNT is shown in Figure 4.7. The black line illustrates the cases where the SAC was released at the oil-water interface, which will be discussed in the next section. The *x*-axis represents the interfacial area occupied by one surfactant molecule, which is inversely proportional to the surfactant interfacial concentration. Without CNT, the graphs describe the typical systems of oil-water-surfactant. At very dilute surfactant interfacial concentration, on the right of the graphs, the

IFT values are calculated as 53.0 and 52.6 mN/m for SDS and C12E8. At the CMCs, corresponding to the area of 49.1 $Å^2$ per SDS molecule and 62.0 $Å^2$ per C12E8 molecule, the IFT is 11.8 and 3.6 mN/m, respectively. The results indicate a good match between the simulation and experimental data of 53.2 mN/m for heptadecane-oil IFT, as well as reported IFT values of 11.2 and 3.4 mN/m at CMCs of SDS and C12E8, respectively [103, 104].

The effects of CNT on the IFTs are quite similar for both the anionic and nonionic surfactants. At low surfactant concentration, the presence of the CNT does not have much influence on the IFT. Since there are few surfactant molecules, the interface can be considered to have only CNTs along with oil-water. It is a well-known fact that the nanoparticles themselves do not remarkably affect IFT, especially at low coverage [142-145]. This helps to explain the overlap of the two curves at low concentrations seen in Figure 4.7. As surfactant concentration increases (see Figure 4.7, where concentration increases from right to left), the IFT decreases for both cases. However, the presence of the CNT reduces the IFT in comparison to the case of only surfactants. This observation was also presented in Ranatunga et al.[40], where non-charged nanoparticles reduced the interfacial tension of oil-water systems with non-ionic surfactants. The explanation was that the nanoparticles occupied a specific area at the interface, leaving less space for the surfactants, i.e., the surfactants were concentrated. Consequently, the *effective* concentration of surfactants increased, making them more active at the interface. We found that the argument can also be applied herein. The impact of the CNT on the reduction of the IFT was significant at surfactant concentrations from 1.02 to 1.66 molecules/nm^2 (98.3 to 60.0 $Å^2$ per SDS). In this concentration range, the CNT was aligned right at the interface, which can be seen in Figure 4.6, to occupy the maximum interfacial area possible. When the surfactant concentration approached the concentration at CMC, the effect of CNT on IFT decreases. At CMC concentration, the IFT values are comparable between the two

cases. This is attributed to the fact that CNT is gradually pushed into the oil phase. The footprint of the CNT at the interface is reduced, which in turn lowers the effectiveness of the surfactant at the interface.

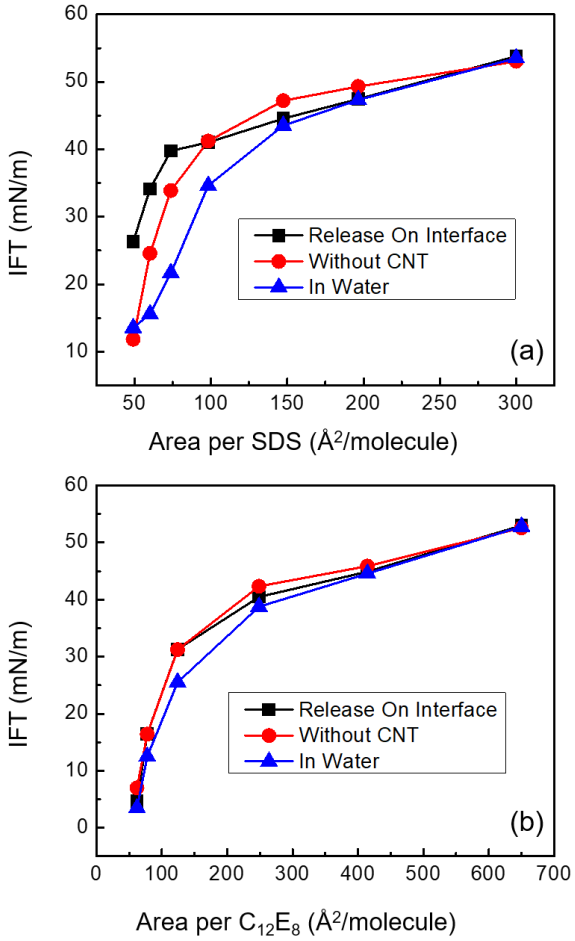

Figure 4.7. Interfacial tension of oil-water at different surfactant interfacial concentrations when releasing SAC in water, at the interface, and with surfactant only. Panels (a), (b) show the cases of SDS, C12E8, respectively. The error bars are not shown to give a clear view of the trends. The maximum error is 4.84%.

c. Behavior of Surfactant-Adsorbed-CNT at the oil-water interface

The simulation results when SACs with different levels of surfactant coverage were placed right at the interface of oil-water are shown in Figure 4.8. The initial configuration for those simulations

can be seen in Figure 4.1c. In all cases, the surfactants in water desorb from the CNT to the interface, similar to the simulations discussed in the previous section. However, the surfactants which are in the oil phase are desorbed from the CNT to create reverse-micelles in oil. We call them reverse-micelles because their structure, with the hydrophilic heads inside the micelle and the hydrophobic tails facing outward, is reversed relative to normal micelles in water. Some of the reverse-micelles were still adsorbed on the CNT since their tails are attracted to both the CNT surface and the oil. The reason for this phenomenon is that the SAC is not at a stable state when it resides in the oil phase because of the hydrophobicity of the CNT. The surfactant tails prefer to be in contact with oil, while the heads do not. Thus, surfactants naturally desorb from the CNT to create reverse-micelles – the structure that both the head and tail desire. Because of the formation of reverse-micelles, the surfactant concentration at the interface decreases. Consequently, the oil-water IFT is expected to increase, as can be seen in Figure 4.7. IFT values are higher for most of the surfactant concentrations, especially at CMC concentration. In this case, most of the surfactant molecules are in micelles in the oil phase, resulting in significant changes in IFT.

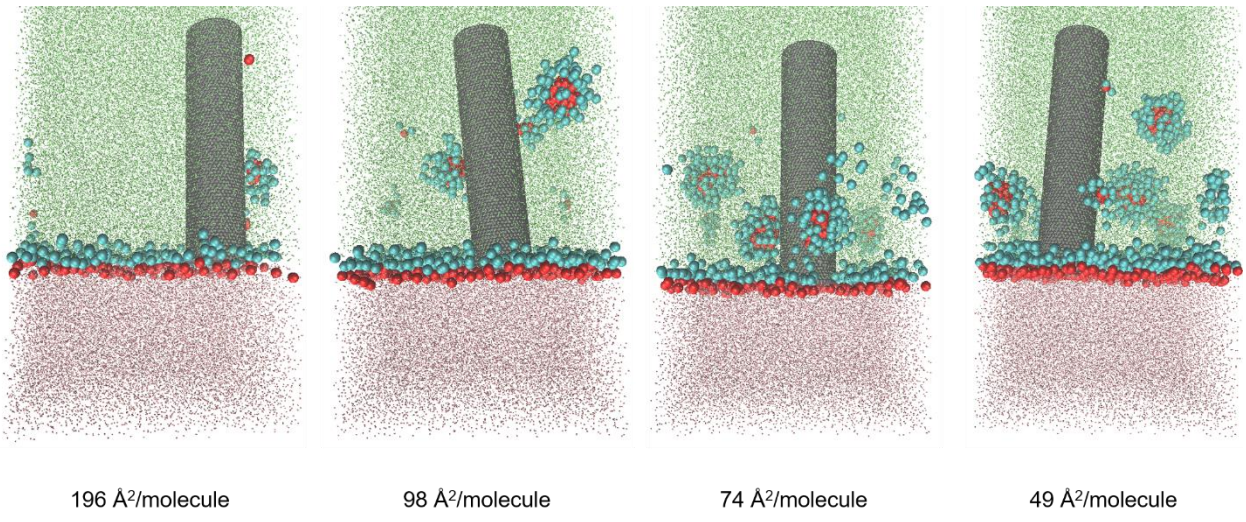

Figure 4.8. Snapshots of the oil-water interface at different SDS surfactant interfacial concentrations when releasing SAC at the interface. The color code is similar to Figure 4.1.

4.4. Conclusions

Dissipative particle dynamics simulations were employed to model surfactant and CNT systems at the oil-water interface. The feasibility of using CNTs as vehicles to carry surfactant molecules to the oil-water interface was explored by studying the behavior of the surfactant-adsorbed-carbon nanotube at the interface in detail. It was found that once the surfactant-adsorbed-CNTs arrive at the oil-water interface, all the surfactant molecules desorb from the CNTs and distribute at the interface, leading to a reduction of the oil-water IFT to values observed at the critical micelle concentration (CMC) of the corresponding surfactants. Both ionic and anionic surfactants were tested. When the system had not reached equilibrium, all the surfactants were on the CNT interface, so that the IFT was the same as the IFT for an oil-water interface. At equilibrium, the contribution of the CNTs on the reduction of IFT depended on the surfactant interfacial concentration. At low concentration, CNTs stayed at the interface, reducing the IFT further than for a system with only surfactant. Increasing surfactant concentration resulted in the gradual push of the CNT into the oil phase from the interface. When the surfactant concentration was high enough, the CNT migrated into the oil phase, and the IFT was not affected.

These findings confirm that it is possible to use CNTs to carry surfactant molecules to the oil-water interface while providing directions to design such systems. There is a maximum amount of surfactant that can be carried for a specific surface area of CNT, and this is determined by the steric repulsion effects of adsorbed non-ionic surfactants and the electrostatic effect of ionic surfactants. Surfactants with smaller hydrophobic tails would be more effective since short tails are more conducive for higher loading of the CNTs. Furthermore, nonionic surfactants are preferred to ionic surfactants of the same size since the electrostatic effect of ionic surfactants hinders their adsorption. The effective oil-water interfacial area available to be covered by the

surfactants is the most important parameter that determines whether the presence of CNTs will modify the IFT. Finally, the diffusion and propagation of the SACs towards the interface can be the time-controlling step in this process since desorption of surfactants from the CNTs occurs relatively fast.

Chapter 5. Synergistic Effects of Surfactants and Nanoparticles at Oil-Water Interface

Abstract[‡]

Nanoparticles (NPs) can reduce the interfacial tension (IFT) of the oil-water system containing surfactants by reducing the interfacial area available to surfactants. The ability to reduce the IFT when surfactants are present in addition to NPs depends on the localization of the NPs at the interface, which is related to the nature of the NPs and the interaction between NPs and surfactant molecules. Using DPD, heterogeneous NPs with different properties and interface coverage were placed at the interface with various surfactant concentrations. The IFT and the surfactant density profiles across the interface were analyzed. It was found that at constant surfactant concentration, adding NPs reduced the IFT; while with the absence of surfactant, NPs expressed no effect on the IFT. Among different types of heterogeneous NPs, the most effective were those that maximized their footprint at the interface, reducing thus the interfacial area available to surfactants. The interactions of the NPs with the surfactant molecules determined exactly which pattern of heterogeneity was most favorable. Based on these results, suggestions for designing NPs for maximum synergistic effects with surfactants were formulated.

5.1. Introduction

Emulsions of oil and water are critical in different applications such as oil recovery [5], food processing [1], drug delivery [6], and catalysis [122]. The emulsions are generally stabilized by emulsifiers, which can be surfactants or nanoparticles. The ability of emulsifiers to stabilize emulsions is due to their natural tendency to remain at the oil-water interface, and consequently modify the interfacial properties. Surfactants stabilize the oil-water emulsions by reducing

[‡] Material in this chapter has been published in T.V. Vu, D.V. Papavassiliou, Journal of Colloid and Interface Science 553 (2019) 50-58.

interfacial tension (IFT) [1, 117, 118], and research on the behavior of surfactants at the oil-water interface has been active for several decades [146-148]. The lower the IFT, the more stable the emulsion is. Nanoparticles (NPs) have also been used in stabilizing emulsions [17, 18]. In most of the previous reports, adding NPs, such as silica or zirconia, has no effect on the IFT of oil-water interfaces, like decane-water [142, 144, 149], or trichloroethylene-water [42].

The co-existence of surfactants and NPs at the oil-water interface is expected to show more complex behavior than when either surfactants or nanoparticles are at the interface on their own. Additional interactions among them can impact the IFT and play a role in applications as diverse as detergency, food preparation [1, 117], and enhanced oil recovery, where NPs are proposed to be used to carry surfactants through an oil reservoir, as well as to further stabilize oil-water emulsions [127, 150-152]. Ranatunga et al. [40], found that nanoparticles reduce the oil-water IFT further than surfactants alone. Wang et al. [50], showed that adding oppositely charged particles decreases the IFT of the water and hexadecane solution containing ionic surfactants. In addition, silica NPs also exhibited a synergistic effect in reducing the IFT of an oil-water interface containing sodium dodecylsulfate surfactant (SDS) [42, 51]. There are also instances where adding NPs had no effect on the oil-water IFT. For example, Luo et al. [153], reported that hydrocarbon NPs did not affect the IFT of the trichloroethylene-water interface with SDS. Studies have also reported an increase of the IFT when NPs and surfactants were present at the oil-water interface as compared to surfactants alone [43, 44, 154]. In a recent study [150], we demonstrated that Carbon nanotubes (CNTs) could affect the IFT of an oil-water system containing surfactants in different ways, and the effect depended on the way CNTs and surfactants were configured in the system.

In previous reports, mostly because of NP fabrication difficulties, there were no comparisons of different types of NPs in the same system to explore the particle properties that contribute crucially to the combined effect of surfactants and NPs. It is challenging to manufacture a range of NPs having almost the same properties, but changing only one characteristic (e.g., tune hydrophobicity, size, shape, etc. systematically). In computations, however, the simulation of NPs with any choice of different properties is possible, which enables a wide range of investigations that could be difficult to conduct experimentally. In this work, we present a comprehensive study to compare the combined effect of different types of NPs in conjunction with surfactants at the interface of oil and water using dissipative particle dynamics (DPD) simulation methods. Homogeneous and heterogeneous NPs were examined. It should be noted however that the adsorption of surfactants on NPs was not considered, since the focus herein is on their behavior on surfactant and NP behavior at the oil-water interface.

After examining the effect of surfactants and NPs separately on the IFT of oil-water systems, this study aims to reveal the mechanism through which different types of heterogeneous NPs can stabilize the oil-water emulsion along with surfactants. The emulsion is considered more stable when its IFT becomes lower. Understanding this mechanism allows suggestions for designing NPs that can stabilize oil-water emulsions in the most effective way. Thus, the contributions of this study are (a) to present the computational protocol for simulating such systems, (b) to explore the mechanism through which the synergistic effect of surfactants and NPs affect the IFT, and (c) to determine the key properties of NPs that contribute to emulsion stability.

5.2. Simulation Details

Heptadecane ($C_{17}H_{36}$) was used to represent oil, and each molecule consisted of three oil beads connected by 2 harmonic bonds. Sodium dodecylsulfate (SDS) was chosen to represent

surfactants, which contained one head and two tail beads. This choice allowed the construction of models that can be validated by experimental data [69, 73, 100, 103, 155]. In the simulations, all the NPs were spherical particles with diameters of 4 r_c. The NP beads were arranged so that the distance between two neighboring beads was 0.3 r_c, in order to avoid any penetration of solvent beads into the NPs [106, 128]. Different types of NPs were used. The general notation adopted herein for designating different types of NPs is *"*A *x-y", *where A could be an amphiphilic Janus particle designated as JP, or A could be a particle with a surface of heterogeneous wettability designated as H. A Janus particle (A ≡ JP) was one in which the two sides of the NP had different hydrophilicities. In heterogeneous nanoparticles (A ≡ H), the hydrophobic and hydrophilic beads were randomly distributed on the particle surface. The pair *x-y* represents the percentage of hydrophobic and hydrophilic beads on the NP surface. The hydrophobic over hydrophilic percentages were 0-100, 25-75, 50-50, 75-25, 100-0. For instance, JP 25-75 denotes a Janus particle with 25% hydrophobic beads and 75% hydrophilic beads on its surface (see Figure 5.1a). We labeled the homogeneous hydrophobic and hydrophilic NPs as 100-0 and 0-100, respectively, since there was only one type of beads on the surface of these NPs. The surfactants and NPs were placed randomly in both position and orientation at the oil-water interface. The representation of each molecule in our simulation is shown in Figure 5.1.

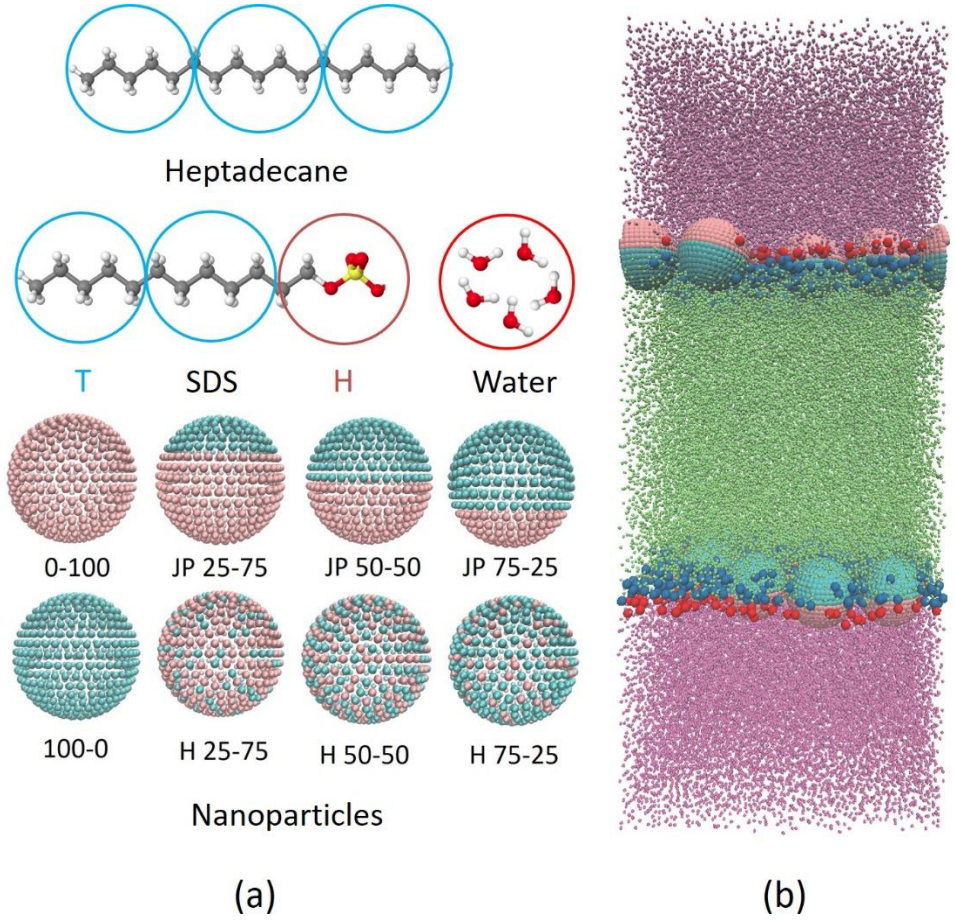

Figure 5.1. (a) Representation of the molecules used in the DPD simulation. Hydrogen, carbon, oxygen, and sulfur atoms are represented as white, gray, red, yellow spheres, respectively. (b) Simulation set up of surfactants and NPs at the oil-water interface. Surfactant head, tail, water, oil, NP hydrophilic, and hydrophobic beads are expressed in red, blue, purple, green, pink, cyan, respectively.

For different beads in our simulation systems, the repulsion parameter used is listed in Table 5.1. The parameters for water, oil, surfactant head, and tail beads were adopted from our previous studies [69, 150]. The NP beads were simplified as hydrophobic and hydrophilic beads; thus, their behavior was chosen to be consistent with the model parameters of surfactant tail and water, respectively.

Table 5.1. Pair-wise interaction parameters used in the simulations. (H stands for the surfactant head beads, T for the surfactant tail beads, W and O for water and oil, respectively, and Pho and Phi represent hydrophobic and hydrophilic beads on the surface of the NPs.)

	H	**T**	**W**	**O**	**Pho**	**Phi**
H	20	42	10	54	54	15
T		15	54	12	15	54
W			15	90	54	15
O				15	15	54
Pho					15	54
Phi						15

The simulation setup is shown in Figure 5.1b. The simulation box was 20 x 20 x 50 in DPD dimensionless units with periodic boundary conditions in all directions; thus, there are two oil-water interfaces as seen in Figure 5.1b. Following previous reports [69, 142, 144], surfactants and NPs were placed at the oil-water interface to save computational time. The NP coverage (i.e., the percent of the interfacial area covered by NPs) was varied from 0 – 37% of the oil-water interface. In earlier research [69], it has been shown that the interfacial concentration of surfactant reaches the maximum at critical micelle concentration (CMC). This maximum value depends on the temperature, type of oil, and surfactant. At 25^{o}C, the maximum concentration of SDS at the interface of n-heptadecane and water is 1.96 molecule/nm^2 [103]. Therefore, the surfactant interfacial concentrations in our study were kept at less than 1.96 molecule/nm^2.

The NVT ensemble (constant number of beads, volume, temperature) was applied in all the simulations. Because the number density of beads on NPs is different from that in liquid, when

changing NP coverage at the oil-water interface, the total number of beads in the simulation box changes. Consequently, when the volume of the simulation box is fixed, the system pressure will change, even though the number density of the liquid is maintained at 5. Therefore, the Berendsen barostat [156] was applied to the system to determine the effect of adjusting NP coverage on interfacial tension. The role of the Berendsen barostat was to automatically adjust the simulation box to keep the pressure constant. In all simulations, equilibrium would be reached after 5 x 10^5 time-steps. Thus, the duration of the simulation runs was set at 1 x 10^6 time-steps, which corresponds to 5.5 μs in real unit.

5.3. Results and Discussion

a. Effects of Surfactants and NPs when Present at the oil-water interface Individually

First, the effects of NPs and surfactants on the oil-water IFT were investigated. Figure 5.2 is the plot of the oil-water IFT as a function of surfactant and NP coverage. The NP coverage was calculated as $c = n\pi R^2/S$, where n is the total number of NPs at the interface, R is the NP radius, and S is the interfacial area between oil and water. In Figure 5.2a, as the *x*-axis increases, the area available to one surfactant molecule increases (i.e., the surfactant interfacial concentration decreases). The inset in Figure 5.2a is the plot of IFT with the abscissa as the SDS interfacial concentration. The surfactant concentration range was between 8 nm^2/molecule (almost no surfactant) and 0.49 nm^2/molecule (corresponding to the interfacial concentration of surfactant at the critical micelle concentration, CMC, of SDS [103]). The pure oil-water mixture exhibits the IFT of 51.3 mN/m, which is comparable to measured experimental data for heptadecane-water [103]. Increasing surfactant concentration leads to the decrease of the IFT. At the interfacial concentration of 0.49 nm^2/molecule, the oil-water IFT reaches 12.2 mN/m, which is the value of oil-water IFT at CMC with SDS surfactant [103]. The observed trend agrees with the expected

behavior of oil-water IFT in the presence of surfactants [103, 157, 158]. With NPs, some previous studies both with experiments and simulations have reported that the presence of NPs at the oil-water interface does not reduce the IFT [143, 145, 159]. This is confirmed in our study, as can be seen in Figure 5.2b. For a clear view, only the plot with JP 50-50 is presented, since the same trend was observed with all types of NPs. When increasing the NP coverage of the interface from 0 to 37.5%, the IFT stays unchanged at a value close to pure oil-water IFT.

The explanation for the different behavior of surfactants and NPs could be found by distinguishing the driving forces for their positionings at the oil-water interface. Their presence at the interface helps reduce the excess free energy, which is given as [40, 123],

$$G = \gamma . S \tag{5.1}$$

where γ is the oil-water interfacial tension and S is the interfacial contact area of oil and water. Surfactants and NPs modify the free energy by different mechanisms: surfactants lower the IFT, while NPs reduce the contact area. The distinct behaviors of surfactants and NPs observed in this study are thus consistent with previous findings, which demonstrates the validity of our model. Based on this model, we next examine the joint effect of NPs and surfactants at the oil-water interface.

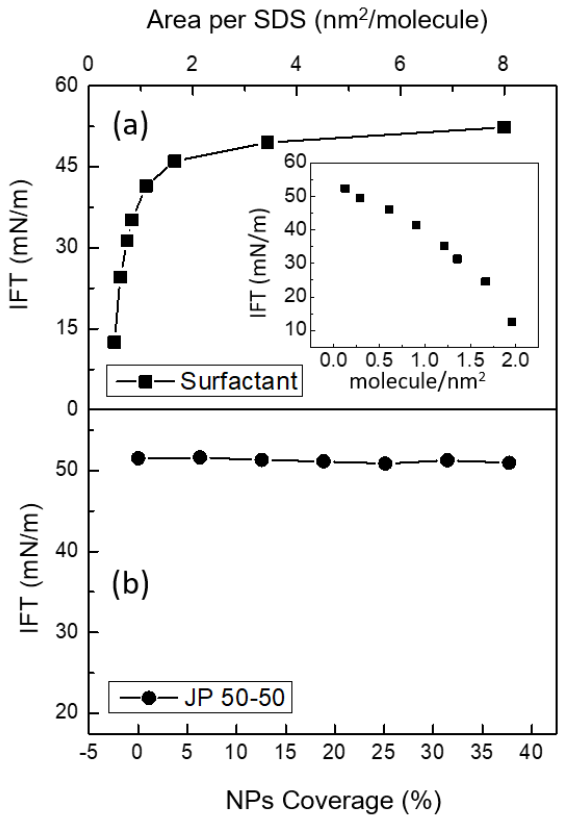

Figure 5.2. Dependence of the oil-water IFT on surfactant concentration (a), and NP coverage (b). The inset is the plot with the x-axis as surfactant interfacial concentration.

Figure 5.3 is a set of snapshots of the oil-water interface taken with the different types of NPs. The NPs tend to stay at different places due to opposite driving forces. One is the desire of each bead to stay in their favored phase – the hydrophobic beads prefer to face the oil phase, while the hydrophilic beads tend to move to the water phase, thus turning the NP accordingly. The other is the inclination of the whole NP to reside at the interface, leading to a reduced oil-water contact area. In all NPs, the tendency of the NP to reside at the interface dominates the former effect. The relative positions of the NPs with the interface in Figure 5.3 indicate this tendency. The 0-100 NPs stay almost entirely in the water phase since they are purely hydrophilic. Increasing the hydrophobic-hydrophilic ratio in the NP gradually brings it farther from the water phase. For JP 50-50, the center of mass of the NPs stays on the plane of the oil-water interface. When the

percentage of hydrophobic beads on the surface reaches 100%, the NPs settle mostly in the oil phase. A similar trend is observed with the heterogeneous NPs. Although the positioning of NPs does not have any impact on the IFT, as already shown in Figure 5.2, it will be useful later in the discussion to explain the effect of NPs when surfactants are also present.

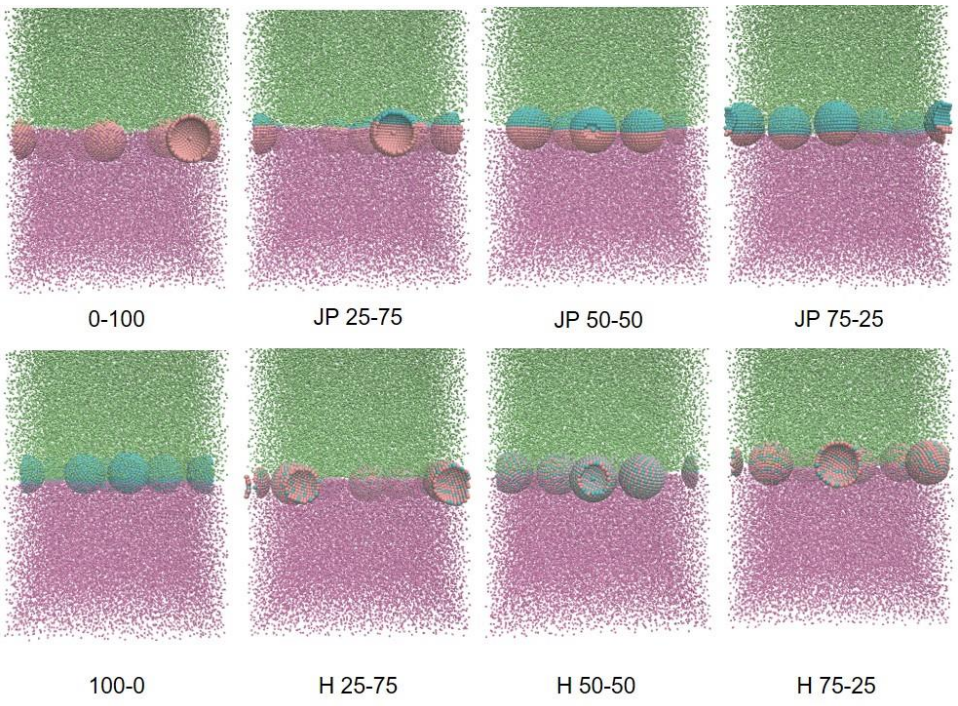

Figure 5.3. Snapshots of the oil-water interface with different types of NPs. The color scheme is used as in Figure 5.1.

b. Synergistic Effect of Surfactants and Nanoparticles at the oil-water interface

This section starts by examining the co-effect of surfactant and one kind of NPs, the JP 50-50. The change of the oil-water IFT as a function of JP 50-50 coverage and at different surfactant concentrations is seen in Figure 5.4. Without the presence of surfactant, the NPs do not have a noticeable impact on the IFT, as already discussed. When surfactants are present, the IFT decreases with NPs coverage. Increasing the NPs coverage from 0 to 37.5% reduces the IFT from 46.49 mN/m to 30.55 mN/m, and from 40.1 mN/m to 12.15 mN/m in the cases of 0.61 and 0.91 SDS

molecule/nm^2, respectively. Note that the effect of JP 50-50 on the IFT is more pronounced at higher NPs coverage. At 0% NP coverage, the reduction in IFT by adding 0.91 SDS molecule/nm^2 compared to the pure oil-water IFT is only 10 mN/m. When the NPs cover 37.5% of the interface, this reduction increases up to 38.7 mN/m (a reduction of about 75%). Note from Figure 5.2 that surfactants by themselves only reduce the IFT by about 25% at this concentration. Given that NPs do not alter the IFT, one would expect the same reductions between the two cases at different NP coverage. Thus, the explanation can only be found by considering the role of surfactants.

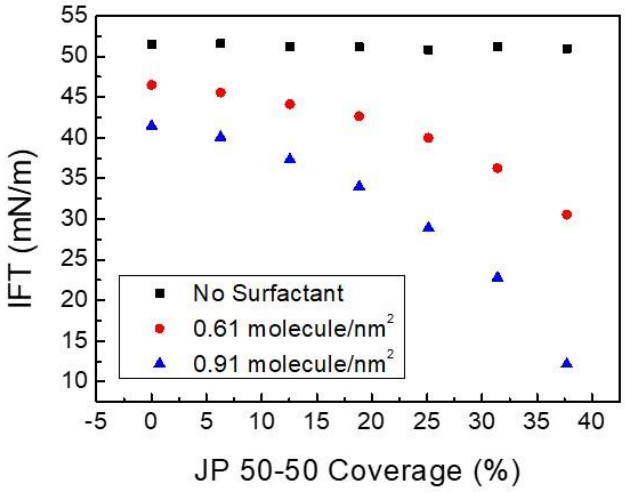

Figure 5.4. Dependence of IFT on JP 50-50 coverage at different surfactant concentrations

Figure 5.5 is a collection of snapshots of the oil-water interface with the presence of 0.91 SDS molecule/nm^2 at different NP coverage. The snapshots on the top row of Figure 5.5 clearly show that the surfactant distribution at the interface becomes denser when NP coverage increases. There is less free space between the NPs for the surfactant molecules to occupy.

To quantify the effect of the presence of NPs on the configuration of surfactants at the interface, we created contour plots of surfactant concentration, as can be seen on the bottom row of Figure 5.5. The plot was constructed by dividing the interface into 50x50 bins. The total number of

surfactant molecules in each bin was counted and then was averaged over 50,000 time-steps. To do this calculation, the NPs and surfactants were allowed to reach an equilibrium configuration, and then the NPs were fixed in their positions, while water, oil, and surfactants could move for the duration of the averaging process. The effect of adding NPs at the interface can be seen clearly in the plots. At 0% NP coverage, the surfactants are uniformly distributed at the interface with the local concentration in each bin within the range of 0.65 – 0.95 molecule/nm^2, which is reasonable since the average concentration of surfactants was 0.91 molecule/nm^2. Introducing JP 50-50 to the interface shifts the local concentration to higher concentration values. When there are 12 JP 50-50 particles at the interface, corresponding to 37.5% coverage, the surfactant concentration is between 1.8-2.4 molecule/nm^2. Thus, it can be seen that increasing JP 50-50 coverage results in more concentrated surfactant at the interface.

The increase of surfactant concentration is explained by the tendency of NPs to stay at the interface. NPs occupy the interface, leaving less space available to the surfactants. Since the surfactant molecules also desire to reside at the interface, the same number of surfactant molecules is packed in a smaller area, which leads to the increase of concentration. This concentration is named *effective concentration,* to distinguish from the overall concentration that is calculated over the whole interfacial area. By comparing Figure 5.5 and Figure 5.4, one can identify the relation between effective concentration and the IFT. For example, at 12% coverage, the effective concentration is 0.95-1.2 molecule/nm^2 (from Figure 5.5), and the IFT is 35-40 mN/m (from Figure 5.4), which is consistent with the correlation between IFT and surfactant concentration in Figure 2a. Similarly, the same observation can be made with 25% and 37% coverage. Such evidence suggests that the IFT is determined by the effective concentration of surfactant instead of the

overall concentration. Moreover, it can be concluded that NPs reduce IFT by increasing effective surfactant concentration.

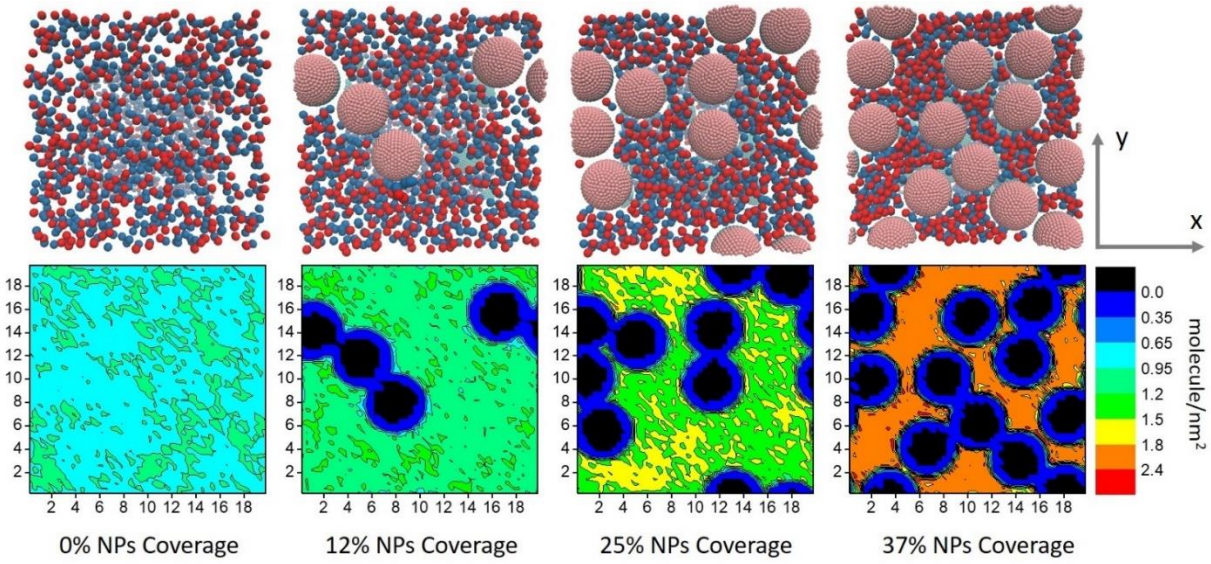

Figure 5.5. (*Top row*) Snapshots of the oil-water interface with 0.91 molecule/nm^2 surfactant at JP 50-50 coverages of 0, 12%, 25%, 37%. The color scheme is similar to that in Figure 1b. Oil, water beads are not shown for clarification. (*Bottom row*) Contour plots of the surfactant concentration at the interface at different JP 50-50 coverages.

The effects of different types of NPs on the oil-water IFT with the presence of surfactants are examined next. Figure 5.6 is a demonstration of the change of the IFT as a function of surfactant concentration with the presence of different types of NPs. The coverage of NPs in the simulation was kept constant at 25%. The insets in each graph show the cases of JP and H NPs with hydrophobic to hydrophilic ratios of 25-75, 50-50, 75-25 only. When NPs are not present, the plot exhibits the typical curve of IFT as a function of surfactant concentration as in Figure 5.2a. The IFT decreases with the presence of any NPs. In both Figures 5.5a and 5.5b, at low surfactant concentration, NPs do not have any noticeable impact on the IFT. The reason is that in this regime, the interface could be considered as containing only NPs. From the preceding discussion, it was demonstrated that NPs can only affect the IFT when surfactants are present. The effect of each

type of NPs is seen when increasing surfactant concentration. In both cases of Janus and heterogeneous nanoparticles, the 25-75, 50-50, and 75-25 NPs exhibit larger effects than the 0-100 and 100-0 NPs. Thus, we grouped them together to examine their effect. When 0-100 and 100-0 NPs were used, the reductions of IFT were lower, especially at high surfactant concentrations. The explanation can be found by looking at the snapshots of the interface in Figure 5.7. Because the 0-100 and 100-0 are purely hydrophilic or hydrophobic, they tend to settle mostly within the water or oil phase, respectively. Some of the 0-100 NPs are even pushed fully into the water phase due to the high concentration of surfactants at the interface, which has been observed in our previous study [150]. For the group of NPs with hydrophobic-hydrophilic bead ratios of 25-75, 50-50, 75-25, their tendency to reside at the interface is stronger than pure NPs as they exhibit both hydrophobic and hydrophilic properties. The interfacial areas occupied by 0-100 and 100-0 NPs are thus smaller in comparison to other types of NPs. Consequently, the effective surfactant concentration is lower, resulting in a lower reduction of IFT.

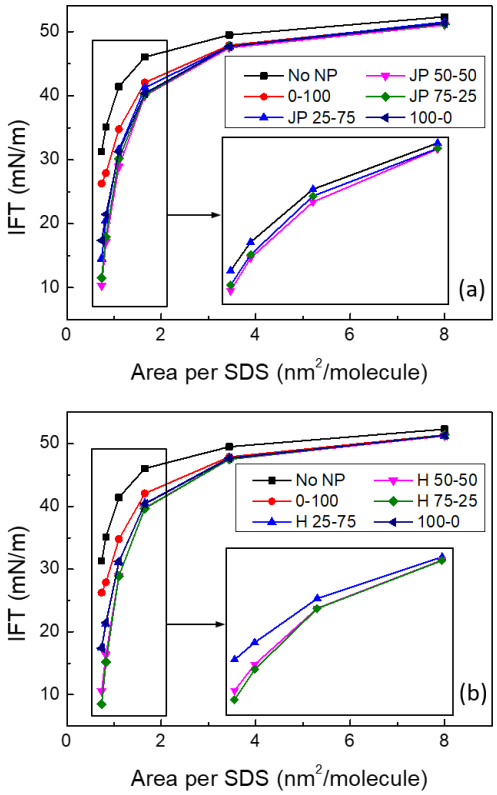

Figure 5.6. Oil-water IFT as a function of surfactant concentration with various types of NPs (a) Janus particles (b) Heterogeneous particles. The inset only shows the cases of 25-75, 50-50, 75-25 NPs for clarification.

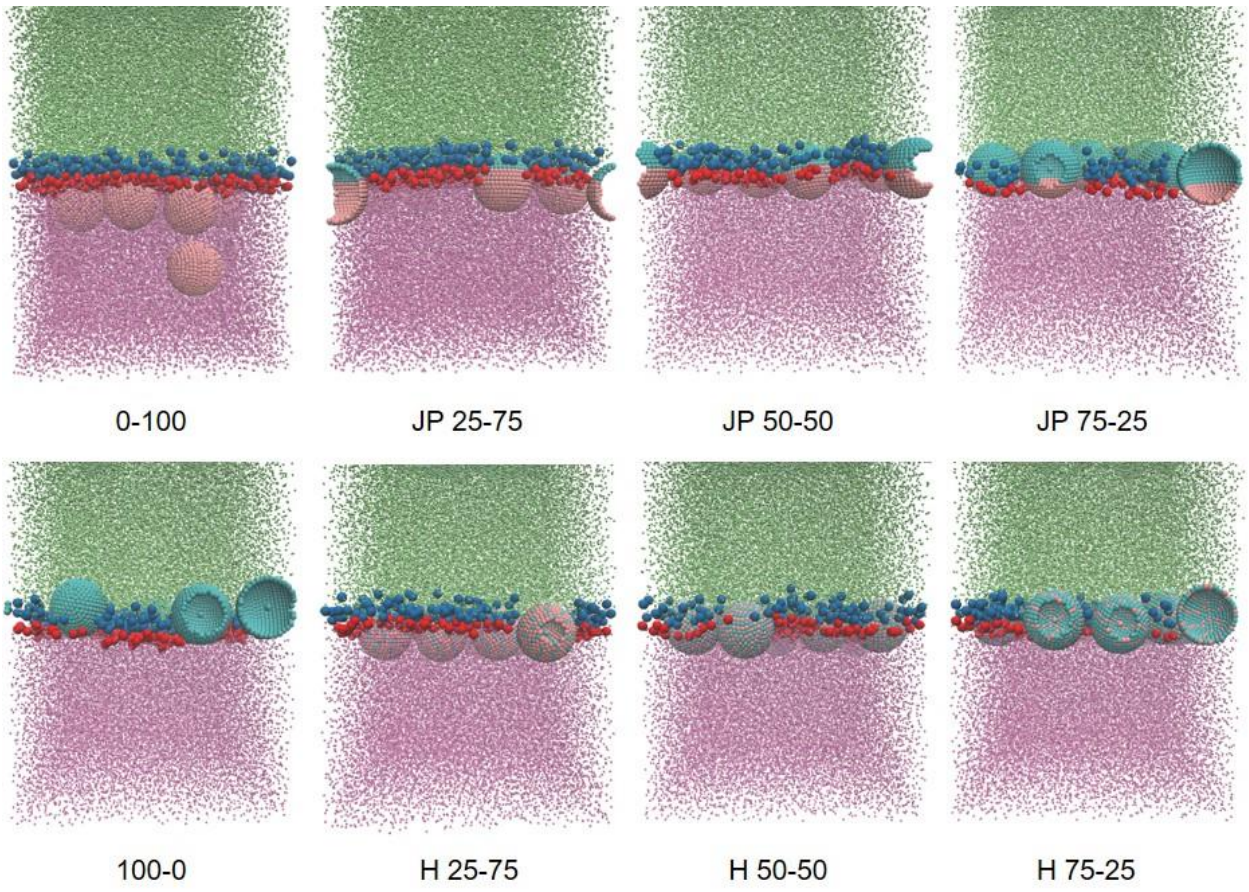

Figure 5.7. Snapshots of the oil-water interface with NPs at 25% coverage and surfactant concentration of 1.36 molecule/nm^2. The color scheme is consistent with Figure 5.1. Note that a 0-100 NP is fully into the water phase in 5the top-left snapshot.

To develop a more quantitative description of the snapshots in Figure 5.7, the density profiles of surfactants and NPs in each system were plotted in Figure 5.8. The correlation between the properties of each NP and the IFT could be found by analyzing Figures 5.6 to 5.8. The peaks of each component indicate the location in the *z*-direction (perpendicular to the oil-water interface) where most of those components are present. The positions of the surfactant peaks are relatively stable; thus, they are used to indicate the oil-water interface. The larger part of 0-100 and 100-0 NPs are within the water and oil phases, respectively, which is consistent with Figure 5.7. The secondary peaks of NP 0-100 show the positions of the NPs that leave the interface to the water

phases as can be seen in Figure 5.7. In both cases of Janus and heterogeneous nanoparticles, increasing the hydrophobic ratio shifts the NPs to the oil phase. The overlap of the positions of the peaks indicates the region where NPs and surfactants align right at the interface, which is exactly in the middle of the oil and water phases ($z \approx 15$ and $z \approx 35$). The overlap happens with JP 50-50 and H 75-25, which are also the NPs that yield the highest effect in lowering the IFT in cases of Janus and heterogeneous NPs. This result suggests that the NP that aligns right in the middle of the interface has a higher impact on reducing the IFT. This observation could be explained using the effective concentration concept. When the middle part of NP (i.e., the equator of the NP sphere) stays right at the interface, the interfacial area occupied by the NP is higher, which increases the effective concentration of surfactant. The IFT is, therefore, lower than the case of NP that shifts to either the oil or water phase. In summary, among different NPs, the JP 50-50 and H 75-25 are the most effective in reducing the IFT due to their positioning exactly in the middle of the interface.

With the Janus particles, it is understandable that the JP 50-50 exhibits the best combined effect with surfactants. The JP 50-50 has two sides with an equal number of hydrophobic and hydrophilic beads. Naturally, one would expect the JP 50-50 to settle with its middle at the interface, with the hydrophobic side in the oil phase and the hydrophilic side in the water phase, as shown in Figure 5.3 where surfactants are not present. However, for the heterogeneous particles, the H 75-25 is slightly more effective in reducing IFT than the H 50-50, which is unexpected considering that the H 50-50 is closer to the interface than H 75-25 in Figure 5.3. For an explanation, in Figure 5.9, we plot the density profile of the hydrophilic and hydrophobic parts of NPs along with the head and tails of surfactants.

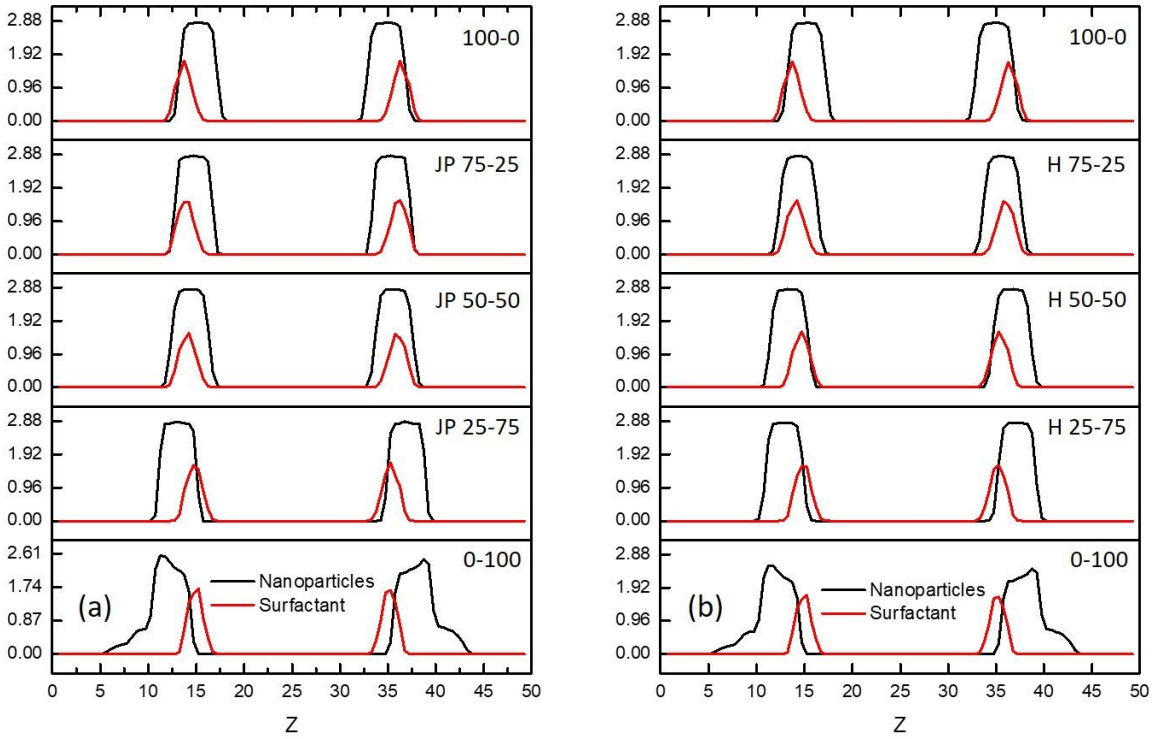

Figure 5.8. Density profiles of surfactants and NPs along *z*-direction corresponding to the snapshots in Figure 5.7. (a) Janus particles, and (b) Heterogeneous particles. The oil phase is in the center of the *z*-axis, at about $z = 25$ (see Figure 5.1b), and the water phase is at low and high *z* values (because of the periodic boundary conditions of the simulations).

The basic difference between Janus and heterogeneous particles lies in the relative positions of the hydrophobic and hydrophilic density peaks. The peaks are separated in the density profile of JP 50-50, while they overlap in the case of heterogeneous particles, which is the result of the different ways of distributing hydrophobic and hydrophilic beads on the surface of these particles. Going from H 25-75 to H 75-25, the ratio of hydrophobic and hydrophilic peak areas increases as expected. For JP 50-50, the surfactant heads and tails are aligned with the hydrophilic and hydrophobic sides of the particle, respectively, to yield the highest co-effect. With the heterogeneous particle, the hydrophobic and hydrophilic beads are not separated; thus, the positioning of the particles relative to the surfactant molecules plays an important role. As can be

seen on the density profiles, the NPs move toward the surfactant tails as their hydrophobic ratios increase. For H 75-25, the peak for NPs is at the same position as the surfactant tails' peak; while in the case of H 50-50, it overlaps with the surfactant heads' peak. The reason is that in an SDS molecule, there are 2 tails and 1 head beads. The attraction of the two tails pulls the NP with a higher hydrophobic ratio (which is H 75-25) closer to the tail. Moreover, an NP and the two tail beads can reduce the number of direct contacts between oil and water molecules further than an NP and one head. Consequently, in the case of H 75-25, the oil-water IFT is lower than H 50-50. For the H 25-75, the tails are almost away from the NPs region; therefore, the co-effect is significantly weakened. In fact, the IFT curve of H 25-75 is quite close to that of 100-0 even though the NP 100-0 has a lower tendency of settling at the interface. This could also be explained by the double number of tails in comparison to the number of heads in an SDS molecule. Although the NP 100-0 has a small footprint at the interface, its combination with the two tails gives the same effect as the combination of the H 25-75 with only one head. The much higher effect of NP 100-0 than the NP 0-100 can also be explained similarly.

To recap, the JP 50-50 and H 75-25 exhibit the highest synergistic effects with SDS surfactant in reducing the oil-water IFT. The key factor that affects the impact of the NPs is their ability to position adjacent to the surfactant molecules. For SDS, the alignment of the NPs with the surfactant tails is more important than the heads due to the higher number of tail beads in one surfactant molecule.

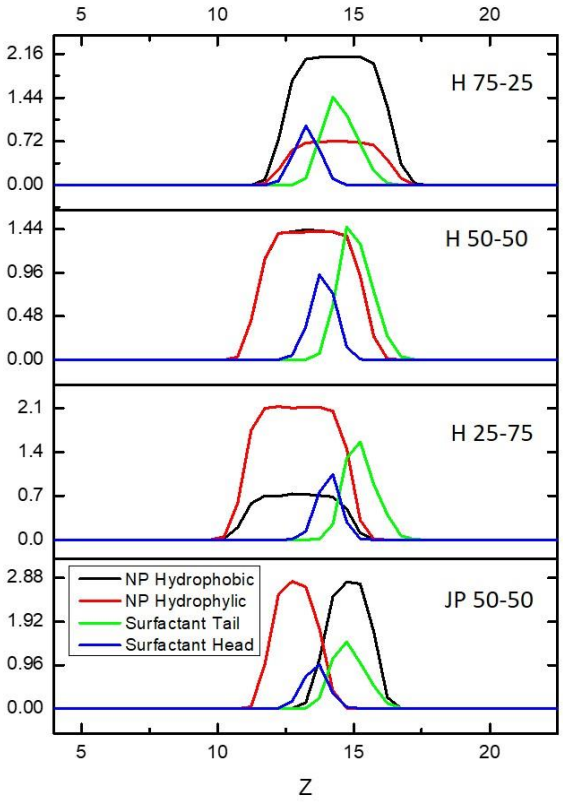

Figure 5.9. Density profiles of surfactant head, tail, and NP hydrophobic, hydrophilic parts for cases of H 75-25, H 50-50, H 25-75, JP 50-50. The interface is at the point of intersection between the surfactant head and tail distributions.

5.4. Conclusions

The contour plots (Figure 5.5) for the surfactant interfacial density provide a clear observation for the increase of surfactant concentration when adding NPs at the oil-water interface. Thus, the role of NPs in further reducing the oil-water IFT with surfactants, which has also been reported in the literature [40, 42, 50, 51, 150] is confirmed. The synergistic effect between NPs and surfactants can be explained by considering that the presence of NPs leads to the less interfacial area available to be occupied by surfactants so that fewer surfactant molecules are needed to generate a larger IFT reduction than when they are alone at the interface.

The utilization of computational simulation allows the investigation of a range of parameters that has not been conducted by experiments. Moving forward from previous reports [40, 42, 142, 149], we demonstrated that the wettability of NPs is the most important factor in the combined effect with surfactants. Among different types of NPs, the maximum synergism occurs when the NPs reside at the interface, maximizing the interfacial area they occupy and minimizing the area that is available to surfactants. This happens when the NPs equator line is at the interface, which is observed with the JP 50-50 particles and the H 75-25 particles. For JP 50-50, the equal number of hydrophobic and hydrophilic beads on the NP makes it settle in the middle of the interface. In the case of the heterogeneous particle, the H 75-25 is the most effective type of particle because the attraction of the two surfactant tail beads pulls the H 75-25 closer to the surfactant tail, reducing the number of direct contacts between oil and water molecules. These conclusions were confirmed by examining the density profiles of the surfactant head and tail beads of the molecule and the density of the hydrophilic and hydrophobic parts of the NPs.

The observation of the different behavior of the various NPs also allows some suggestions for the design of NPs for stabilizing emulsions using fewer NPs and surfactants. For Janus particles, the JP 50-50 should be used. For heterogeneous particles, the optimal ratio of hydrophobic over hydrophilic surface coverage depends on the structure of the surfactant molecules. When a surfactant with a long tail and a short head is used, the portion of hydrophobic beads on the particle should increase to shift it close to the tail region at the interface, and vice versa.

Chapter 6. Effect of Janus Particles and Surfactants on the Coalescence of Emulsions

Abstract

The synergistic effect of sodium dodecyl sulfate surfactants and Janus nanoparticles on the stability of oil-in-water emulsion was investigated using dissipative particle dynamics. Two oil droplets with different Janus particle surface coverages and surfactant surface concentrations were pushed towards each other for coalescing. The coalescence progressed by moving the Janus particles away from the point of drop contact, followed by the diffusion of surfactant from the contact area to allow the direct oil-oil contact. The emulsion stability was quantified using the difference of free energy between the final and the initial state of coalescence. At particle coverage of less than 70% of the drop surface, Janus particles alone could not thermodynamically stabilize the emulsion. However, when combined with surfactants, Janus particles would improve emulsion stability by increasing the effective surfactant concentration on the emulsion surface. A model to predict the emulsion stability from the particle coverage and surfactant concentration was constructed. The model suggested that the emulsion will be stable if the effective surfactant concentration is higher than 80% of the critical micelle concentration on the drop surface.

6.1. Introduction

Emulsions of oil and water have been important in different applications including food processing [2], production of pharmaceuticals [3], material synthesis [4], oil recovery [5], and drug delivery [6]. In general, emulsions are stabilized using surfactants, which decrease the oil-water interfacial tension (IFT) and, thus, the surface free energy [1, 117, 118]. The effectiveness of surfactants as emulsifiers depends on the type of surfactant (ionic or non-ionic surfactant), its molecular length and hydrophilic-lipophilic balance, its concentration, and the pH of the suspension [1, 160-162]. Nanoparticles (NPs) can also function as emulsifiers [17, 18, 163, 164]. The mechanism for

stabilizing an emulsion by particles is different than the one for surfactants. Particles that assemble at the interface limit the direct interaction between oil and water leading to a reduction of free energy [40, 123].

Coalescence is one of the common mechanisms of emulsion breaking along with flocculation and creaming [165]. The coalescence of surfactant emulsions has been investigated intensively in the literature [166-170]. Studies on Pickering emulsions (i.e., emulsions that are stabilized by solid particles) suggested that the stability depends on the particle shape, coverage, surface chemistry, and the collision speed between droplets [171, 172].

While prior reports have studied the coalescence of emulsions stabilized by surfactants or JPs, the knowledge of their combined effects on coalescence is still not yet well-understood. In this study, we aim to explore the different mechanisms of coalescence of emulsions stabilized by surfactants and Janus particles (JPs) using dissipative particle dynamics (DPD) simulation. We also built a model to predict the emulsion stability from the JP coverage and surfactant surface concentration.

6.2. Simulation Details

We employed the dissipative particle dynamics (DPD) simulation method in this study. DPD is a coarse-grain molecular dynamics method, where several atoms or molecules are represented by a single "bead" [68, 73]. As the motion of several molecules is described by that of one bead, the computational time will be reduced significantly. DPD has been applied for studying surfactants, polymers, and nanoparticles [106, 173-175]. The details of the method [73] and the parameterization can be found in our early publications [49, 69, 150]. We only briefly describe the construction of our simulation here. All the quantities reported herein are in dimensionless units.

Figure 6.1 showed the simulation setup and the representation of the components in this study. Five water molecules were grouped into one water bead. Heptadecane was used to represent the oil, with three oil beads connected by two harmonic bonds. Sodium dodecyl sulfate (SDS), an anionic surfactant was used as the surfactant, which was represented by two hydrophobic beads (tail) and one hydrophilic bead (head) connected by 2 harmonic bonds. The interaction parameters and bonding, angle coefficients were given in chapter 5. In a previous study [49], we have demonstrated that Janus particles with one hemisphere being polar and the other half of the spherical surface being apolar would result in the highest reduction of interfacial tension compared to other nanoparticles (NPs) when combined with SDS surfactants at the oil-water interface. Thus, this type of JP was used in our simulation. The JPs were modeled as hollow spheres containing 560 beads with a JP diameter of 2.35 r_c, where r_c is the reduced unit used in our simulation. The distribution of polar and apolar beads on the JP surface resulted in a contact angle of $90.5^o \pm 0.3^o$ on the oil-water interface. The components in the simulation were chosen to match experimental data in the literature [103, 176].

The simulation size was $80\times50\times50$ r_c^3 in all cases. Periodic boundary conditions were applied in all 3 dimensions. Two oil-in-water droplets with diameters of 30 r_c each were placed 40 r_c apart at the beginning of the simulation. The JP concentrations at the emulsion surface were described as the *JP coverage*, which is the ratio between the area covered by JPs and the surface area of the emulsion drop. The surfactant concentrations were normalized by the surface concentration of surfactant at the critical micelle concentration (CMC), which is the maximum surface concentration at the oil-water interface for one kind of surfactant [1]. For SDS, this surface concentration is 3.1×10^{-10} [mol/cm^2] [104]. By definition, the JP coverage and surfactant

concentrations were in the range of 0-1. The JP coverages and surfactant concentrations were 0 to 0.7 and 0 to 0.8, respectively.

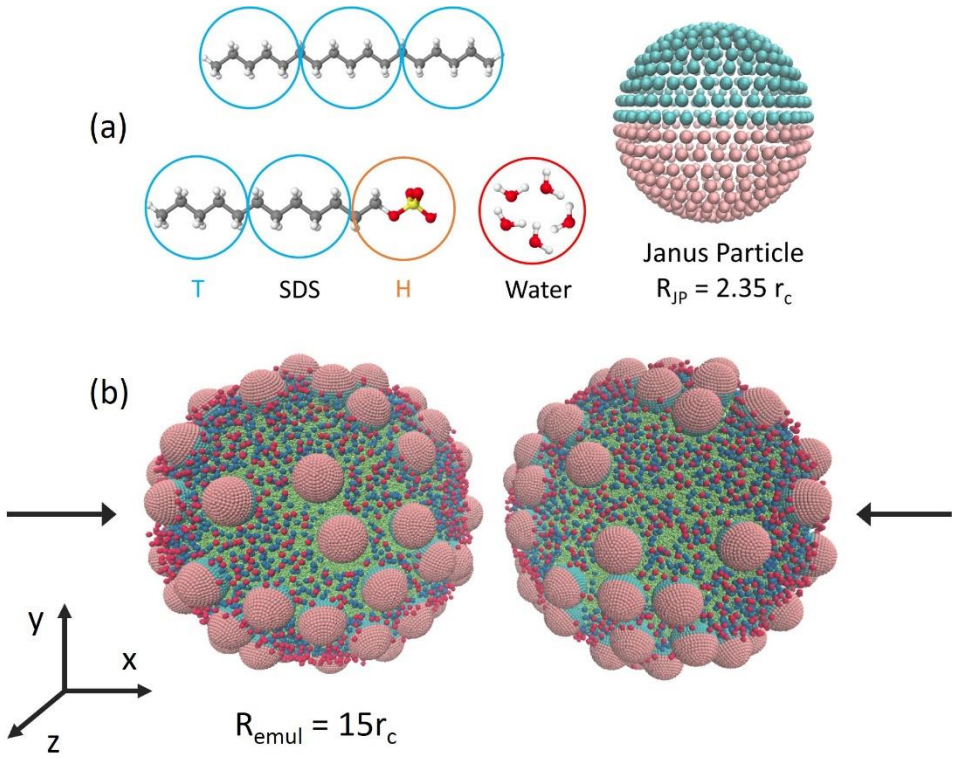

Figure 6.1. Simulation setup and representation of the components used in the system. (a) Beads of the DPD model for water, heptadecane, SDS head (H), tail (T), and the Janus nanoparticles (JPs); (b) Snapshot of the system containing oil-in-water drops stabilized by SDS surfactants and JPs. The arrows show the direction of coalescence. The coordinate axes represented the orientation of the system. Purple, green, red, blue, pink, cyan beads represent water, oil, surfactant head, surfactant tail, and the Janus nanoparticle's polar and apolar, respectively. R_{emul}, R_{JP}, r_c are the radius of the emulsion drops, the radius of the JP, and the unit length.

The NVT ensemble (constant number of atoms, volume, and temperature) was employed. The pressure was kept constant using the Berendsen barostat [177]. The initial system was equilibrated for 10^6 timesteps to allow the uniform distribution of surfactants and JPs on the emulsion surface. The centers of mass (COMs) of the two drops were fixed at the original position during the equilibrium. For the coalescence of emulsions, we applied the steered molecular dynamics (SMD)

algorithm [178, 179]. A fictitious spring with a force constant of 200 k_BT/r_c was used to couple the two droplets and pull them toward each other at a constant relative velocity (pulling velocity) of 0.0001 r_c per timestep. The surfactants and JPs were allowed to freely move on the droplet surface. The potential of mean force (PMF) of the system can be calculated via SMD. According to Jarzynski's equality, the PMF reflects the free energy difference between two states during a nonequilibrium process [179]. Therefore, a correlation between the configuration of the system and the PMF profile can be made to explain the behavior of surfactants and JPs during coalescence.

6.3. Results and Discussion

Figure 6.2 showed the snapshots of the emulsion drops at different states of coalescence. We can observe quite similar progress for all three cases. The drops were first in contact through the interaction of surfactants or the interaction between JPs on the surface of the two different drops The drops were deformed to different levels depending on the effectiveness of surfactants or JPs to stabilize the drops until the oil molecules in the two emulsion drops were in direct contact (second row). Once the first oil-oil contact was made, the two emulsions merged rapidly, forming a new drop with a transitional shape (third row). At the end of coalescence, the new emulsion evolved to a spherical shape to reduce its total surface area. The process agreed with published experimental studies [180]. It is important to note that for emulsions with only NPs, the JP coverage was chosen to be less than 0.7 to avoid arrested coalescence [181], which prevented the new emulsion drops from reaching a spherical shape. We also observed arrested coalescence when JP coverages were higher than 0.7, but the phenomenon is outside the scope of this study. In addition, the surfactant concentrations were kept at 0-0.8, less than CMC surface concentration to prevent surfactant desorption from the droplets, which will further complicate the behavior of the system. As the JP coverages were lower than 0.7, the coalescence of JP-stabilized drops happened

quite easily as the droplets did not undergo a high degree of deformation as reported in the literature [171].

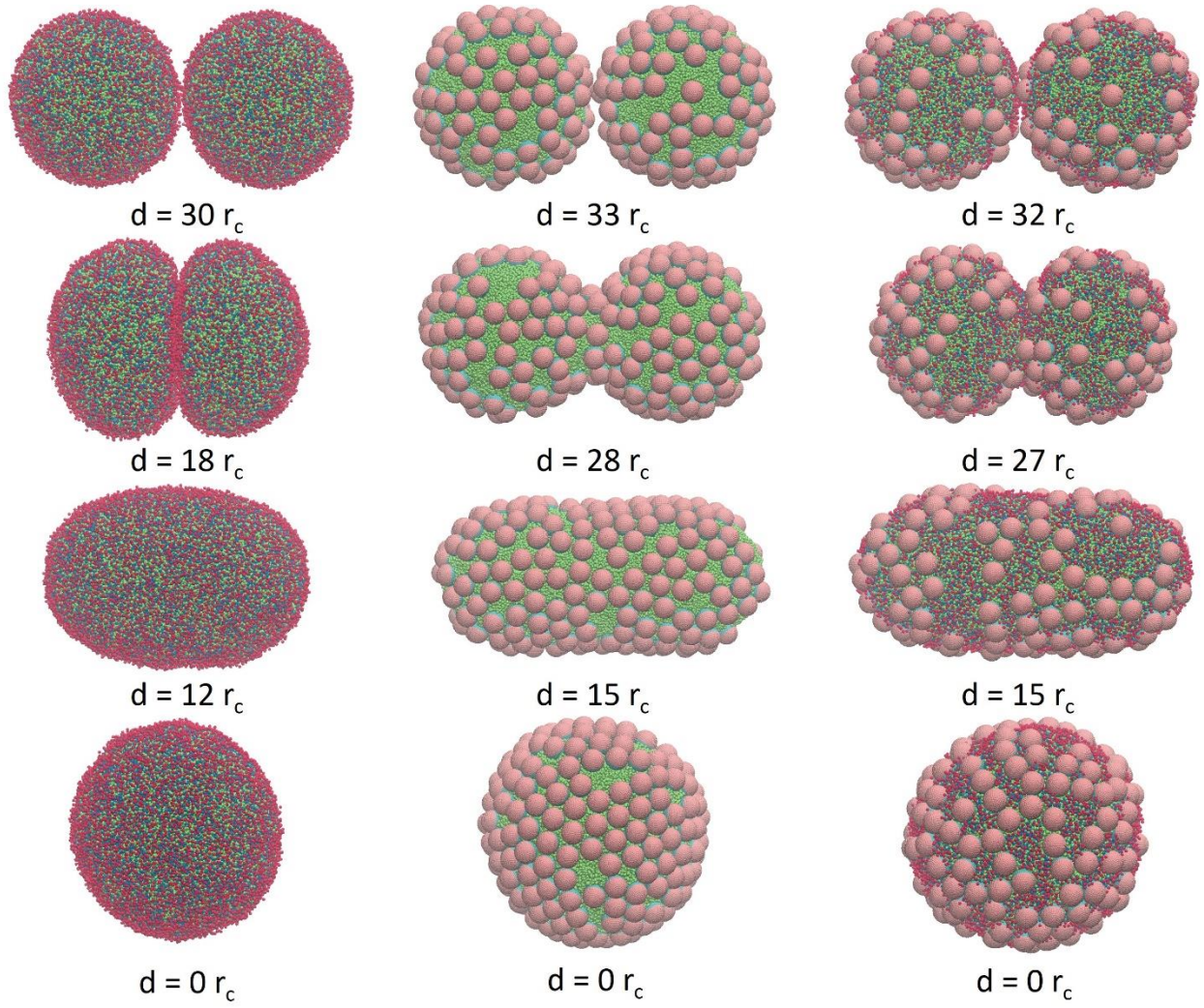

Figure 6.2. Snapshots of the droplets at different states of coalescence. The drops were stabilized by SDS at 0.7 CMC concentration (left column), JPs at 0.7 coverage (middle column), JPs at 0.42 coverage and SDS at 0.35 CMC concentrations (right column). d is the distance between the centers of mass of the two emulsion drops. The color code is similar to Figure 6.1.

Figure 6.3 showed the snapshots of surfactants in the contact area at different coalescence states. These are two droplets with only SDS surfactant present on their surface. When the two emulsion droplets were far from each other, the surface concentration of surfactant was distributed in the

range of 0.6-0.8 and 0.8-1. It should be noted that because we projected the curved surfaces shown in Figures 6.3a-b onto the yz plane in Figure 6.3d-e, the area of the region further from the center decreased, leading to an increase in surfactant concentration. The area of the region near the center should be approximately close to the area on the curvature as the projection had little effect there. Therefore, the surfactant concentration in the center was comparable to the expected concentration of 0.7 (the yellow region in Figure 6.3g). Right before fusion of the oil (Figure 6.3e), the surfactant concentration reduced to 0.4-0.6 (green color on Figure 6.3h), indicating that surfactants diffused away from the contact region. The reason was that the local concentration of surfactants at the contact area increased due to the squeezing of surfactants from two emulsion drops. The concentration gradient between the contact area and the remaining area led to the diffusion of surfactant away from the contact area. Once the surfactant concentration on its original emulsion reached a critical value (0.4-0.6), there was a higher possibility of oil-oil contact. The *bridging* region (i.e., the region where the first oil-oil contact occurs) in Figure 6.3f (the blank area) corresponds to the green area in Figure 6.3h further confirming our hypothesis. In summary, for emulsions with only surfactants, the coalescence happened due to the diffusion of surfactant away from the contact area, which reduced the local surfactant concentration to 0.4-0.6 CMC surface concentration, allowing a higher chance of oil-oil contact.

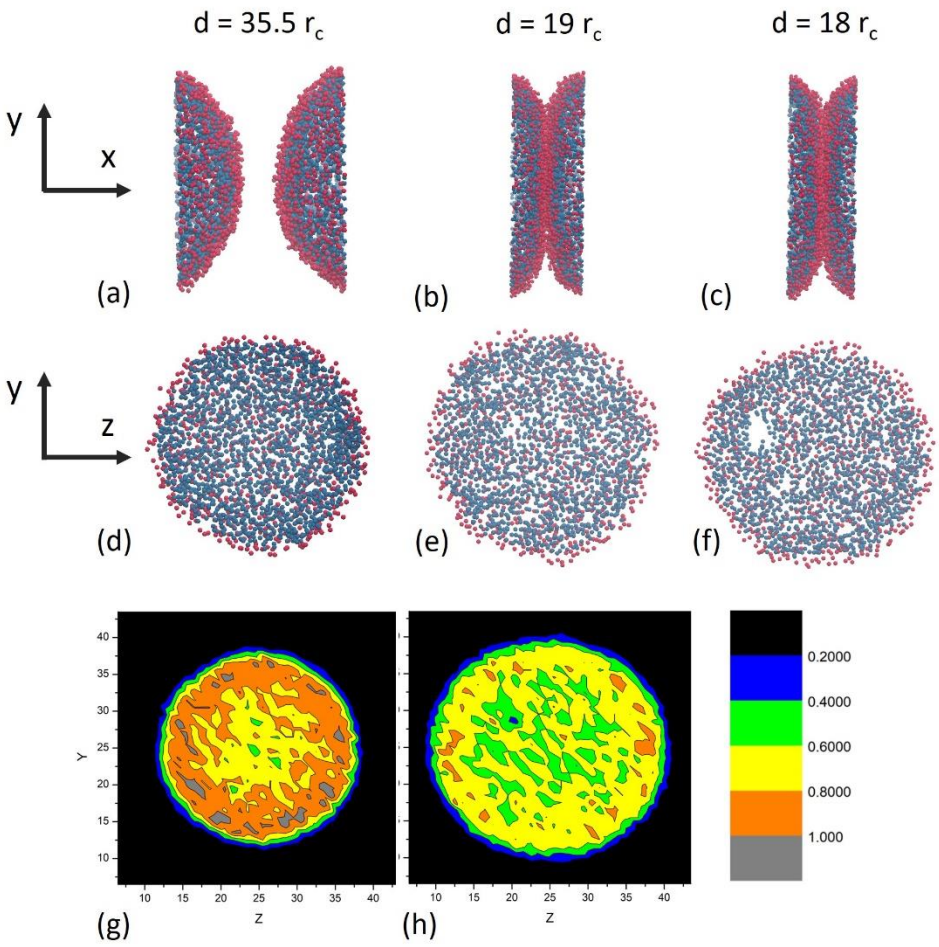

Figure 6.3. Snapshots of the surfactants in the contact area at different coalescence states with corresponding COMs distances: the droplets were not in contact (left column), the first oil-oil contact was created (right column), before the beginning of oil-oil contact (middle column). The first and second rows showed the view on the *xy* and *yz* planes, respectively. Figures (g) and (h) showed the contour plots of figures (d) and (e), respectively. The color scheme is similar to Figure 6.1. The surfactant concentration was 0.7 of the CMC surface concentration.

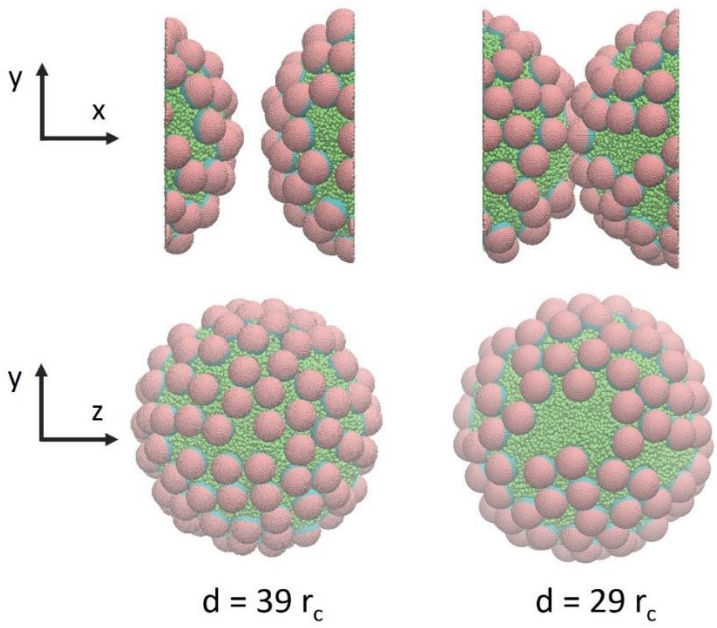

Figure 6.4. Snapshots of emulsion drops stabilized by 0.7 JPs coverage at different coalescence states. The first and second rows showed the view on the *yz* and *xy* planes, respectively.

For JPs, Figure 6.4 showed that the JPs at the contact area were pushed away from their original position due to steric effects. This mechanism of coalescence agreed with the early report by Fan et al. [171]. As the volume of a single surfactant is much smaller than a JP, the surfactants can cover the interface more uniformly compared to JPs. As can be seen from Figure 6.4, there are voids in between JPs; thus, once the JPs in the contact region were push away, the fusion of oils from the two emulsions occurs very quickly and the oil bridge is formed.

Figure 6.5 illustrated the coalescence of emulsions stabilized by both JPs and SDS surfactants. Due to their higher volume, the JPs from different emulsion drops were in contact first. Then the steric effect expelled them from the contact area. The drops did not collapse right after that because of the presence of surfactants. The global surfactant concentration was 0.35 CMC surface concentration. The *effective* surfactant concentration, which was calculated after accounting for the area occupied by JPs was 0.6 of the CMC. As can be seen in Figure 6.5g, the local surfactant

concentration was in the range of 0.4-0.8. Similar to the case of surfactant only, the surfactants gradually diffused away from the contact area until the concentration was 0.4-0.6 (the green region in Figure 6.5h). The bridging region (blank area in Figure 6.5e) also occurred in the area where surfactant concentration was 0.4-0.6, which is consistent with Figure 6.3. In conclusion, when the two emulsions approach, the steric effect moved JPs out of the contact region. The surfactants gradually diffused away until reaching 0.4-0.6 concentration, which was enough to allow oil-oil direct contact, bridging between the two droplets and then coalescence.

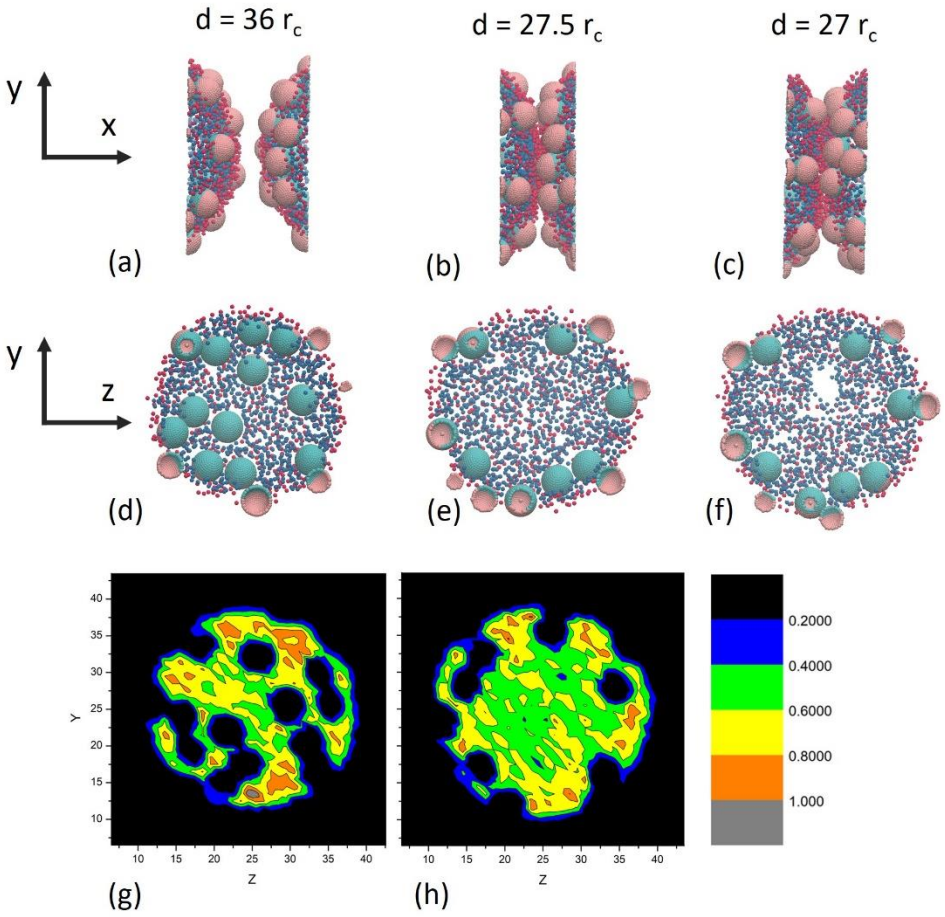

Figure 6.5. Snapshots of the JPs and surfactants in the contact area at different coalescence states with corresponding COMs distances: the droplets were not in contact (left column), the first oil-oil contact was created (right column), before the beginning of oil-oil contact (middle column). The first and second rows showed the view on the *yz* and *xy* planes, respectively. Figures (g) and

(h) showed the contour plots of figures (d) and (e), respectively. The color scheme is similar to Figure 6.1. The JPs coverage was 0.42, the surfactant concentration was 0.35 CMC surface concentration.

Figure 6.6 showed the plot of the potential of mean force as a function of the distance between the emulsions during coalescence. When the emulsions were not in contact (state (a)), the PMF stayed at 0 as expected. The energy built up as the drops came in contact because the contact area became crowded with surfactants and JPs from the 2 emulsion drops. The energy increased until state (b) when the bridging occurred. The energy difference between this state and the initial state could be considered as the energy barrier needed for coalescence. After that, the PMF reduced as the oil molecules from the two drops merged, which is energy favorable. The energy decreased to a plateau when the new drop gradually turned into a spherical shape, minimizing free energy by minimizing its surface area. The energy difference between the final and the initial state (ΔE) can be used to quantify the stability of the emulsion. A negative ΔE indicated the generation of a more stable state when the two drops coalesce, i.e., the emulsions were not thermodynamically stable and vice versa. With the same JP coverage of 0.42, increasing surfactant concentration from 0.2 to 0.5 led to more stable emulsions. The explanation can be found by comparing the initial and the final state. The coalescence led to the reduction of surface area by $2^{1/3}$ times, which means the JPs coverage and surfactant concentration increases by $2^{1/3}$ times. When the JP coverage and surfactant concentration were small, this increment resulted in a larger reduction of interfacial free energy. However, when surfactant concentration was high (0.5 CMC surface concentration), the new emulsion was overcrowded by the emulsifiers. Their repulsion resulted in an energy unfavorable state.

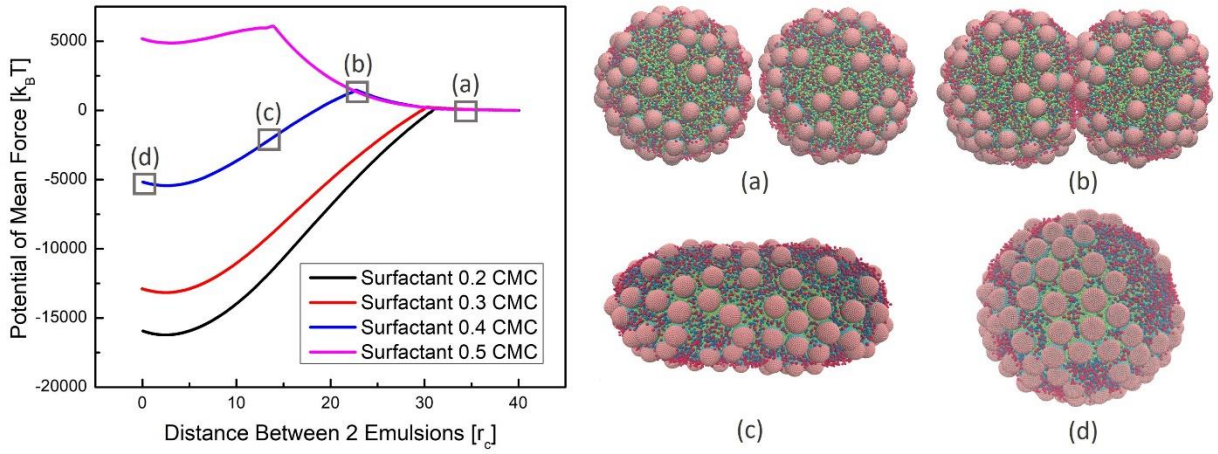

Figure 6.6. Potential of mean force (PMF) profile of the system during coalescence. The snapshots on the right showed the emulsions at the indicated state in the plot. The JP coverage was 0.42.

Using the energy difference (ΔE), we can quantify the effect of surfactants and JPs on emulsion stability. Figure 6.7a showed the change of ΔE as a function of JP coverage and surfactant concentration. Increasing surfactant concentration led to a more stable emulsion, which is expected. With the same surfactant concentration, increasing JP coverage also helped stabilize the emulsion. It should be noted that within the range of JP coverage in this study (0-0.7), without surfactant, the JP coverage does not have much effect on the emulsion stability (the points on the far left of Figure 6.7a). In fact, we only observed thermodynamically stable emulsion when the JP coverage was >0.9. However, that range was not considered in this study due to the complexity of having arrested coalescence with the presence of surfactants.

In a previous study, we have proven that the effective surfactant concentration on the interface was more important than the total concentration in determining the interfacial tension [49]. Thus, we transformed the axes of the plots by calculating the effective concentration when accounting for the area occupied by JPs in Figure 6.7b. It can be seen that ΔE increases approximately linearly with surfactant effective concentration. When the JP coverage was less than 0.7, the surfactants

played a more important role in stabilizing the emulsion, JPs only helped to increase the effective surfactant concentration. An emulsion droplet with surfactant effective concentration > 0.8 is thermodynamically stable.

The new plots can be fitted using a simple linear model with an R^2 of 0.88. In fact, the plot in Figure 6.7b can be divided into two regions with the effective concentration of surfactants smaller or greater than 0.6. In the region where the effective concentration was lower than 0.6, the number of surfactant molecules was not enough to sufficiently prevent the direct oil-oil contact. Thus, increasing the concentration did not improve the stability significantly, which resulted in a lower slope. When the concentration was higher than 0.6, the total amount of surfactants was large enough; therefore adding more surfactants helped better stabilize the emulsion droplet. The slope was thus higher than the lower concentration region. However, for simplicity, we can just use a linear model to explain the effects of surfactants and JPs on emulsion stability. By substituting the effective concentration with the surfactant concentration and the JP coverage, we have the following equation to predict emulsion stability:

$$\Delta E = \frac{a\, C_{Surf}}{(1-\phi)} - b$$

where C_{surf} is the surface concentration of surfactant (normalize by CMC) and ϕ is the JP coverage. The parameters a and b are a = 42436 and b = 32505. It should be noted that the points with surfactant concentrations of 0 were not included in the determination of the model and its parameters, i.e., the model can only be used when surfactants are present.

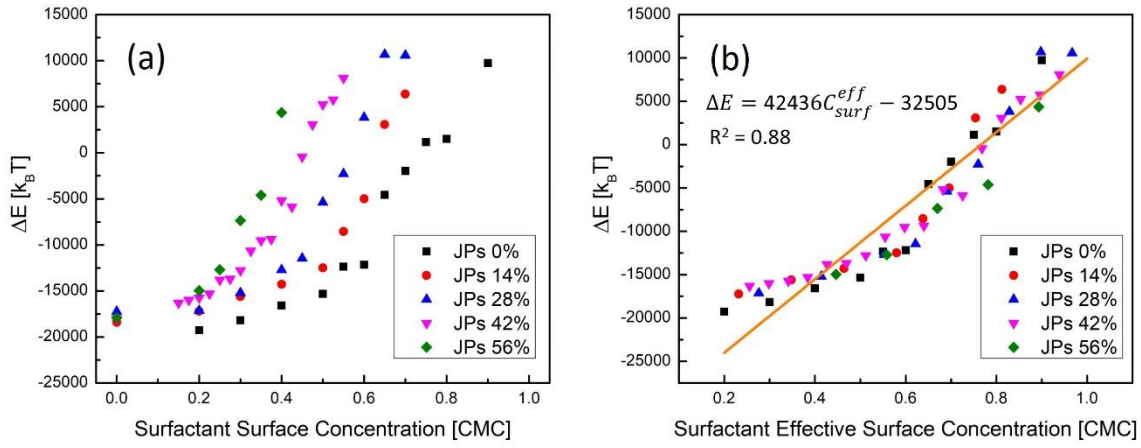

Figure 6.7. Energy difference between the final and the initial state as a function of JPs coverage and surfactant concentration. The surfactant concentration was used as total concentration (a), or effective concentration after accounting for the area occupied by JPs (b).

6.4. Conclusions

In this study, the synergistic effect of sodium dodecyl sulfate surfactants and Janus nanoparticles on the stability of oil-in-water emulsion was investigated using dissipative particle dynamics. During coalescence, the emulsions were contacted first by the Janus particles due to their high volume, leading to the particles being pushed away from the contact region. Without surfactants, the two emulsions merged immediately. The presence of surfactants prevented the coalescence by inhibiting direct oil-oil contact. Further pulling of the emulsions resulted in the diffusion of surfactant from the contact region until a critical value of 0.4-0.6 of CMC surface concentration, at which the two emulsions coalesced. The merged emulsions underwent a transition in shape and formed a new emulsion with a spherical shape to minimize the surface area. The difference of free energy between the final state after coalescence and the initial state was used to quantify the emulsion stability. The results showed that when the particle coverage was less than 0.7 emulsion area, Janus particles alone cannot thermodynamically stabilize the oil-in-water emulsion. However, when combined with surfactants, Janus particles can improve emulsion stability by

increasing the effective surfactant concentration on the emulsion surface. A model to predict the emulsion stability from the particle coverage and surfactant concentration was constructed. The model suggested a linear correlation between the emulsion stability and the effective surfactant concentration. The emulsion is thermodynamically stable if the effective surfactant concentration is higher than 0.8 of CMC surface concentration.

Chapter 7. Effect of Janus Particles and Non-ionic Surfactants on the Collapse of the Oil-Water Interface under Compression

Abstract[§]

Janus particles (JPs) and surfactants express different behaviors at the oil-water interface under compression. When both are present at the interface, their synergies result in a different collapse mechanism than the individual ones depending on the JPs and surfactants concentrations. The DPD coarse-grained modeling was used to probe the synergies between Janus nanoparticles and nonionic surfactant on the stability of an oil-water interface under compression. The interface was covered at 0-55% area by JPs and contained surfactants at 0-55% of the interfacial surfactant concentration corresponding to the critical micelle concentration (CMC). Compression of the interface with only surfactants resulted in the expulsion of surfactant molecules to the water phase once the interfacial concentration of surfactant molecules reached the CMC value. Compression of a Janus particle-laden interface past the closed-packing point led to a buckled interface so that the total interfacial area remained constant upon further compression. When both surfactants and JPs were present at the interface, JPs still caused buckling, which helped retain the surfactant molecules at the interface. The interface exhibited a higher level of deformation in presence of surfactants. When the surfactant concentration was high, under compression, the surfactants were partitioned into the water phase, but the buckling of the interface persisted.

7.1. Introduction

Oil-water emulsions are important in various applications including pharmaceutics, food processing, oil recovery, and drug delivery [1, 5, 6]. In general, emulsions are stabilized using

[§] Material in this study has been published in T.V. Vu, S. Razavi, D.V. Papavassiliou, Journal of Colloid and Interface Science (2021).

surfactants, which decrease the oil-water interfacial tension (IFT) and, thus, the surface free energy [1, 117, 118]. The effectiveness of surfactants as emulsifiers depends on the type of surfactant (ionic or non-ionic surfactant), its molecular length and hydrophilic-lipophilic balance, its concentration, and the pH of the suspension [1, 160-162]. Solid micro- and nano-sized particles (NPs) can also function as emulsifiers [17, 18, 163, 164]. The mechanism for stabilizing the emulsion by particles is different than the one for surfactants. Particles that assemble at the interface limit the direct interaction between oil and water leading to a reduction of free energy [40, 123]. The adsorption of NPs at fluid interfaces is controlled by many particle attributes including wettability, surface charge, size, shape, and particle hardness (soft vs. hard particle) [123, 182-186]. Among different types of anisotropic nanoparticles, amphiphilic particles (i.e., Janus particles) are unique. Janus particles (JPs) are anisotropic since their surface has areas of distinct wettability, where one particle side is hydrophilic and the other side is hydrophobic [19, 20]. Due to their amphiphilicity, JPs have a high tendency to adsorb onto the interface. Theoretical predictions have shown that JPs can possess up to 3-fold higher desorption energy from the interface compared to homogeneous nanoparticles [187]. The surface of JPs can also be modified by various techniques, such as metal vapor deposition, chemical processing, spin-coating, and electroless deposition to achieve a desired set of interfacial properties [188-191]. Thus, JPs have a high potential for tuned interfacial properties when targeting specific applications [188, 190, 192].

Surfactants in combination with NPs have also been used as emulsion co-stabilizers where particles and surfactant molecules function synergistically [5, 193, 194]. In previous studies, we demonstrated that carbon nanotubes could be used as surfactant carriers to an oil-water interface, which could lead to improved oil recovery [150]. Furthermore, the interparticle interactions can be tuned in presence of surfactants. Rahman et. al. demonstrated that the microstructure of the

polystyrene particle-laden air-water interface can be altered by the addition of Tween 80 or sodium dodecyl sulfate (SDS) surfactants [48]. Three distinct interfacial microstructures were identified corresponding to the different ratios of the attractive to repulsive interparticle interactions controlled by the surfactant concentration. While the synergistic effect of homogeneous NPs and surfactants on the oil-water interfacial tension and emulsion stability has been examined in the literature [40, 49-52], a number of studies have also reported on the competitive interfacial behavior in these mixed systems. For example, Smits et. al. reported that adding octadecylamine surfactant molecules could lead to the desorption of aminated silica particles from the decane-water interface due to displacement by surfactants [53]. A recent study by the same group demonstrated that the charges of NPs and surfactants determine whether their combination would lead to synergistic or competitive adsorption. Negatively charged silica NPs could only adsorb to the oil-water interface if it was covered with an oil-soluble cationic surfactant (octadecyl amine). In contrast, increasing the cationic surfactant concentration resulted in reversible desorption of positively charged NPs that were already adsorbed at the interface [54].

In many applications, the emulsions encounter extreme deformation due to applied compressions or because of submission to shear stresses. The stabilization of the emulsions then depends strongly on the response of the stabilizers under these conditions. Surfactant molecules can be exchanged easily between the interface and the bulk phase; thus, the surfactant concentration in the bulk impacts the surface rheology [55]. In contrast, NPs have different response mechanisms to deformation due to their stronger adsorption onto the oil-water interface (i.e., desorption energy on the order of thousands k_BT per particle in comparison to several k_BT per surfactant molecule) [56]. Previous studies for the particle-laden air-water interface subjected to compression have shown that the surface wettability of the NPs dictates the interfacial response. Under compression,

hydrophilic NPs were irreversibly expulsed to the bulk aqueous phase, while the more hydrophobic NPs formed a solid monolayer at the air-water interface that collapsed by buckling and folding [57-61]. Other factors that contribute to the response of NPs to compression are the particle surface charge and presence of an electrolyte, particle shape and softness, and the pH of the suspension [57, 62-64]. A comprehensive review of factors influencing the interfacial rheological behavior of particle-laden interfaces can be found in a recent review article [65].

Despite their high potential for applications, few studies have been dedicated to the response of JPs to applied stresses. Razavi et. al. showed that the amphiphilicity of the JPs controlled their collapse behavior on air-water interfaces [66]. Under applied compressions, JPs with a low degree of amphiphilicity formed a porous multi-layer particle film at the interface, while JPs with higher amphiphilicity resulted in a buckled monolayer at the interface similar to that of hydrophobic NPs [57]. Yin and coworkers also reported that Janus nanosheets exhibit a wrinkling and folding collapse mode. In addition, the oil-water interface covered by Janus nanosheets displayed a larger deformation compared to the bare interface under an applied vertical stress [67]. Compression of the interface containing both NPs and surfactants shows interesting effects. In a recent study, Yazhgure et. al. observed that changing cetrimonium bromide (CTAB) surfactant concentration could alter the collapse mechanism of silica NPs on the air-water interface [45]. At low CTAB concentrations (1×10^{-6} to 4×10^{-5} M), the adsorbed NPs formed a solid-like monolayer, while at higher concentrations, the NP layer was more fragile and formed aggregates when collapsing. Due to the observed increase in the interfacial tension with the addition of NPs, it was concluded that surfactants modify the hydrophobicity of the NPs, which resulted in the change of collapse mechanism.

While these prior studies focused on homogeneous NPs, there is a gap in knowledge on the behavior of a system composed of both surfactants and surface anisotropic JPs, at oil-water interfaces, especially their response to applied stresses. Herein we are tackling this problem using dissipative particle dynamics (DPD) simulation. The main contributions of this study are as follows: (a) we detail the construction and validation of a model containing JPs and surfactants at the oil-water interface with the DPD approach; (b) we investigate the behavior of oil-water interface stabilized with JPs only and surfactants only and the response of the interface to applied compressions; and (c) we explore the synergistic response of JPs and surfactants to interfacial compression.

7.2. Simulation Details

The details of the method [73] and the development of the model that is used here can be found in the previous chapters or our prior published studies [49, 69, 150, 195]. The units reported in this research are reduced dimensionless units [69].

In short, in this study, we used one water bead to represent 6 water molecules. Dodecane ($C_{12}H_{26}$) was used as the oil, represented by 2 oil beads connected by a harmonic bond with a length of 1 r_c and bonding coefficient of 100 k_BT/r_c^2, where r_c is the dimensionless cut-off distance for the DPD model, k_B is the Boltzmann constant and T is the temperature. The nonionic surfactant octaethylene glycol monododecyl ether (C12E8) was chosen as the surfactant. As the DPD method requires all the beads to have roughly the same volume [73], it was reasonable to describe the C12E8 as 6 beads, including 4 hydrophilic head beads and 2 hydrophobic tail beads, connected consequently by 5 harmonic bonds with a bonding coefficient of 100 k_BT/r_c^2. The nanoparticles were modeled as the set of beads distributed on a sphere of diameter 4 r_c. Since the beads themselves are repulsive of each other, the diameter of a nanoparticle was determined using the first peak in the radial

distribution function, which was located at 4.7 r_c (see Figure A1 in Appendix A). For comparison, the approximate length of a surfactant molecule was 3.5 r_c. The NP beads were distributed uniformly on the sphere surface with a distance of 0.3 r_c apart from each other. This arrangement ensured that the solvent beads did not penetrate the NPs, which would result in unphysical behavior. The hydrophobic and hydrophilic NPs used in our simulation represent amidine polystyrene latex and gold, respectively. The oil, surfactant molecules, and NPs were chosen so that the model can be validated by the readily available experimental data in the literature [104, 176]. In a previous study [49], we have demonstrated that Janus particles, which consist of one hydrophobic hemisphere and the other hemisphere as hydrophilic, would result in the highest reduction of interfacial tension compared to other patchy particles when combined with SDS and C12E8 surfactants. Thus, in this study, we used this kind of JPs (50% of the surface hydrophilic and 50% hydrophobic) for our simulations. The representations of each component in the simulation are shown in Figure 7.1

In DPD, the total interaction force between the beads consists of the sum of three different forces: the conservative force, the drag force, and the random force [73]. The drag and random forces are used to capture the hydrodynamics behavior of the fluid [73]. The conservative force is the most important one to represent the physical properties of the system, such as interfacial tension, adsorption to and desorption from surfaces and interfaces, and micelle formation [69, 196]. Thus, the pairwise interaction parameters for the conservative force needed to be carefully constructed to accurately describe the physical system. The parameters for oil, water, and surfactant components were adopted from our earlier studies by matching the simulation results to the experimental data on the oil-water interfacial tension at different surfactant concentrations and surfactant aggregation number in water [69, 150]. The parameters for nanoparticle beads were

adjusted to match the experimentally reported contact angles of the NPs at the oil-water interface [176], where the NPs represented here are amidine polystyrene latex and gold (see Appendix A). The contact angles of the hydrophobic and hydrophilic NPs were $110.7^{o} \pm 1.2^{o}$ and 80.6 ± 2.2^{o}, respectively. The interaction parameters found for the hydrophobic and hydrophilic beads were used to create the apolar and polar faces of the amphiphilic JP. The contact angle value for a JP residing at the oil-water interface was measured to be $93.2^{o} \pm 0.2^{o}$ (Figure A2 in Appendix A). The interaction parameters for the polar and apolar regions of the JPs with the surfactant beads were chosen to be the same as those between the head and tail beads of the surfactant. The interaction parameters for different types of beads in our simulation system are summarized in Table A1 in Appendix A.

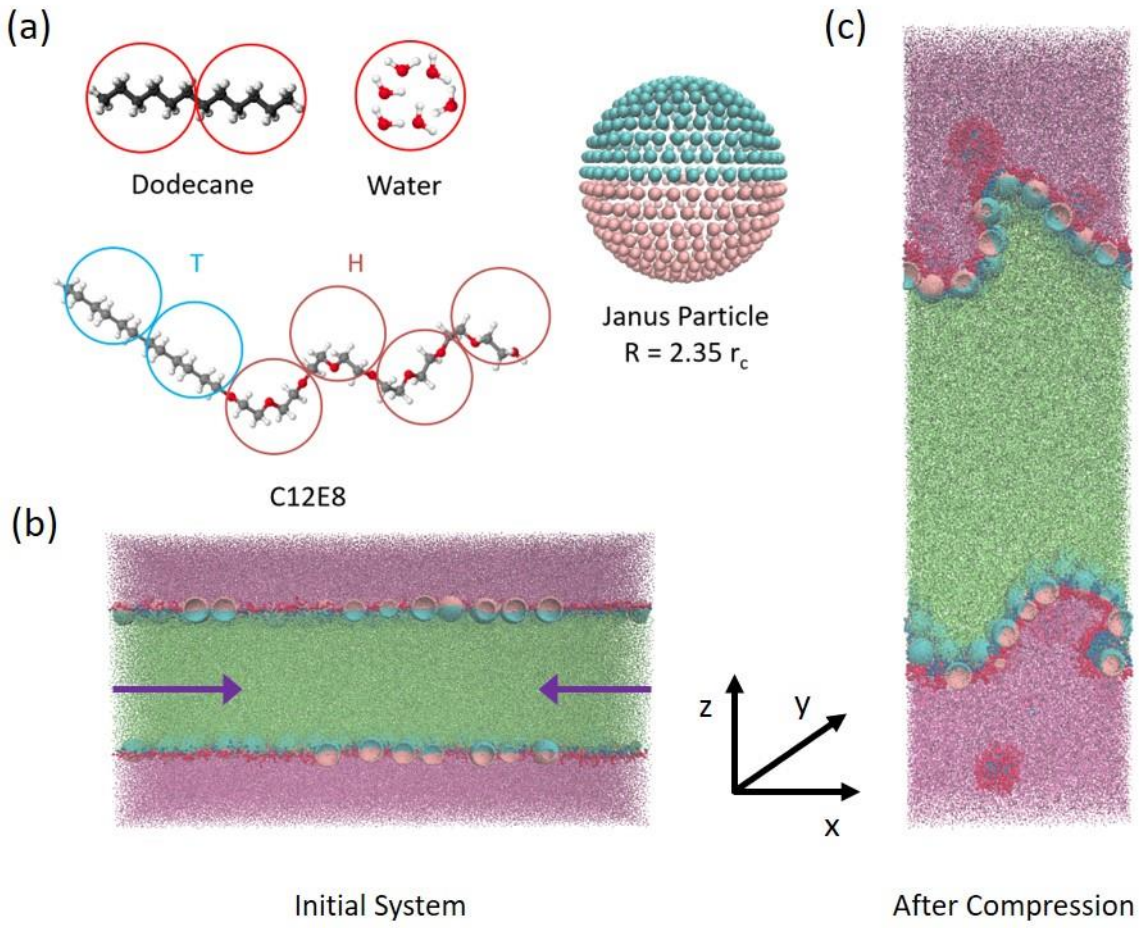

Figure 7.1. Representation of the components used in the system and the configuration of the simulation box. (a) Beads of the DPD model for water, dodecane, C12E8 head (H), tail (T), and the Janus nanoparticles (JPs); (b) Oil-water interfaces with JPs and surfactants at equilibrium before compression, the arrows show the direction of the compression; (c) Snapshot of the interface after compression, where the interface has crumpled, and surfactant micelles have partitioned in the water phase. Purple, green, red, blue, pink, cyan are the colors of water, oil, surfactant head, surfactant tail, and the Janus nanoparticle's polar and apolar beads, respectively. The coordinate axes show the orientation of the simulated system. R and r_c denote the NP radius and the unit of length used in the simulation.

The setup of the simulation is shown in Figure 7.1. The size of the initial computational box was 90×20×50 in DPD reduced units. Periodic boundary conditions were applied, which resulted in two oil-water interfaces, as shown in Figure 7.1b. The surfactants and NPs were distributed at the interface at the beginning of the simulation to avoid the computational time required for adsorption

from the bulk. Different NP coverages were used, ranging from 0-55% of the initial interfacial area at the initial state before compressions. It is known that the maximum surfactant concentration at the interface is the one corresponding to the critical micelle concentration (CMC) in bulk [1]. With C12E8 surfactant, this maximum interfacial concentration is 2.6×10^{-10} mol/cm^2 [104]. The interfacial concentration of surfactant used in our study was adjusted as a percentage of this maximum concentration at the initial state and is reported as % CMC concentration. The range of the surfactant concentration was 0-40% of the CMC concentration in studies that used a combination of surfactants with NPs, and 60-75% of the CMC when surfactants were present at the interface by themselves. For the compression study, the initial simulation box was compressed along the *x*-direction (see Figure 7.1b from 90 r_c to 36 r_c; thus, the final area of the *xy* plane was 40% of its original area. Protocols for choosing the suitable box size and compression speed are presented in Figure A3 in Appendix A.

The NVT ensemble – constant number of beads, volume, and pressure was employed in our study. The Berendsen barostat [177] was applied at the beginning of the simulations to ensure that all studies were carried out under the same pressure. The potential interaction energies between components that were at the interface at the beginning of the simulation were recorded during the compression process. The system equilibrated for a period of 2×10^5 timesteps to make sure that the temperature, pressure, and interfacial tension were stable prior to compressing the interface. The compression was carried out over 2×10^6 timesteps followed by an equilibration period of 2×10^5 timesteps. Next, the calculation of density profiles and the quantification of the interface collapse were performed.

7.3. Results and Discussion

a. Compression of oil-water interface with surfactants

In this section, we investigate the behavior of surfactants at the oil-water interface under compression. Figure 7.2 is a depiction of the evolution of the system during the compression process. As the interfacial area decreased, the surfactants became more concentrated at the interface. It is well-known from the Gibbs equation for soluble surfactants that the surface concentration of the surfactant would reach a maximum at the critical micelle concentration (CMC) [118]. Beyond that concentration, the added surfactants would be incorporated into micelles. Here, we observed the same behavior. For brevity, we will call the interfacial concentration of surfactants corresponding to the CMC in bulk as *interfacial CMC*. Once the amount of surfactant present at the interface reached the interfacial CMC due to the applied compression, the surfactant molecules were ejected from the interface into the water phase, as can be seen in Figure 7.2b. The free molecules of surfactant grouped together to create micelles. At a higher level of compression (Figures 7.2c-7.2d), more surfactant molecules were expelled from the interface to keep the concentration constant at the interfacial CMC. The analysis of density profiles for the surfactant molecules confirmed that upon compression of the interface past the interfacial CMC, the surfactant concentration at the interface remained unchanged at the interfacial CMC regardless of the initial surfactant concentration at the interface (see Figure A4 in Appendix A).

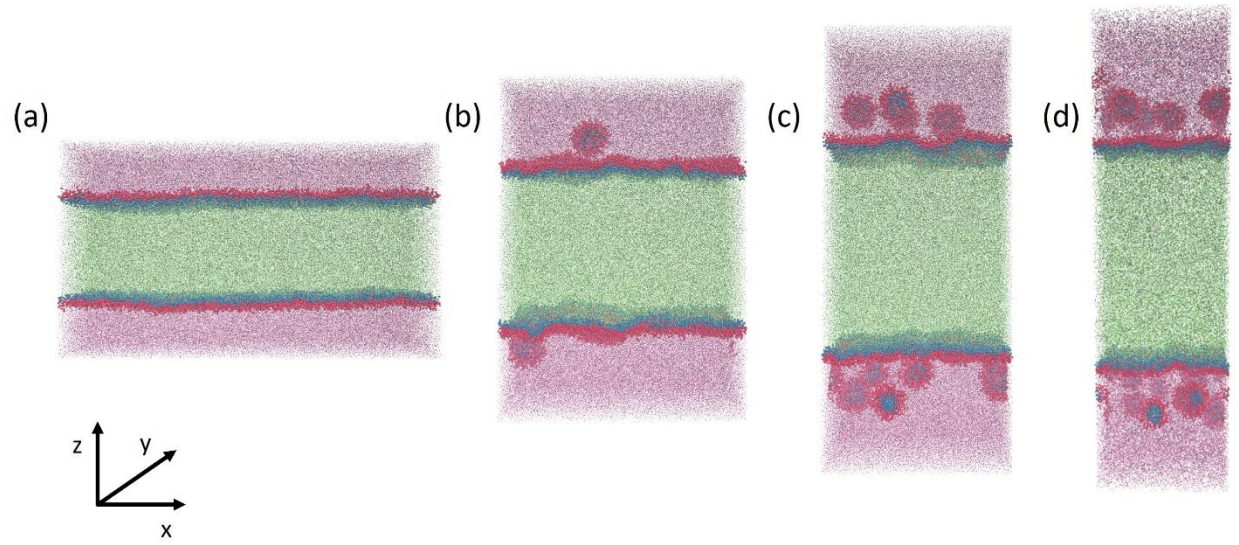

Figure 7.2. Snapshots of the system containing surfactants at the oil-water interface under compression at (a) 100%, (b) 70%, (c) 50%, and (d) 40% of the initial interfacial area. The color scheme is similar to that used in Figure 7.1.

When investigating the response of interfacial layers to applied compressions experimentally, via a Langmuir trough, the plot of surface pressure as a function of the area is conventionally used. It has been shown that the main contribution to the surface pressure is through the interactions of components present at the interface, which are mediated by the two fluids [64]. Thus, the interaction potential energy between surfactant molecules or nanoparticles was used in this computational study to quantify the behavior in both the surfactant-only systems and the mixed particle/surfactant system. The change in the average potential energy acting on one surfactant molecule by other surfactants during the compression process is shown in Figure 7.3a as a function of the fraction of the interfacial area, A/A_o, where A_o is the initial interfacial area before the compression process was initiated. As the interfacial area decreased, the surfactant molecules became more crowded at the interface. Therefore, the potential energy exerted on a molecule from all other surfactant molecules increased. The potential energy increased up to a maximum value at

elevated surfactant concentrations corresponding to the interfacial CMC. After interfacial CMC was reached, some surfactant molecules were expelled from the interface into the bulk water phase; therefore, the overall average distance between surfactant molecules increased, leading to the reduction of the measured potential energy, as seen in Figure 7.3a. The magnitude of the maximum energies was comparable in all cases, indicating that the number of surfactant molecules at the interface at the point of relaxation was the same regardless of the initial concentration. Increasing the initial concentration of surfactant molecules resulted in reaching the maximum in the potential energy at a larger interfacial area, as the interface became saturated with surfactant molecules at a lower level of compression. Figure 7.3b is a plot of the derivative of the data in Figure 7.3a, i.e., it is the rate of change of the average potential energy with the normalized interfacial area, A/A_0. Although no noticeable change was observed in this profile for the case of surfactant molecules, it is included here for comparison with the JP studies discussed in the next section.

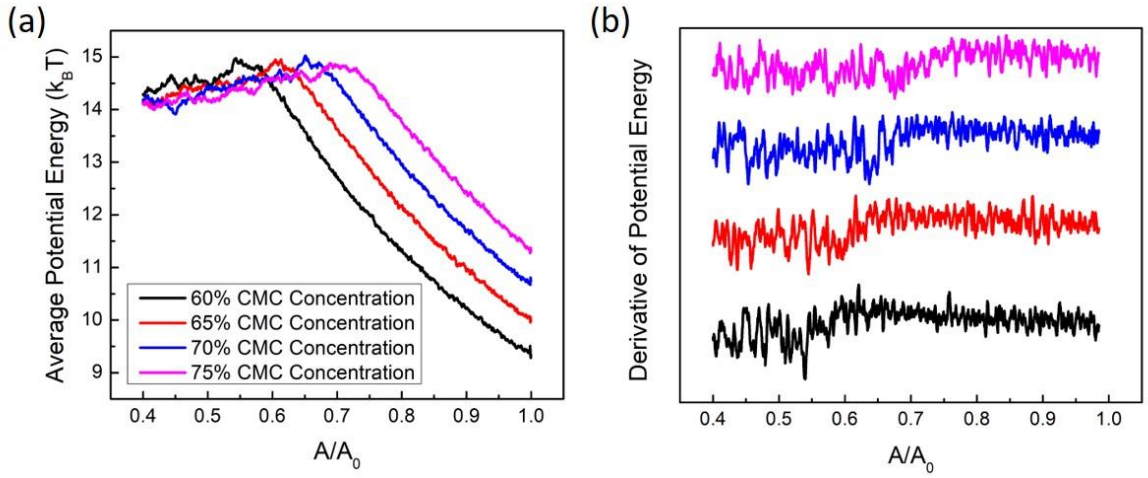

Figure 7.3. Interface with only surfactant, (a) average intermolecular surfactant – surfactant potential energy (APE) as a function of the relative interfacial area, (b) the derivative of the potential energy, -d(APE)/d(A/A_0). Note that the derivative curves in panel (b) are spaced out for visual clarity.

b. Compression of oil-water interface with Janus particles

In this section, we study the responses of the JPs at the oil-water interface under compression with a focus on their behavior compared to the surfactant molecules. Figure 7.4 is a set of snapshots of the system with 55% initial JP coverage at different degrees of compression. As expected, the layer of JPs at the interface became denser when the interface was compressed. Once the JP coverage reached the maximum allowable packing (~ 80 ± 1% coverage of the interfacial area calculated based on the position of the first peak in the radial distribution function, Figure A1), there were two different behaviors available to the particles: interface buckling or particle expulsion from the interface [57-59]. In buckling, the interface bends to create more space, relative to the area of a flat interface projected in the *xy* plane, to accommodate and retain the trapped NPs at the interface. This phenomenon is known to occur when NPs experience attractive interparticle interactions and have a high tendency to stay at the interface as a solid film. In contrast, particle expulsion to the bulk phase occurs in the case of NPs with lower desorption energy (i.e., low contact angle at the fluid interface) and/or repulsive interparticle interactions [57]. For Janus particles in this study, buckling was the favored collapse mode as shown in Figure 7.4. For comparison, the collapse modes of homogeneous hydrophilic and hydrophobic NPs, and JPs under compression are illustrated in Figure 7.5. It is seen that particle expulsion occurred with the hydrophilic and hydrophobic NPs, where a multilayer of NPs was formed at the interface with compression. The JPs resulted in the buckling of the interface. Under compression to 80 ± 1% coverage of the interface, the hydrophilic and hydrophobic NPs were displaced into the water or oil phase, respectively.

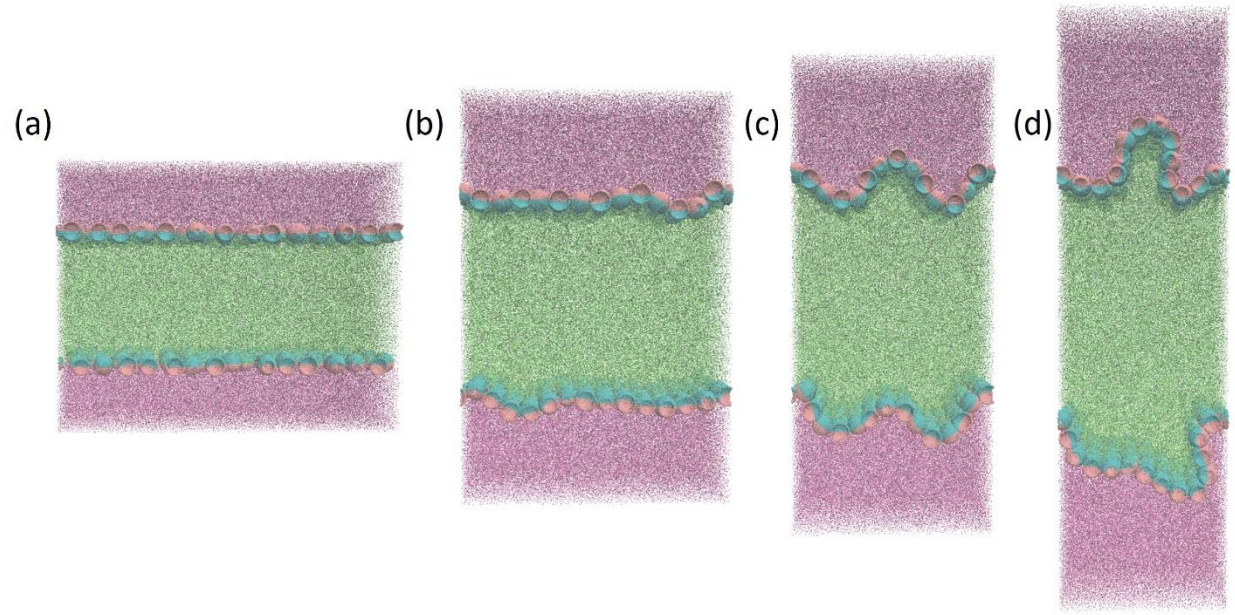

Figure 7.4. Snapshots of the system containing 55% initial JPs coverage at the oil-water interface under compression at (a) 100%, (b) 70%, (c) 50%, (d) 40% of the initial interfacial area. The color scheme is similar to that in Figure 7.1.

In a recent study, Razavi et. al. reported that the behavior of JPs at the air-water interface under compression depends on their amphiphilicity and configuration at the interface [66]. Molecular Dynamics simulations showed that the rotational motion of amphiphilic JPs, around the axis parallel to the plane of the interface, was restricted when compared to that of homogeneous NPs. Langmuir trough experimental studies of the particle monolayers at the air-water interface illustrated that JPs of low amphiphilicity exhibit random orientation at the interface and form a porous multi-layer film at the interface after the collapse, while JPs with a high degree of amphiphilicity reside at the interface with the Janus cap perpendicular to the plane of interface and collapse via wrinkle and fold formation. The angle representing the orientational alignment of particles at the interface was calculated for both homogeneous and Janus particle systems to examine the link between the JP cap alignment with the interface and the particle rotational motion with the buckling behavior under compression. As shown in Figure 7.5d, the polar angle (θ_{polar})

is defined as the angle between a normal vector $\vec{n}$ connecting the center of the particle and a chosen bead (top or bottom) on the NP surface and the basis vector $\vec{k}$ in the z-direction, which is perpendicular to the oil-water interface. This angle could take values from 0 to 180°. The distribution of the polar angle for each NP can be found in Figure A5 of the SI.

For quantification of the orientational distribution of particles, the order parameter (S) is commonly used. This parameter is calculated as follows [197]:

$$S = \langle \frac{3cos^2\theta - 1}{2} \rangle \tag{7.1}$$

where θ is the polar angle and the brackets represent ensemble averaging. For a randomly oriented set of particles, S = 0, whereas S = 1 indicates perfectly aligned particles. The values of S for the hydrophobic and hydrophilic NPs are 0.0006 ± 0.00002 and -0.0115 ± 0.0004, respectively, which are close to 0. Thus, it can be concluded that the homogeneous NPs were randomly oriented at the oil-water interface. When introducing amphiphilicity to the particle, the order parameter S was 0.9736 ± 0.042, indicating that JP caps were perpendicular to the interface as a result of the particle's restricted rotation caused by its high amphiphilicity. This observation agrees with the study by Razavi et. al. that the configuration of JPs trapped at the interface influenced the interparticle interaction and the resulting response of the interfacial monolayer under compression.

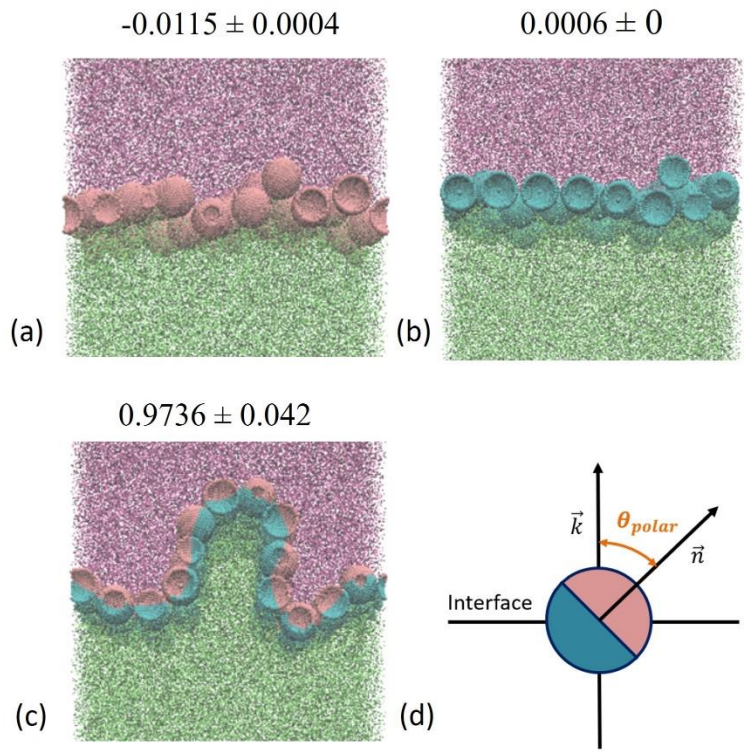

Figure 7.5. Final configuration of the system containing 55% initial coverage of (a) homogeneous hydrophilic NPs, (b) homogeneous hydrophobic NPs, and (c) JPs after compression at 40% of the initial interfacial area. The color scheme is similar to that of Figure 7.1. (d) Schematic with the definition of the orientation angle between vectors $\vec{k}$ and $\vec{n}$. The order parameters (S) calculated from the polar angle data are placed above the corresponding snapshot.

The change of the average intermolecular potential energy between Janus particles during compression is presented in Figure 7.6a. There are several differences in the plot for particle-laden interfaces compared to that for surfactants (Figure 7.3). Surfactants are small molecules that can move freely at the interface, while the JPs consist of many beads that move together. Under the applied compression, the average potential energy of surfactants increased immediately (and linearly) as the average distance between the molecules decreased. In the case of JPs, at the beginning of the compression, the potential energy did not exhibit an appreciable change as the JPs were still far from each other. Once particles come close enough, i.e., within the cut-off radius, suddenly, all the JP beads were in the range where they strongly interact with each other.

Consequently, the potential energy between the particles increased abruptly followed by an almost constant value, which corresponds to regimes beyond the interfacial collapse via buckling. Compressing the interface beyond this point did not lead to a drastic change in the interparticle potential energy because the interfacial area remained constant and the distance between the JPs could not be reduced any further. Therefore, further compression resulted in a higher degree of bending of the interface, while the interparticle separation between JPs remained unchanged. When increasing the initial particle coverage at the interface, the shape of the profile for the interparticle interaction energy remained similar but the onset of the transition to a plateau value shifted to a higher A/A_0. A noteworthy observation is the inflection point on the potential energy plot, which can be seen clearly as a peak in Figure 7.6b that illustrates the derivative of the interparticle interaction energy. This inflection point indicates the onset of 2D to 3D transitions corresponding to the collapse of the interface [57] as illustrated by the snapshot in the inset of Figure 7.6b.

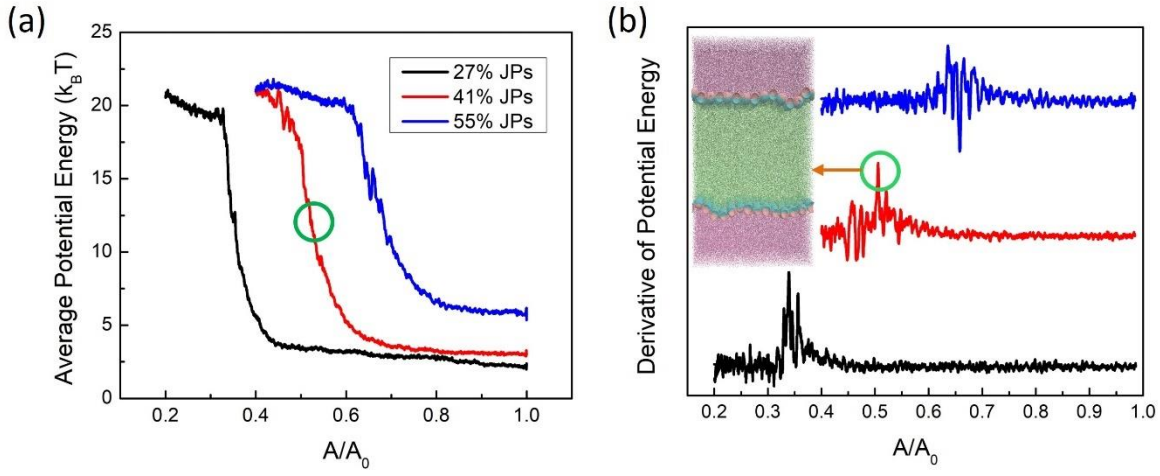

Figure 7.6. Interface with only JPs, (a) average intermolecular JP-JP potential energy (APE) as a function of the relative interfacial area for a particle-laden interface under compression, (b) the derivative of the potential energy curve in (a), $-d(APE)/d(A/A_0)$. The green circle in each plot indicates the area at which the interface starts to crumple as schematically shown in the inset of

(b). Note that the curves are spaced out for visual clarity while the baseline for all the plots in (b) is at the same level.

c. Compression of oil-water interface with Janus particles and surfactants

In the previous sections, we compared the behavior of surfactants and JPs at the interface under compression. In this section, we focus on the synergistic effects of JPs and surfactants at the interface under compression. Figure 7.7 is a collection of snapshots at the end of compression (i.e., $A/A_0 = 0.4$) of the system containing 41% initial JPs coverage with surfactant at different concentrations. Under applied compressions, the interface covered with JPs and surfactant molecules (Figure 7.7b-c) buckled in order to retain the particles at the interface due to their high desorption energy. This phenomenon is analogous to the case of JPs in the absence of surfactants (Figure 7.7a). However, in contrast to the surfactant-only systems, surfactant molecules stayed on the JP-laden interface instead of partitioning into the water phase. The presence of JPs thus enhanced the retention of surfactant molecules at the interface by collapsing via buckling and keeping the interfacial area available to surfactants constant despite the continued compression. In addition, the presence of surfactants further distorted the interface, compared to the JP-only system, as will be quantified later. At a higher surfactant concentration of 30% interfacial CMC (Figure 7.7d), the available interfacial area created by wrinkling in presence of JPs was not enough to accommodate all surfactant molecules; consequently, some surfactant molecules had to migrate to the water phase. At 40% interfacial CMC (Figure 7.7e), a larger number of surfactant molecules appeared in the bulk water phase compared to the case of 30% interfacial CMC.

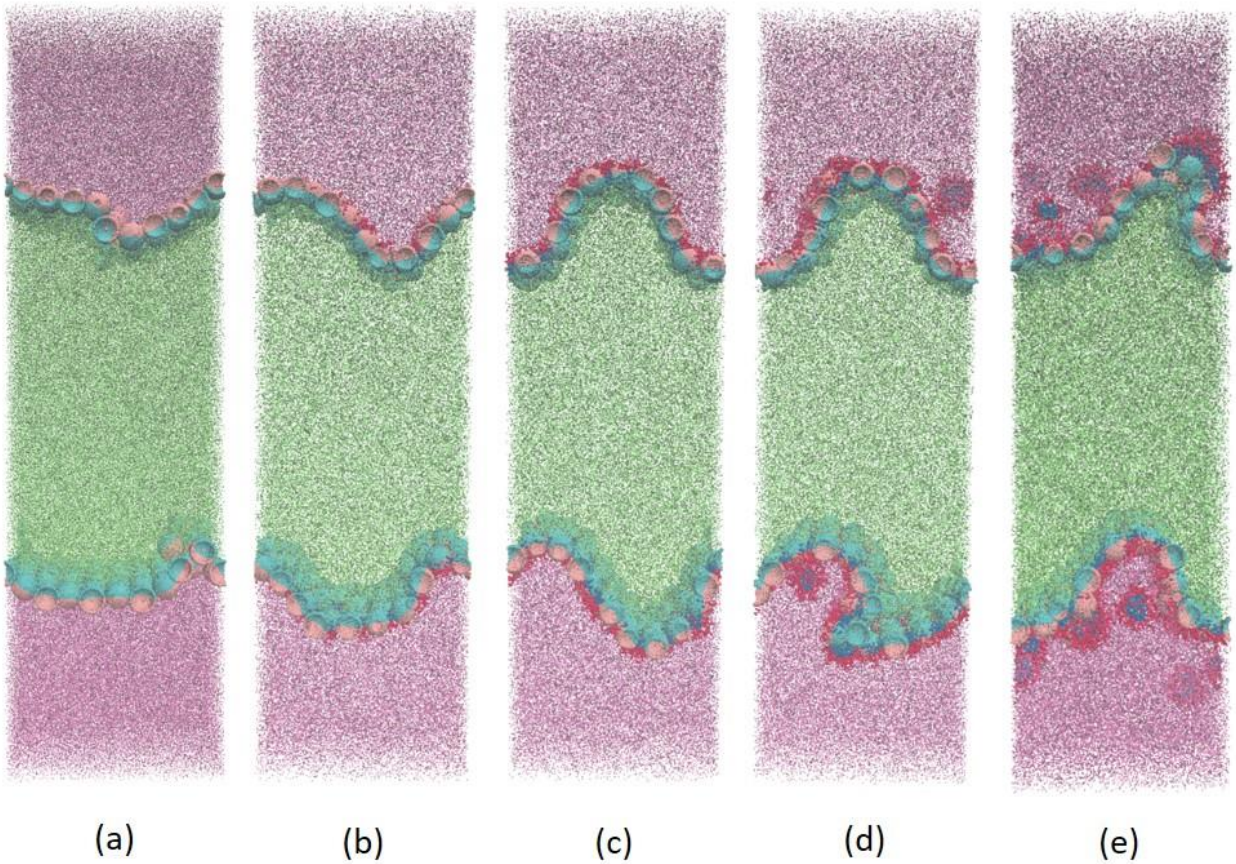

Figure 7.7. Snapshots after compression of the interface to 40% of the initial area for systems containing 41% JPs coverage with (a) no surfactants, (b) 10% CMC, (c) 20% CMC, (d) 30% CMC, (e) 40% CMC surfactant at the interface. The color scheme is similar to that of Figure 7.1. Note the surfactant and particle interfacial concentrations were calculated based on the total initial area of the interface in the absence of compressions.

As can be seen in the snapshots of Figure 7.7, JPs remained attached to the interface for all cases with different surfactant concentrations and with the Janus cap perpendicular to the interface as confirmed by the order parameter in Figure 7.5c. This behavior allowed the use of JPs to quantify the change incurred to the interface in presence of surfactants. To track the shape of the interface, we plotted the density profile of JPs along the *z*-direction at different surfactant concentrations, as illustrated in Figure 7.8a. The peaks on each plot show the position where most JPs settled, which coincides with the location of the interface. Without surfactant, the peaks were sharp and narrow,

indicating that the JPs were concentrated in a small space, which also means the interface is bent to a lesser extent. Adding surfactants led to wider peaks as shown on the 10, 20% CMC plots. Since the total number of JPs is the same for all cases, the total area of the peaks is constant, meaning the heights of the peaks were reduced to compensate for the increased width. These changes of the peaks indicate the modification of the interface with added surfactants. The interface endured a higher degree of bending, in line with the observations made in Figure 7.7. The reason is that although surfactants are small molecules, they do occupy space at the interface and interact with JPs. Therefore, in presence of surfactants, the interface buckled earlier (at a higher A/A_0), to retain the JPs, which have large desorption energy, at the interface.

To clarify the combined effect of surfactants and JPs, we performed a calculation of surfactant concentration at the interface during compression. The initial surfactant concentrations were calculated based on the entire interfacial area of the interface. When we factored in the area occupied by JPs, the interfacial area available to surfactants is smaller. Therefore, the *effective surfactant concentrations* would be 0, 17, 34, 51, 68% of the interfacial CMC instead of the nominal values of 0, 10, 20, 30, 40%. At the beginning of compression, the JPs covered 41% of the interface for all cases. The final area of the interface in the *xy* plane was 40% of the initial area, meaning that without buckling the available flat interfacial area would only be sufficient to accommodate the retention of JPs, and all the surfactant molecules would be expected to get pushed into the water phase. However, the presence of JPs buckled the interface and prevented it from further shrinking, which kept the interfacial area unchanged beyond the point of buckling. The effective surfactant concentrations for the 10 and 20% CMC cases at the point of buckling were 56 and 98% CMC, respectively. As these values are lower than the interfacial CMC, the surfactant molecules were not desorbed from the interface. For the cases of 30 and 40% CMC, the

surfactant molecules were partitioned to the water phase before the buckling had occurred, and the effective surfactant concentration was kept at the CMC. This behavior was also reflected in Figure 7.8a as the density profiles for the JPs were unchanged when the surfactant concentration changed from 30 to 40% CMC. The reason is that as the interface was saturated with surfactants and JPs, the excess surfactants were pushed into the water phase, but the shape of the interface did not change.

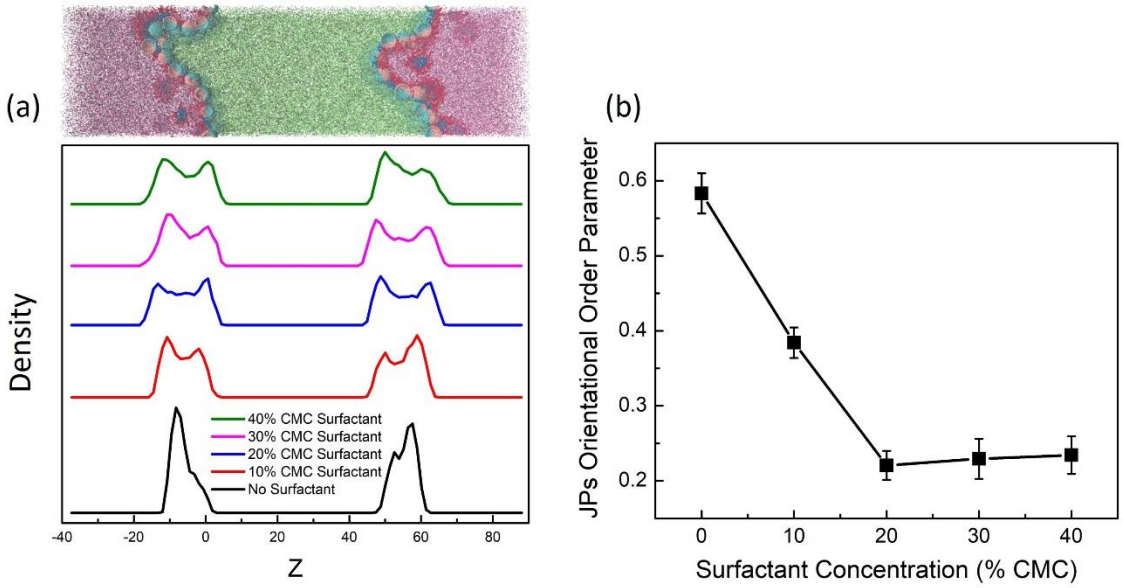

Figure 7.8. (a) Density profiles of JPs along the z-direction with the presence of surfactants at the oil-water interface and after compression of the interface to 40% of its initial area. The snapshot on top represents the system orientation used in the plots. Note that the baselines of all the plots are at the same level. (b) Change in the level of interface distortion with the surfactant concentration. The interface distortion level was quantified using the order parameter of JPs.

In the previous section, it was demonstrated that JPs aligned themselves such that the Janus cap remains perpendicular to the interface. Assuming that they behave the same way when the interface is distorted, we can use the orientational configuration of JPs to quantify the degree of buckling of the interface. As illustrated in Figure 7.7, once buckled, the interface was no longer flat, meaning that it was not aligned along the z-direction (i.e., on the *xy* plane). Assuming the JPs always remain

perpendicular to the interface, tracking the distribution of the angle between the vector $\vec{n}$, normal to the JP cap, and the basis vector $\vec{k}$ of the z-direction (used in Figure 7.5d) can provide insights on the shape of the interface and the effect of surfactants on interfacial distortions. The orientational order parameter (S) could be used as an indicator for the level of distortion of the interface. Considering that JPs orient themselves perpendicular to the interface, as confirmed in Figure 7.5c, a lower value of the parameter is an indirect measurement of the interface degree of wrinkling and indicates a more severe distortion from a flat interface. Figure 7.8b is an illustration of the change of the orientational order parameter of the JPs as a function of surfactant concentration. When increasing the nominal surfactant concentration from 0 to 20% CMC, the order parameter dropped from 0.58 ± 0.03 to 0.22 ± 0.02, showing that the presence of surfactant further deformed the interface compared to the JP-only system. In addition, the interface reached saturation at a surfactant concentration of 20% interfacial CMC, which is illustrated by the plateau from 20 to 40% CMC. This observation indicated that there were no notable changes in the shape of the interface at surfactant concentrations higher than 20% CMC. Thus, we can conclude that the interface reached a limit of deformation.

The change in the average intermolecular potential energy between JPs during compression and with different surfactant concentrations is illustrated in Figure 7.9a. It is shown that adding surfactants resulted in the reduction of the potential energy between JPs. In the presence of surfactant molecules at the interface, JPs could not come close to each other as in the case of particle-only systems. As the interparticle potential energy depends on the distance between the particles, its value was reduced in presence of surfactants because the surfactants were effectively increasing the interparticle spacing. At lower nominal surfactant concentrations of 10 to 20% CMC, the shape of the potential plot remained similar. In addition to the lower value of the

potential energy, the other difference between the plots in this regime and that of JP only system was the position of the inflection point, representing the buckling, which occurred at a larger normalized area for the mixed system as reflected in the potential energy derivative plot (Figure 7.9b). This is expected since the surfactants occupied parts of the available interfacial area, thus, the buckling occurred at a lower degree of compression in the mixed system. At higher initial surfactant concentrations (30 and 40% CMC), the sudden rise of the potential energy disappeared; instead, the potential energy increased slowly and to a much smaller value at the final compressed state, compared to the system with lower surfactant concentration (<20% CMC). This behavior was also captured on the derivative plot (Figure 7.9b) as the peak gradually disappeared when the surfactant concentration increased. To explain this behavior, we should recall that JPs consist of many beads. The beads must move together; thus, when their distances were reduced to a critical level, there was an abrupt surge in the potential as many of them were close to each other. This phenomenon expressed itself as peaks in the potential energy derivative plot. As the number of surfactant molecules at the interface rose, the average distance between JPs increased as they could not come as close to each other as before. With high enough surfactant concentration, the surfactants could block the JPs from reaching the critical distance of 4.7 r_c, which is the JPs diameter. This can be observed by looking at the plots of the radial density distribution for the JPs in Figure 7.9c. Note that to obtain these plots, we only used the center of mass of each JP instead of all the JP beads. The first peak in each plot, at around 4.7 r_c, represented the average interparticle distance between the closest neighbor particles. The height of this peak decreased as the initial surfactant concentration increased, indicating that the average interparticle distance between the closest neighbors increased. When the initial surfactant concentration was higher than 20% CMC, there appeared a secondary peak at 6 r_c, with an even higher height than the first peak, which

suggested the shift of the JPs to larger distances from each other on average. The results from the radial density distribution confirmed that the presence of surfactants blocks the JPs from reaching the distance that separated them in a particle-only system. Consequently, the sudden jump in the potential plot was not observed.

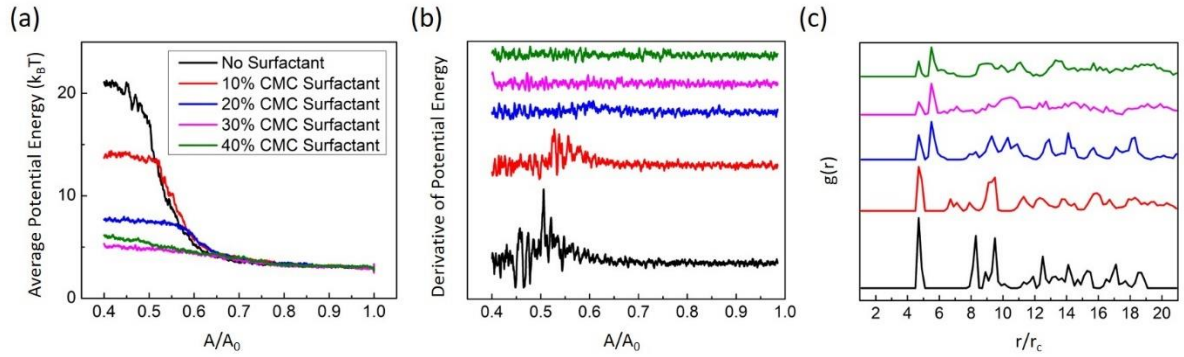

Figure 7.9. Interface with 41% JPs coverage at various initial surfactant concentrations, (a) average intermolecular JP-JP potential energy (APE) as the function of the relative interfacial area; (b) the derivative of the potential energy, -d(APE)/d(A/A_0); (c) radial density distribution of the JPs after compression to 40% A/A_0. Note that the curves are spaced out for visual clarity and the baseline for all the plots in (b) is at the same level.

7.4. Conclusions

In this study, we provided the first report on the combined behavior of nonionic surfactant molecules and Janus particles at the oil-water interface subjected to compression. When the interface contains only surfactants, the compression beyond a critical area results in the partition of surfactant molecules into the water phase and the formation of micelles in the bulk in order to keep the interfacial concentration of the surfactant constant, in accordance with the CMC value in bulk [1]. In contrast, Janus particles remained adsorbed to the interface even under the applied compressions, which resulted in buckling of the interface. The average potential energy between components at the interface during compression further showcased the distinct behavior of surfactants and Janus particles. The plot for Janus particles exhibited an inflection point

representing the onset of interface collapse via buckling, whereas this point did not exist in the corresponding plot for surfactant-only systems, where the interface remained flat under the applied compression. The individual behavior of surfactants and Janus particles was in agreement with several previous experimental studies [57, 66, 69].

When both surfactants and Janus particles were present at the interface, we observed a synergism under compression that has not been reported before (to the best of our knowledge). Due to their high desorption energy, the presence of Janus particles at the interface led to the wrinkling of the interface under the applied compression. Due to the additional area available to surfactants in the buckled stated compared to a flat interface, the surfactants remained at the interface when their effective interfacial concentration was kept at a value lower than the interfacial CMC. In contrast, surfactant-only interfaces stay flat, and the surfactants partition into the bulk phase under compression [1, 117]. This highlights the role of Janus particles in the behavior of the mixed system.

With the assumption that Janus particles always orient themselves vertically to the interface, we employed the order parameter of Janus particles as indications of the degree of deformation of the interface. The JP density profile and the distribution of the JP orientation angles indicated that the presence of surfactants at the interface distorted the interface at a higher level compared to Janus particles alone. At higher concentrations, adding surfactants did not affect the configuration of the interface as the excess surfactant molecules were desorbed into the water phase. The synergism of surfactants and Janus particles at the interface was also reflected in the potential energy. The addition of surfactants reduced the interaction potential energy between Janus particles as the presence of surfactants increased the interparticle spacing at the interface. In addition, the inflection point, marking the onset of the interfacial collapse via crumpling, gradually disappeared

with the addition of surfactants, and the surfactants distorted the interface at a higher level compared to JPs by themselves.

This mechanistic understanding of the combined effects of surfactants and JPs in stabilizing the oil-water interface can be used to design emulsifiers and processes for the separation of oil and water. The presence of JPs that leads to buckling of the interface could be explored in applications for interfaces that are not flat, e.g., for cases when drops are drying, and a higher mass transfer area can be achieved.

Chapter 8. Summary and Future Works

8.1. Summary

This dissertation focused on the effects of surfactants and NPs on the properties of the oil-water interface when used simultaneously as emulsifiers. The main conclusions can be drawn as follows:

- We established a protocol to estimate and validate the interaction parameters for DPD simulations of systems containing surfactants at the oil-water interface. The procedure to describe the interfacial regions is summarized as follows: The exact number of surfactant molecules to be placed at the interface at the CMC for the simulation was calculated from the Gibbs adsorption equations. The surfactant molecules were then described to satisfy the two criteria: (a) the interface is saturated with the number of placed surfactants, and (b) the interface is flat, stable. Finally, the conservative interaction parameters were varied to match the IFT of the oil-water-surfactant system at CMC. This protocol could be applied to other coarse-grained simulation methods.
- The feasibility of using CNTs as vehicles to carry surfactant molecules to the oil-water interface was explored by studying the behavior of the surfactant-adsorbed-carbon nanotube at the interface. It was found that once the surfactant-adsorbed-CNTs arrive at the oil-water interface, all the surfactant molecules desorb from the CNTs and distribute at the interface, leading to a reduction of the oil-water IFT to values observed at the critical micelle concentration (CMC) of the corresponding surfactants. At equilibrium, the contribution of the CNTs on the reduction of IFT depended on the surfactant interfacial concentration. At low concentration, CNTs stayed at the interface, reducing the IFT further than for a system with only surfactant. Increasing surfactant concentration resulted in the gradual push of the CNTs into the oil phase from the interface. When the surfactant concentration was high enough, the CNTs migrated into the oil phase, and the IFT was not affected.

- Adding NPs to an oil-water interface with the presence of surfactants further reduces the oil-water IFT, leading to a more stable emulsion. The synergistic effect between NPs and surfactants can be explained by considering that the presence of NPs leads to the less interfacial area available to be occupied by surfactants so that fewer surfactant molecules are needed to generate a larger IFT reduction than when they are alone at the interface. We demonstrated that the wettability of NPs is the most important factor in the combined effect with surfactants. Among different types of NPs, the maximum synergism occurs when the NPs reside at the interface, maximizing the interfacial area they occupy and minimizing the area that is available to surfactants. This happens when the NPs equator line is at the interface, which is observed with the JP 50-50 particles and the H 75-25 particles. For JP 50-50, the equal number of hydrophobic and hydrophilic beads on the NP makes it settle in the middle of the interface. In the case of the heterogeneous particle, the H 75-25 is the most effective type of particle because the attraction of the two surfactant tail beads pulls the H 75-25 closer to the surfactant tail, reducing the number of direct contacts between oil and water molecules. The observation of the different behavior of the various NPs also allows some suggestions for the design of NPs for stabilizing emulsions using fewer NPs and surfactants. For Janus particles, the JP 50-50 should be used. For heterogeneous particles, the optimal ratio of hydrophobic over hydrophilic surface coverage depends on the structure of the surfactant molecules. When a surfactant with a long tail and a short head is used, the portion of hydrophobic beads on the particle should increase to shift it close to the tail region at the interface, and vice versa.
- During coalescence, the emulsions were contacted first by the Janus particles due to their high volume, leading to the particles being pushed away from the contact region. Without surfactants, the two emulsions merged immediately. The presence of surfactants prevented the

coalescence by inhibiting direct oil-oil contact. Further pulling of the emulsions resulted in the diffusion of surfactant from the contact region until a critical value of 0.4-0.6 of CMC surface concentration, at which the two emulsions coalesced. The merged emulsions underwent a transition in shape and formed a new emulsion with a spherical shape to minimize the surface area. The difference of free energy between the final state after coalescence and the initial state was used to quantify the emulsion stability. The results showed that when the particle coverage was less than 0.7 emulsion area, Janus particles alone cannot thermodynamically stabilize the oil-in-water emulsion. However, when combined with surfactants, Janus particles can improve emulsion stability by increasing the effective surfactant concentration on the emulsion surface. A model to predict the emulsion stability from the particle coverage and surfactant concentration was constructed. The model suggested a linear correlation between the emulsion stability and the effective surfactant concentration. The emulsion is thermodynamically stable if the effective surfactant concentration is higher than 0.8 of CMC surface concentration.

- Under interfacial compression, the oil-water interface changes shape and behaves in different ways depending on the type of surface-active additives. When the interface contains only surfactants, compression beyond a critical area results in the partition of surfactant molecules into the water phase and the formation of micelles in the bulk in order to keep the interfacial concentration of the surfactant constant, in accordance with the CMC value in bulk. In contrast, Janus particles remained adsorbed to the interface even under severe compression, which resulted in buckling of the interface. When both surfactants and Janus particles were present at the interface, we observed a synergism under compression that has not been reported before. Due to their high desorption energy, the presence of Janus particles at the interface led to the wrinkling of the interface under the applied compression. Due to the additional area available to surfactants in the

buckled state compared to a flat interface, the surfactants remained at the interface when their effective interfacial concentration was kept at a value lower than the interfacial CMC. In contrast, surfactant-only interfaces stay flat, and the surfactants partition into the bulk phase under compression. This highlights the role of Janus particles in the behavior of the mixed system. The presence of surfactants at the interface distorted the interface at a higher level compared to Janus particles alone. At higher concentrations, adding surfactants did not affect the configuration of the interface as the excess surfactant molecules were desorbed into the water phase.

8.2. Suggestions for Future Research

Based on the methodology and findings from this thesis, several research topics can be developed:

- Effect of surfactants and different types of NPs at the interface under compression. We have just studied the Janus particles while the other types of NPs such as homogeneous NPs were not considered. The contact angle of NPs can affect the behavior of the system under stress.
- Effect of NPs shape and size on emulsion stability when used separately or combined with surfactants. When the NPs are larger, the steric effect becomes more pronounced. However, the total area covered by NPs is higher with small NPs. Thus, we are uncertain about the efficiency of NPs in stabilizing emulsion when increasing their size. The shape of NPs can determine how they orient and locate at the interface; therefore, it is also an important property to investigate.
- The detailed mechanism of emulsions breakage when stabilized by different types of NPs with or without surfactants. As we have studied only the Janus particles, there are many other properties of NPs that should be considered such as contact angle, wettability, etc.
- Synergism of NPs and surfactants when considering adsorption of surfactants on NP surface. When surfactants adsorb on NPs surface, there are less surfactant at the interface. Moreover, the adsorption is dynamic; thus, it is expected that it will influence the synergism.

REFERENCES

[1] M.J. Rosen, J.T. Kunjappu, Surfactants and interfacial phenomena, John Wiley & Sons2012.
[2] I. Kralova, J. Sjöblom, Surfactants Used in Food Industry: A Review, Journal of Dispersion Science and Technology 30(9) (2009) 1363-1383.
[3] D. Attwood, Surfactant systems: their chemistry, pharmacy and biology, Springer Science & Business Media2012.
[4] R.J. Farn, Chemistry and technology of surfactants, John Wiley & Sons2008.
[5] D.W. Green, G.P. Willhite, Enhanced oil recovery, Henry L. Doherty Memorial Fund of AIME, Society of Petroleum Engineers …1998.
[6] M. Jaiswal, R. Dudhe, P.K. Sharma, Nanoemulsion: an advanced mode of drug delivery system, 3 Biotech 5(2) (2015) 123-127.
[7] D. Myers, Surfactant science and technology, John Wiley & Sons2020.
[8] X. Cui, S. Mao, M. Liu, H. Yuan, Y. Du, Mechanism of surfactant micelle formation, Langmuir 24(19) (2008) 10771-10775.
[9] A.J. Konop, R.H. Colby, Role of condensed counterions in the thermodynamics of surfactant micelle formation with and without oppositely charged polyelectrolytes, Langmuir 15(1) (1999) 58-65.
[10] M.J. Rosen, Q. Zhou, Surfactant− surfactant interactions in mixed monolayer and mixed micelle formation, Langmuir 17(12) (2001) 3532-3537.
[11] S. Marrink, D. Tieleman, A. Mark, Molecular dynamics simulation of the kinetics of spontaneous micelle formation, The Journal of Physical Chemistry B 104(51) (2000) 12165-12173.
[12] D. Stigter, Micelle formation by ionic surfactants. II. Specificity of head groups, micelle structure, The Journal of Physical Chemistry 78(24) (1974) 2480-2485.
[13] J. Lu, R. Thomas, J. Penfold, Surfactant layers at the air/water interface: structure and composition, Advances in Colloid and Interface science 84(1-3) (2000) 143-304.
[14] D. Beneventi, B. Carre, A. Gandini, Role of surfactant structure on surface and foaming properties, Colloids and Surfaces A: Physicochemical and Engineering Aspects 189(1-3) (2001) 65-73.
[15] D. Taylor, R. Thomas, J. Penfold, Polymer/surfactant interactions at the air/water interface, Advances in colloid and interface science 132(2) (2007) 69-110.
[16] L. Rekvig, M. Kranenburg, B. Hafskjold, B. Smit, Effect of surfactant structure on interfacial properties, EPL (Europhysics Letters) 63(6) (2003) 902.
[17] E. Vignati, R. Piazza, T.P. Lockhart, Pickering Emulsions: Interfacial Tension, Colloidal Layer Morphology, and Trapped-Particle Motion, Langmuir 19(17) (2003) 6650-6656.
[18] Y. Chevalier, M.-A. Bolzinger, Emulsions stabilized with solid nanoparticles: Pickering emulsions, Colloids and Surfaces A: Physicochemical and Engineering Aspects 439 (2013) 23-34.
[19] N. Glaser, D.J. Adams, A. Böker, G. Krausch, Janus Particles at Liquid−Liquid Interfaces, Langmuir 22(12) (2006) 5227-5229.
[20] A. Walther, A.H.E. Müller, Janus particles, Soft Matter 4(4) (2008) 663-668.
[21] R. Aveyard, Can Janus particles give thermodynamically stable Pickering emulsions?, Soft Matter 8(19) (2012) 5233-5240.
[22] H. Fan, A. Striolo, Nanoparticle effects on the water-oil interfacial tension, Physical Review E 86(5) (2012) 051610.

[23] T.N. Hunter, R.J. Pugh, G.V. Franks, G.J. Jameson, The role of particles in stabilising foams and emulsions, Advances in colloid and interface science 137(2) (2008) 57-81.
[24] S. Levine, B.D. Bowen, S.J. Partridge, Stabilization of emulsions by fine particles I. Partitioning of particles between continuous phase and oil/water interface, Colloids and surfaces 38(2) (1989) 325-343.
[25] R. Aveyard, B.P. Binks, J.H. Clint, Emulsions stabilised solely by colloidal particles, Advances in Colloid and Interface Science 100 (2003) 503-546.
[26] B. Binks, S. Lumsdon, Catastrophic phase inversion of water-in-oil emulsions stabilized by hydrophobic silica, Langmuir 16(6) (2000) 2539-2547.
[27] B. Binks, S. Lumsdon, Pickering emulsions stabilized by monodisperse latex particles: effects of particle size, Langmuir 17(15) (2001) 4540-4547.
[28] B.P. Binks, C.P. Whitby, Nanoparticle silica-stabilised oil-in-water emulsions: improving emulsion stability, Colloids and Surfaces A: Physicochemical and Engineering Aspects 253(1-3) (2005) 105-115.
[29] T.S. Horozov, B.P. Binks, Particle-stabilized emulsions: a bilayer or a bridging monolayer?, Angewandte Chemie 118(5) (2006) 787-790.
[30] F. Tu, B.J. Park, D. Lee, Thermodynamically stable emulsions using Janus dumbbells as colloid surfactants, Langmuir 29(41) (2013) 12679-12687.
[31] S. Sacanna, W. Kegel, A. Philipse, Thermodynamically stable pickering emulsions, Physical review letters 98(15) (2007) 158301.
[32] B. Binks, P. Fletcher, Particles adsorbed at the oil− water interface: A theoretical comparison between spheres of uniform wettability and "Janus" particles, Langmuir 17(16) (2001) 4708-4710.
[33] B.J. Park, D. Lee, Equilibrium orientation of nonspherical Janus particles at fluid–fluid interfaces, ACS nano 6(1) (2012) 782-790.
[34] B.J. Park, C.-H. Choi, S.-M. Kang, K.E. Tettey, C.-S. Lee, D. Lee, Geometrically and chemically anisotropic particles at an oil–water interface, Soft Matter 9(12) (2013) 3383-3388.
[35] A.F. Mejia, A. Diaz, S. Pullela, Y.-W. Chang, M. Simonetty, C. Carpenter, J.D. Batteas, M.S. Mannan, A. Clearfield, Z. Cheng, Pickering emulsions stabilized by amphiphilic nano-sheets, Soft Matter 8(40) (2012) 10245-10253.
[36] E. Vignati, R. Piazza, T.P. Lockhart, Pickering emulsions: interfacial tension, colloidal layer morphology, and trapped-particle motion, Langmuir 19(17) (2003) 6650-6656.
[37] J. Frelichowska, M.-A. Bolzinger, Y. Chevalier, Pickering emulsions with bare silica, Colloids and Surfaces A: Physicochemical and Engineering Aspects 343(1-3) (2009) 70-74.
[38] L. Liu, X. Pu, Y. Zhou, X. Wu, D. Luo, Z. Ren, Phase inversion of Pickering emulsions by electrolyte for potential reversible water-in-oil drilling fluids, Energy & Fuels 34(2) (2020) 1317-1328.
[39] M. Tang, T. Wu, X. Xu, L. Zhang, F. Wu, Factors that affect the stability, type and morphology of Pickering emulsion stabilized by silver nanoparticles/graphene oxide nanocomposites, Materials Research Bulletin 60 (2014) 118-129.
[40] R.J.K.U. Ranatunga, C.T. Nguyen, B.A. Wilson, W. Shinoda, S.O. Nielsen, Molecular dynamics study of nanoparticles and non-ionic surfactant at an oil–water interface, Soft Matter 7(15) (2011) 6942-6952.
[41] S. Ahualli, G.R. Iglesias, W. Wachter, M. Dulle, D. Minami, O. Glatter, Adsorption of Anionic and Cationic Surfactants on Anionic Colloids: Supercharging and Destabilization, Langmuir 27(15) (2011) 9182-9192.

[42] H. Ma, M. Luo, L.L. Dai, Influences of surfactant and nanoparticle assembly on effective interfacial tensions, Physical Chemistry Chemical Physics 10(16) (2008) 2207-2213.
[43] F. Ravera, E. Santini, G. Loglio, M. Ferrari, L. Liggieri, Effect of Nanoparticles on the Interfacial Properties of Liquid/Liquid and Liquid/Air Surface Layers, The Journal of Physical Chemistry B 110(39) (2006) 19543-19551.
[44] D.C.E. Calzolari, D. Pontoni, M. Deutsch, H. Reichert, J. Daillant, Nanoscale structure of surfactant-induced nanoparticle monolayers at the oil–water interface, Soft Matter 8(45) (2012) 11478-11483.
[45] P.A. Yazhgur, B.A. Noskov, L. Liggieri, S.Y. Lin, G. Loglio, R. Miller, F. Ravera, Dynamic properties of mixed nanoparticle/surfactant adsorption layers, Soft Matter 9(12) (2013) 3305-3314.
[46] L. Mingxiang, L.D. Lenore, Molecular dynamics simulations of surfactant and nanoparticle self-assembly at liquid–liquid interfaces, Journal of Physics: Condensed Matter 19(37) (2007) 375109.
[47] A.J. Worthen, L.M. Foster, J. Dong, J.A. Bollinger, A.H. Peterman, L.E. Pastora, S.L. Bryant, T.M. Truskett, C.W. Bielawski, K.P. Johnston, Synergistic Formation and Stabilization of Oil-in-Water Emulsions by a Weakly Interacting Mixture of Zwitterionic Surfactant and Silica Nanoparticles, Langmuir 30(4) (2014) 984-994.
[48] S.E. Rahman, N. Laal-Dehghani, S. Barman, G.F. Christopher, Modifying interfacial interparticle forces to alter microstructure and viscoelasticity of densely packed particle laden interfaces, Journal of Colloid and Interface Science 536 (2019) 30-41.
[49] T.V. Vu, D.V. Papavassiliou, Synergistic effects of surfactants and heterogeneous nanoparticles at oil-water interface: Insights from computations, Journal of Colloid and Interface Science 553 (2019) 50-58.
[50] W. Wang, Z. Zhou, K. Nandakumar, Z. Xu, J.H. Masliyah, Effect of charged colloidal particles on adsorption of surfactants at oil–water interface, Journal of Colloid and Interface Science 274(2) (2004) 625-630.
[51] N.R. Biswal, N. Rangera, J.K. Singh, Effect of Different Surfactants on the Interfacial Behavior of the n-Hexane–Water System in the Presence of Silica Nanoparticles, The Journal of Physical Chemistry B 120(29) (2016) 7265-7274.
[52] H. Katepalli, V.T. John, A. Bose, The Response of Carbon Black Stabilized Oil-in-Water Emulsions to the Addition of Surfactant Solutions, Langmuir 29(23) (2013) 6790-6797.
[53] J. Smits, F. Vieira, B. Bisswurn, K. Rezwan, M. Maas, Reversible Adsorption of Nanoparticles at Surfactant-Laden Liquid–Liquid Interfaces, Langmuir 35(34) (2019) 11089-11098.
[54] J. Smits, R.P. Giri, C. Shen, D. Mendonça, B. Murphy, P. Huber, K. Rezwan, M. Maas, Synergistic and Competitive Adsorption of Hydrophilic Nanoparticles and Oil-Soluble Surfactants at the Oil–Water Interface, Langmuir 37(18) (2021) 5659-5672.
[55] D. Langevin, Rheology of Adsorbed Surfactant Monolayers at Fluid Surfaces, Annual Review of Fluid Mechanics 46(1) (2014) 47-65.
[56] B.P. Binks, Particles as surfactants—similarities and differences, Current Opinion in Colloid & Interface Science 7(1) (2002) 21-41.
[57] S. Razavi, K.D. Cao, B. Lin, K.Y.C. Lee, R.S. Tu, I. Kretzschmar, Collapse of Particle-Laden Interfaces under Compression: Buckling vs Particle Expulsion, Langmuir 31(28) (2015) 7764-7775.
[58] S. Bordács, A. Agod, Z. Hórvölgyi, Compression of Langmuir Films Composed of Fine Particles: Collapse Mechanism and Wettability, Langmuir 22(16) (2006) 6944-6950.

[59] T.S. Horozov, B.P. Binks, R. Aveyard, J.H. Clint, Effect of particle hydrophobicity on the formation and collapse of fumed silica particle monolayers at the oil–water interface, Colloids and Surfaces A: Physicochemical and Engineering Aspects 282-283 (2006) 377-386.
[60] R. Aveyard, J.H. Clint, D. Nees, Small solid particles and liquid lenses at fluid/fluid interfaces, Colloid and Polymer Science 278(2) (2000) 155-163.
[61] H. Xu, S. Melle, K. Golemanov, G. Fuller, Shape and Buckling Transitions in Solid-Stabilized Drops, Langmuir 21(22) (2005) 10016-10020.
[62] B. Madivala, J. Fransaer, J. Vermant, Self-Assembly and Rheology of Ellipsoidal Particles at Interfaces, Langmuir 25(5) (2009) 2718-2728.
[63] M. Rey, T. Yu, K. Bley, K. Landfester, D.M.A. Buzza, N. Vogel, Amphiphile-Induced Anisotropic Colloidal Self-Assembly, Langmuir 34(34) (2018) 9990-10000.
[64] V. Garbin, Collapse mechanisms and extreme deformation of particle-laden interfaces, Current Opinion in Colloid & Interface Science 39 (2019) 202-211.
[65] E.L. Correia, N. Brown, S. Razavi, Janus Particles at Fluid Interfaces: Stability and Interfacial Rheology, Nanomaterials 11(2) (2021) 374.
[66] S. Razavi, B. Lin, K.Y.C. Lee, R.S. Tu, I. Kretzschmar, Impact of Surface Amphiphilicity on the Interfacial Behavior of Janus Particle Layers under Compression, Langmuir 35(48) (2019) 15813-15824.
[67] T. Yin, Z. Yang, F. Zhang, M. Lin, J. Zhang, Z. Dong, Assembly and mechanical response of amphiphilic Janus nanosheets at oil-water interfaces, Journal of Colloid and Interface Science 583 (2021) 214-221.
[68] P. Hoogerbrugge, J. Koelman, Simulating microscopic hydrodynamic phenomena with dissipative particle dynamics, EPL (Europhysics Letters) 19(3) (1992) 155.
[69] T.V. Vu, D.V. Papavassiliou, Oil-water interfaces with surfactants: A systematic approach to determine coarse-grained model parameters, The Journal of Chemical Physics 148(20) (2018) 204704.
[70] L. Rekvig, B. Hafskjold, B. Smit, Molecular Simulations of Surface Forces and Film Rupture in Oil/Water/Surfactant Systems, Langmuir 20(26) (2004) 11583-11593.
[71] L. Rekvig, B. Hafskjold, B. Smit, Chain Length Dependencies of the Bending Modulus of Surfactant Monolayers, Physical Review Letters 92(11) (2004) 116101.
[72] Y. Li, Y. Guo, M. Bao, X. Gao, Investigation of interfacial and structural properties of CTAB at the oil/water interface using dissipative particle dynamics simulations, Journal of Colloid and Interface Science 361(2) (2011) 573-580.
[73] R.D. Groot, P.B. Warren, Dissipative particle dynamics: Bridging the gap between atomistic and mesoscopic simulation, The Journal of Chemical Physics 107(11) (1997) 4423-4435.
[74] P. Espanol, P. Warren, Statistical mechanics of dissipative particle dynamics, EPL (Europhysics Letters) 30(4) (1995) 191.
[75] S. Plimpton, Fast Parallel Algorithms for Short-Range Molecular Dynamics, Journal of Computational Physics 117(1) (1995) 1-19.
[76] W. Humphrey, A. Dalke, K. Schulten, VMD: Visual molecular dynamics, Journal of Molecular Graphics 14(1) (1996) 33-38.
[77] M.R. Porter, Handbook of surfactants, Springer2013.
[78] D. Myers, Surfactant science and technology, John Wiley & Sons2005.
[79] D.O. Shah, Improved oil recovery by surfactant and polymer flooding, Elsevier2012.

[80] M.S. Leaver, U. Olsson, H. Wennerstrom, R. Strey, U. Wurz, Phase behaviour and structure in a non-ionic surfactant-oil-water mixture, Journal of the Chemical Society, Faraday Transactions 91(23) (1995) 4269-4274.
[81] S. Trabelsi, J.-F. Argillier, C. Dalmazzone, A. Hutin, B. Bazin, D. Langevin, Effect of Added Surfactants in an Enhanced Alkaline/Heavy Oil System, Energy & Fuels 25(4) (2011) 1681-1685.
[82] B. Brooks, H. Richmond, Phase inversion in non-ionic surfactant—oil—water systems—II. Drop size studies in catastrophic inversion with turbulent mixing, Chemical engineering science 49(7) (1994) 1065-1075.
[83] S. Karaborni, N. Van Os, K. Esselink, P. Hilbers, Molecular dynamics simulations of oil solubilization in surfactant solutions, Langmuir 9(5) (1993) 1175-1178.
[84] B. Smit, A. Schlijper, L. Rupert, N. Van Os, Effects of chain length of surfactants on the interfacial tension: molecular dynamics simulations and experiments, Journal of physical chemistry 94(18) (1990) 6933-6935.
[85] B. Smit, P. Hilbers, K. Esselink, L. Rupert, N. Van Os, A. Schlijper, Computer simulations of a water/oil interface in the presence of micelles, Nature 348(6302) (1990) 624-625.
[86] A.R. van Buuren, S.J. Marrink, H.J. Berendsen, A molecular dynamics study of the decane/water interface, The Journal of Physical Chemistry 97(36) (1993) 9206-9212.
[87] R. Larson, L. Scriven, H. Davis, Monte Carlo simulation of model amphiphile-oil–water systems, The Journal of chemical physics 83(5) (1985) 2411-2420.
[88] S.S. Jang, S.-T. Lin, P.K. Maiti, M. Blanco, W.A. Goddard, P. Shuler, Y. Tang, Molecular dynamics study of a surfactant-mediated decane− water interface: effect of molecular architecture of alkyl benzene sulfonate, The Journal of Physical Chemistry B 108(32) (2004) 12130-12140.
[89] S. Poteau, J.-F. Argillier, D. Langevin, F. Pincet, E. Perez, Influence of pH on stability and dynamic properties of asphaltenes and other amphiphilic molecules at the oil− water interface, Energy & Fuels 19(4) (2005) 1337-1341.
[90] W.-X. Shi, H.-X. Guo, Structure, Interfacial Properties, and Dynamics of the Sodium Alkyl Sulfate Type Surfactant Monolayer at the Water/Trichloroethylene Interface: A Molecular Dynamics Simulation Study, The Journal of Physical Chemistry B 114(19) (2010) 6365-6376.
[91] R.D. Groot, K.L. Rabone, Mesoscopic Simulation of Cell Membrane Damage, Morphology Change and Rupture by Nonionic Surfactants, Biophysical Journal 81(2) (2001) 725-736.
[92] S. Yamamoto, Y. Maruyama, S.-a. Hyodo, Dissipative particle dynamics study of spontaneous vesicle formation of amphiphilic molecules, The Journal of chemical physics 116(13) (2002) 5842-5849.
[93] L. Rekvig, M. Kranenburg, J. Vreede, B. Hafskjold, B. Smit, Investigation of Surfactant Efficiency Using Dissipative Particle Dynamics, Langmuir 19(20) (2003) 8195-8205.
[94] N. Denham, M.C. Holmes, A.V. Zvelindovsky, The Phases in a Non-Ionic Surfactant (C12E6)−Water Ternary System: A Coarse-Grained Computer Simulation, The Journal of Physical Chemistry B 115(6) (2011) 1385-1393.
[95] V.V. Ginzburg, K. Chang, P.K. Jog, A.B. Argenton, L. Rakesh, Modeling the Interfacial Tension in Oil−Water−Nonionic Surfactant Mixtures Using Dissipative Particle Dynamics and Self-Consistent Field Theory, The Journal of Physical Chemistry B 115(16) (2011) 4654-4661.
[96] B. Duan, X. Zhang, B. Qiao, B. Kong, X. Yang, Description of Ionic Surfactant/Water System by Adjusting Mesoscopic Parameters, The Journal of Physical Chemistry B 113(26) (2009) 8854-8859.

[97] M. Ndao, F. Goujon, A. Ghoufi, P. Malfreyt, Coarse-grained modeling of the oil–water–surfactant interface through the local definition of the pressure tensor and interfacial tension, Theoretical Chemistry Accounts 136(1) (2017) 21.
[98] M. Suttipong, N.R. Tummala, A. Striolo, C.S. Batista, J. Fagan, Salt-specific effects in aqueous dispersions of carbon nanotubes, Soft Matter 9(14) (2013) 3712-3719.
[99] M. Suttipong, B.P. Grady, A. Striolo, Self-assembled surfactants on patterned surfaces: confinement and cooperative effects on aggregate morphology, Physical Chemistry Chemical Physics 16(31) (2014) 16388-16398.
[100] M.D. Vo, D.V. Papavassiliou, Effect of Sodium Dodecyl Sulfate Adsorption on the Behavior of Water inside Single Walled Carbon Nanotubes with Dissipative Particle Dynamics Simulation, Molecules 21(4) (2016) 500.
[101] E.E. Keaveny, I.V. Pivkin, M. Maxey, G.E. Karniadakis, A comparative study between dissipative particle dynamics and molecular dynamics for simple- and complex-geometry flows, The Journal of Chemical Physics 123(10) (2005) 104107.
[102] F. van Voorst Vader, Adsorption of detergents at the liquid-liquid interface. Part 1, Transactions of the Faraday Society 56(0) (1960) 1067-1077.
[103] S.J. Rehfeld, Adsorption of sodium dodecyl sulfate at various hydrocarbon-water interfaces, The Journal of Physical Chemistry 71(3) (1967) 738-745.
[104] M.J. Rosen, D.S. Murphy, Effect of the nonaqueous phase on interfacial properties of surfactants. 2. Individual and mixed nonionic surfactants in hydrocarbon/water systems, Langmuir 7(11) (1991) 2630-2635.
[105] J.H. Irving, J.G. Kirkwood, The Statistical Mechanical Theory of Transport Processes. IV. The Equations of Hydrodynamics, The Journal of Chemical Physics 18(6) (1950) 817-829.
[106] M.D. Vo, B. Shiau, J.H. Harwell, D.V. Papavassiliou, Adsorption of anionic and non-ionic surfactants on carbon nanotubes in water with dissipative particle dynamics simulation, The Journal of Chemical Physics 144(20) (2016) 204701.
[107] A.F.M. Barton, Solubility parameters, Chemical Reviews 75(6) (1975) 731-753.
[108] Z. Mai, E. Couallier, M. Rakib, B. Rousseau, Parameterization of a mesoscopic model for the self-assembly of linear sodium alkyl sulfates, The Journal of Chemical Physics 140(20) (2014) 204902.
[109] N.J. Turro, A. Yekta, Luminescent probes for detergent solutions. A simple procedure for determination of the mean aggregation number of micelles, Journal of the American Chemical Society 100(18) (1978) 5951-5952.
[110] H. Wu, J. Xu, X. He, Y. Zhao, H. Wen, Mesoscopic simulation of self-assembly in surfactant oligomers by dissipative particle dynamics, Colloids and Surfaces A: Physicochemical and Engineering Aspects 290(1) (2006) 239-246.
[111] R. Aveyard, B.P. Binks, S. Clark, J. Mead, Interfacial tension minima in oil-water-surfactant systems. Behaviour of alkane-aqueous NaCl systems containing aerosol OT, Journal of the Chemical Society, Faraday Transactions 1: Physical Chemistry in Condensed Phases 82(1) (1986) 125-142.
[112] E. Deguillard, N. Pannacci, B. Creton, B. Rousseau, Interfacial tension in oil–water–surfactant systems: On the role of intra-molecular forces on interfacial tension values using DPD simulations, The Journal of Chemical Physics 138(14) (2013) 144102.
[113] M.-T. Lee, A. Vishnyakov, A.V. Neimark, Calculations of Critical Micelle Concentration by Dissipative Particle Dynamics Simulations: The Role of Chain Rigidity, The Journal of Physical Chemistry B 117(35) (2013) 10304-10310.

[114] chemapps.stolaf.edu/jmol/. https://chemapps.stolaf.edu/jmol/jmol.php?model=O%28CCOCCOCCCCCCCCCCCC%29CCOCCOCCOCCOCCOCCO.
[115] J. Pang, Y. Wang, G. Xu, T. Han, X. Lv, J. Zhang, Molecular Dynamics Simulations of SDS, DTAB, and C12E8 Monolayers Adsorbed at the Air/Water Surface in the Presence of DSEP, The Journal of Physical Chemistry B 115(11) (2011) 2518-2526.
[116] D. Danino, Y. Talmon, R. Zana, Aggregation and Microstructure in Aqueous Solutions of the Nonionic Surfactant C12E8, Journal of Colloid and Interface Science 186(1) (1997) 170-179.
[117] A.W. Adamson, A.P. Gast, Physical chemistry of surfaces, 6th ed., John Wiley & Sons, New York, 1967.
[118] P.C. Hiemenz, R. Rajagopalan, Principles of Colloid and Surface Chemistry, 3rd ed., CRC press, New York, 1997.
[119] J. Sheng, Modern chemical enhanced oil recovery: theory and practice, Gulf Professional Publishing2010.
[120] B. Liu, W. Wei, X. Qu, Z. Yang, Janus Colloids Formed by Biphasic Grafting at a Pickering Emulsion Interface, Angewandte Chemie 120(21) (2008) 4037-4039.
[121] D. Suzuki, S. Tsuji, H. Kawaguchi, Janus Microgels Prepared by Surfactant-Free Pickering Emulsion-Based Modification and Their Self-Assembly, Journal of the American Chemical Society 129(26) (2007) 8088-8089.
[122] S. Crossley, J. Faria, M. Shen, D.E. Resasco, Solid Nanoparticles that Catalyze Biofuel Upgrade Reactions at the Water/Oil Interface, Science 327(5961) (2010) 68-72.
[123] L.C. Bradley, W.-H. Chen, K.J. Stebe, D. Lee, Janus and patchy colloids at fluid interfaces, Current Opinion in Colloid & Interface Science 30 (2017) 25-33.
[124] J.C. Melrose, Role of Capillary Forces In Detennining Microscopic Displacement Efficiency For Oil Recovery By Waterflooding, (1974).
[125] L.L. Wesson, J.H. Harwell, Surfactant adsorption in porous media, Surfactants: fundamentals and applications in the petroleum industry (2000) 121-158.
[126] J. Neves Libório De Avila, L. Louise Grecco Cavalcanti De Araujo, S. Drexler, J. de Almeida Rodrigues, R. Sandra Veiga Nascimento, Polystyrene nanoparticles as surfactant carriers for enhanced oil recovery, Journal of Applied Polymer Science 133(32) (2016).
[127] C. Chen, S. Wang, M.J. Kadhum, J.H. Harwell, B.-J. Shiau, Using carbonaceous nanoparticles as surfactant carrier in enhanced oil recovery: A laboratory study, Fuel 222 (2018) 561-568.
[128] M.D. Vo, D.V. Papavassiliou, Effects of Temperature and Shear on the Adsorption of Surfactants on Carbon Nanotubes, The Journal of Physical Chemistry C 121(26) (2017) 14339-14348.
[129] A. Maiti, J. Wescott, P. Kung, Nanotube–polymer composites: insights from Flory–Huggins theory and mesoscale simulations, Molecular Simulation 31(2-3) (2005) 143-149.
[130] C. Matteo, D. Marco, Z. Francesco, Wrapping Nanotubes with Micelles, Hemimicelles, and Cylindrical Micelles, Small 5(19) (2009) 2191-2198.
[131] M. Suttipong, N.R. Tummala, B. Kitiyanan, A. Striolo, Role of Surfactant Molecular Structure on Self-Assembly: Aqueous SDBS on Carbon Nanotubes, The Journal of Physical Chemistry C 115(35) (2011) 17286-17296.
[132] M. Suttipong, A. Striolo, Equimolar mixtures of aqueous linear and branched SDBS surfactant simulated on single walled carbon nanotubes, RSC Advances 5(109) (2015) 90049-90060.

[133] N.R. Tummala, A. Striolo, SDS Surfactants on Carbon Nanotubes: Aggregate Morphology, ACS Nano 3(3) (2009) 595-602.
[134] M.J. Rosen, H. Wang, P. Shen, Y. Zhu, Ultralow Interfacial Tension for Enhanced Oil Recovery at Very Low Surfactant Concentrations, Langmuir 21(9) (2005) 3749-3756.
[135] D. Wang, C. Liu, W. Wu, G. Wang, Novel Surfactants that Attain Ultra-Low Interfacial Tension between Oil and High Salinity Formation Water without adding Alkali, Salts, Co-surfactants, Alcohols and Solvents, SPE EOR Conference at Oil & Gas West Asia, Society of Petroleum Engineers, Muscat, Oman, 2010, p. 11.
[136] M.F. Islam, E. Rojas, D.M. Bergey, A.T. Johnson, A.G. Yodh, High Weight Fraction Surfactant Solubilization of Single-Wall Carbon Nanotubes in Water, Nano Letters 3(2) (2003) 269-273.
[137] L. Vaisman, H.D. Wagner, G. Marom, The role of surfactants in dispersion of carbon nanotubes, Advances in Colloid and Interface Science 128-130 (2006) 37-46.
[138] O. Matarredona, H. Rhoads, Z. Li, J.H. Harwell, L. Balzano, D.E. Resasco, Dispersion of Single-Walled Carbon Nanotubes in Aqueous Solutions of the Anionic Surfactant NaDDBS, The Journal of Physical Chemistry B 107(48) (2003) 13357-13367.
[139] R. Kumar, D. Milanova, Effect of surface tension on nanotube nanofluids, Applied Physics Letters 94(7) (2009) 073107.
[140] V. Sa, K.G. Kornev, Analysis of Stability of Nanotube Dispersions Using Surface Tension Isotherms, Langmuir 27(22) (2011) 13451-13460.
[141] P. Katiyar, J.K. Singh, A coarse-grain molecular dynamics study of oil–water interfaces in the presence of silica nanoparticles and nonionic surfactants, The Journal of Chemical Physics 146(20) (2017) 204702.
[142] X.-C. Luu, J. Yu, A. Striolo, Nanoparticles Adsorbed at the Water/Oil Interface: Coverage and Composition Effects on Structure and Diffusion, Langmuir 29(24) (2013) 7221-7228.
[143] R. Pichot, F. Spyropoulos, I.T. Norton, Competitive adsorption of surfactants and hydrophilic silica particles at the oil–water interface: Interfacial tension and contact angle studies, Journal of Colloid and Interface Science 377(1) (2012) 396-405.
[144] H. Fan, D.E. Resasco, A. Striolo, Amphiphilic Silica Nanoparticles at the Decane−Water Interface: Insights from Atomistic Simulations, Langmuir 27(9) (2011) 5264-5274.
[145] T. Fereidooni Moghadam, S. Azizian, S. Wettig, Synergistic behaviour of ZnO nanoparticles and gemini surfactants on the dynamic and equilibrium oil/water interfacial tension, Physical Chemistry Chemical Physics 17(11) (2015) 7122-7129.
[146] J.K. Beattie, A.M. Djerdjev, The pristine oil/water interface: Surfactant-free hydroxide-charged emulsions, Angewandte Chemie International Edition 43(27) (2004) 3568-3571.
[147] D. Evans, D. Mitchell, B. Ninham, Oil, water, and surfactant: properties and conjectured structure of simple microemulsions, The Journal of Physical Chemistry 90(13) (1986) 2817-2825.
[148] B. Smit, P.A.J. Hilbers, K. Esselink, L.A.M. Rupert, N.M. van Os, A.G. Schlijper, Computer simulations of a water/oil interface in the presence of micelles, Nature 348(6302) (1990) 624-625.
[149] X.-C. Luu, J. Yu, A. Striolo, Ellipsoidal Janus Nanoparticles Adsorbed at the Water–Oil Interface: Some Evidence of Emergent Behavior, The Journal of Physical Chemistry B 117(44) (2013) 13922-13929.
[150] T.V. Vu, D.V. Papavassiliou, Modification of Oil–Water Interfaces by Surfactant-Stabilized Carbon Nanotubes, The Journal of Physical Chemistry C 122(48) (2018) 27734-27744.
[151] E. Nourafkan, Z. Hu, D. Wen, Nanoparticle-enabled delivery of surfactants in porous media, Journal of Colloid and Interface Science 519 (2018) 44-57.

[152] L.N. Nwidee, M. Lebedev, A. Barifcani, M. Sarmadivaleh, S. Iglauer, Wettability alteration of oil-wet limestone using surfactant-nanoparticle formulation, Journal of Colloid and Interface Science 504 (2017) 334-345.
[153] M. Luo, L.L. Dai, Molecular dynamics simulations of surfactant and nanoparticle self-assembly at liquid–liquid interfaces, Journal of Physics: Condensed Matter 19(37) (2007) 375109.
[154] N.G. Eskandar, S. Simovic, C.A. Prestidge, Interactions of hydrophilic silica nanoparticles and classical surfactants at non-polar oil–water interface, Journal of Colloid and Interface Science 358(1) (2011) 217-225.
[155] P. Angelikopoulos, H. Bock, Directed Self-Assembly of Surfactants in Carbon Nanotube Materials, The Journal of Physical Chemistry B 112(44) (2008) 13793-13801.
[156] H.J.C. Berendsen, J.P.M. Postma, W.F.v. Gunsteren, A. DiNola, J.R. Haak, Molecular dynamics with coupling to an external bath, The Journal of Chemical Physics 81(8) (1984) 3684-3690.
[157] K.J. Mysels, Surface tension of solutions of pure sodium dodecyl sulfate, Langmuir 2(4) (1986) 423-428.
[158] P. Joos, D. Vollhardt, M. Vermeulen, Interfacial tension of sodium dodecyl sulfate solutions at the hexane-water interface, Langmuir 6(2) (1990) 524-525.
[159] T. Fereidooni Moghadam, S. Azizian, Effect of ZnO Nanoparticle and Hexadecyltrimethylammonium Bromide on the Dynamic and Equilibrium Oil–Water Interfacial Tension, The Journal of Physical Chemistry B 118(6) (2014) 1527-1534.
[160] J.R. Bloor, J.C. Morrison, C.T. Rhodes, Effect of pH on the Micellar Properties of a Nonionic Surfactant, Journal of Pharmaceutical Sciences 59(3) (1970) 387-391.
[161] J.E. Strassner, Effect of pH on Interfacial Films and Stability of Crude Oil-Water Emulsions, Journal of Petroleum Technology 20(03) (1968) 303-312.
[162] M. Abe, N. Tsubaki, K. Ogino, Solution properties of mixed surfactant system: V. The effect of alkyl groups in nonionic surfactant on surface tension of anionic-nonionic surfactant systems, Journal of Colloid and Interface Science 107(2) (1985) 503-508.
[163] B.P. Binks, C.P. Whitby, Nanoparticle silica-stabilised oil-in-water emulsions: improving emulsion stability, Colloids and Surfaces A: Physicochemical and Engineering Aspects 253(1) (2005) 105-115.
[164] S.U. Pickering, CXCVI.—Emulsions, Journal of the Chemical Society, Transactions 91(0) (1907) 2001-2021.
[165] P. Kumar, K.L. Mittal, Handbook of microemulsion science and technology, CRC press1999.
[166] E. Fredrick, P. Walstra, K. Dewettinck, Factors governing partial coalescence in oil-in-water emulsions, Advances in Colloid and Interface Science 153(1) (2010) 30-42.
[167] I.B. Ivanov, K.D. Danov, P.A. Kralchevsky, Flocculation and coalescence of micron-size emulsion droplets, Colloids and Surfaces A: Physicochemical and Engineering Aspects 152(1) (1999) 161-182.
[168] R.P. Borwankar, L.A. Lobo, D.T. Wasan, Emulsion stability — kinetics of flocculation and coalescence, Colloids and Surfaces 69(2) (1992) 135-146.
[169] K. Boode, P. Walstra, Partial coalescence in oil-in-water emulsions 1. Nature of the aggregation, Colloids and Surfaces A: Physicochemical and Engineering Aspects 81 (1993) 121-137.
[170] T.M. Dreher, J. Glass, A.J. O'Connor, G.W. Stevens, Effect of rheology on coalescence rates and emulsion stability, AIChE Journal 45(6) (1999) 1182-1190.

[171] H. Fan, A. Striolo, Mechanistic study of droplets coalescence in Pickering emulsions, Soft Matter 8(37) (2012) 9533-9538.
[172] F. Sicard, A. Striolo, Numerical analysis of Pickering emulsion stability: insights from ABMD simulations, Faraday Discussions 191(0) (2016) 287-304.
[173] F. Sicard, A. Striolo, Buckling in armored droplets, Nanoscale 9(25) (2017) 8567-8572.
[174] M.D. Vo, D.V. Papavassiliou, Physical adsorption of polyvinyl pyrrolidone on carbon nanotubes under shear studied with dissipative particle dynamics simulations, Carbon 100 (2016) 291-301.
[175] R.D. Groot, Electrostatic interactions in dissipative particle dynamics—simulation of polyelectrolytes and anionic surfactants, The Journal of Chemical Physics 118(24) (2003) 11265-11277.
[176] A. Maestro, E. Guzmán, F. Ortega, R.G. Rubio, Contact angle of micro- and nanoparticles at fluid interfaces, Current Opinion in Colloid & Interface Science 19(4) (2014) 355-367.
[177] H.J.C. Berendsen, J.P.M. Postma, W.F. van Gunsteren, A. DiNola, J.R. Haak, Molecular dynamics with coupling to an external bath, The Journal of Chemical Physics 81(8) (1984) 3684-3690.
[178] S. Park, K. Schulten, Calculating potentials of mean force from steered molecular dynamics simulations, The Journal of chemical physics 120(13) (2004) 5946-5961.
[179] C. Jarzynski, Nonequilibrium equality for free energy differences, Physical Review Letters 78(14) (1997) 2690.
[180] A.S. Kabalnov, Coalescence in emulsions, Modern aspects of emulsion science (1998) 205-260.
[181] A.B. Pawar, M. Caggioni, R. Ergun, R.W. Hartel, P.T. Spicer, Arrested coalescence in Pickering emulsions, Soft Matter 7(17) (2011) 7710-7716.
[182] B.P. Binks, S.O. Lumsdon, Influence of Particle Wettability on the Type and Stability of Surfactant-Free Emulsions, Langmuir 16(23) (2000) 8622-8631.
[183] V. Garbin, J.C. Crocker, K.J. Stebe, Nanoparticles at fluid interfaces: Exploiting capping ligands to control adsorption, stability and dynamics, Journal of Colloid and Interface Science 387(1) (2012) 1-11.
[184] N. Ballard, A.D. Law, S.A.F. Bon, Colloidal particles at fluid interfaces: behaviour of isolated particles, Soft Matter 15(6) (2019) 1186-1199.
[185] D.M. Goggin, J.R. Samaniuk, Dynamics of pristine graphite and graphene at an air-water interface, AIChE Journal 64(8) (2018) 3177-3187.
[186] O.S. Deshmukh, D. van den Ende, M.C. Stuart, F. Mugele, M.H.G. Duits, Hard and soft colloids at fluid interfaces: Adsorption, interactions, assembly & rheology, Advances in Colloid and Interface Science 222 (2015) 215-227.
[187] B.P. Binks, P.D.I. Fletcher, Particles Adsorbed at the Oil−Water Interface: A Theoretical Comparison between Spheres of Uniform Wettability and “Janus” Particles, Langmuir 17(16) (2001) 4708-4710.
[188] J. Hu, S. Zhou, Y. Sun, X. Fang, L. Wu, Fabrication, properties and applications of Janus particles, Chemical Society Reviews 41(11) (2012) 4356-4378.
[189] S. Razavi, L.M. Hernandez, A. Read, W.L. Vargas, I. Kretzschmar, Surface tension anomaly observed for chemically-modified Janus particles at the air/water interface, Journal of Colloid and Interface Science 558 (2020) 95-99.
[190] J. Zhang, B.A. Grzybowski, S. Granick, Janus Particle Synthesis, Assembly, and Application, Langmuir 33(28) (2017) 6964-6977.

[191] L.C. Bradley, K.J. Stebe, D. Lee, Clickable Janus Particles, Journal of the American Chemical Society 138(36) (2016) 11437-11440.
[192] A. Walther, A.H.E. Müller, Janus Particles: Synthesis, Self-Assembly, Physical Properties, and Applications, Chemical Reviews 113(7) (2013) 5194-5261.
[193] E. Jurado, O. Herrera-Márquez, A. Plaza-Quevedo, J.M. Vicaria, Interaction between non-ionic surfactants and silica micro/nanoparticles. Influence on the cleaning of dried starch on steel surfaces, Journal of Industrial and Engineering Chemistry 21 (2015) 1383-1388.
[194] Z. AlYousef, M. Almobarky, D. Schechter, Enhancing the Stability of Foam by the Use of Nanoparticles, Energy & Fuels 31(10) (2017) 10620-10627.
[195] T.V. Vu, S. Razavi, D.V. Papavassiliou, Effect of Janus particles and non-ionic surfactants on the collapse of the oil-water interface under compression, Journal of Colloid and Interface Science (2021).
[196] R.L. Anderson, D.J. Bray, A. Del Regno, M.A. Seaton, A.S. Ferrante, P.B. Warren, Micelle Formation in Alkyl Sulfate Surfactants Using Dissipative Particle Dynamics, Journal of Chemical Theory and Computation 14(5) (2018) 2633-2643.
[197] S.K. Ghosh, A model for the orientational order in liquid crystals, Il Nuovo Cimento D 4(3) (1984) 229-244.

Appendices

Appendix A. Supporting Information for Chapter 7

Interaction Parameter

Table A1. Pair-wise interaction parameters used in the simulations. H stands for the surfactant head beads, T for the surfactant tail beads, W and O for water and oil, respectively, and P and AP represent polar (hydrophilic) and apolar (hydrophobic) beads of the NPs and on the two faces of JPs.)

	H	**T**	**W**	**O**	**AP**	**P**
H	15	25	14	25	25	15
T		15	30	14.5	15	25
W			15	100	50	20
O				15	15	25
AP					15	25
P						15

Determination of the nanoparticle diameter

Figure A1 is the radial density distribution of the Janus particles (JPs) after compression to 40% A/A_0 of the original interface. The first peak at 4.7 r_c represented the minimum distance between two JPs. Upon compression, the JPs cannot come closer to each other than the distance 4.7 r_c. Thus, this distance was used as the diameter of the JPs.

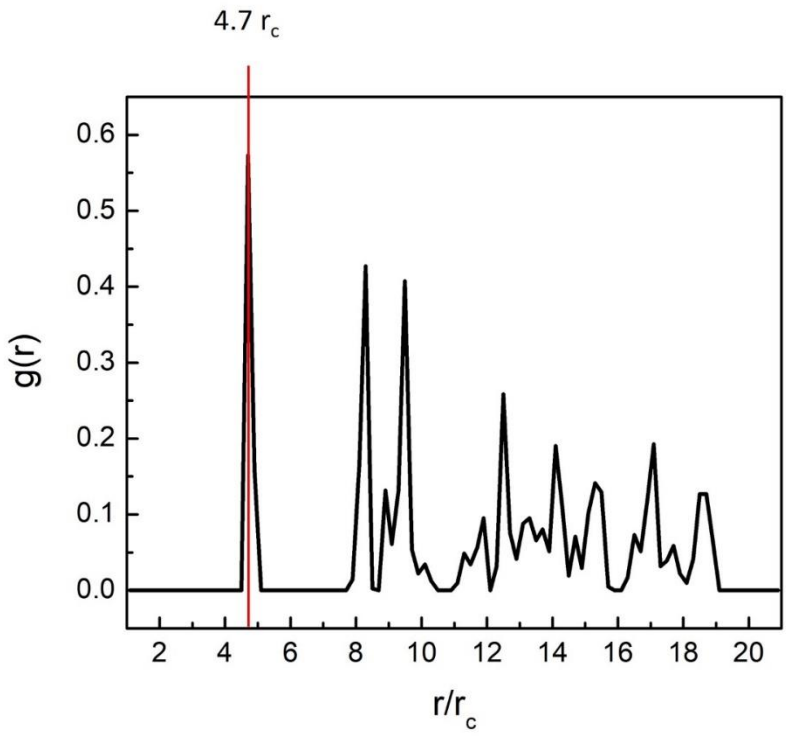

Figure A1. Radial density distribution of the JPs after compression to 40% A/A_0 of the original interface.

Contact angles of NPs

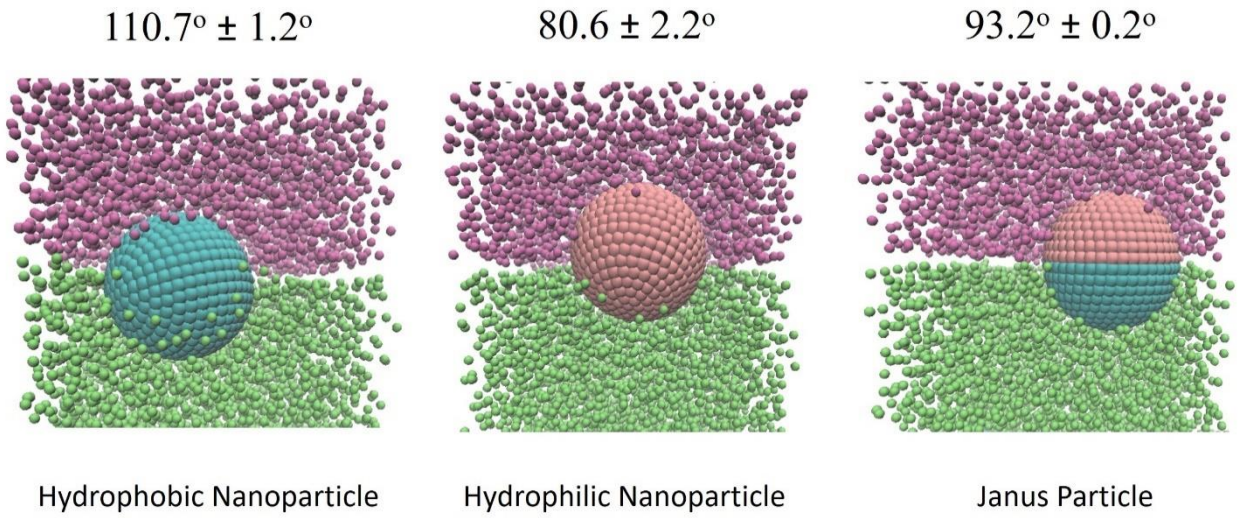

Figure A2. Snapshots of hydrophobic, hydrophilic, and Janus particles at the oil-water interface. The contact angle values of the nanoparticles are shown on top of the corresponding snapshot. Purple, green, pink, cyan are the colors of water, oil, and the Janus nanoparticle's polar and apolar beads, respectively.

Determination of simulation box size and compression speed

The size of the box was chosen to be large enough to allow observation of the collapse of the interface and as small as possible to save computational cost. However, the box size also needs to be large enough to ensure that the width and depth of the wrinkle are invariant with the box size. We carried a series of simulations with the length in the direction of compression (L_x) of 60, 90, 120 r_c. Figure A3 showed that increasing L_x from 60 to 90 r_c led to an increase in both the width and depth of the wrinkle. Changing L_x from 90 to 120 did not significantly affect the size of the wrinkle. Thus, the value of L_x was chosen as 90 to ensure the independence of the wrinkle size with regards to the box size.

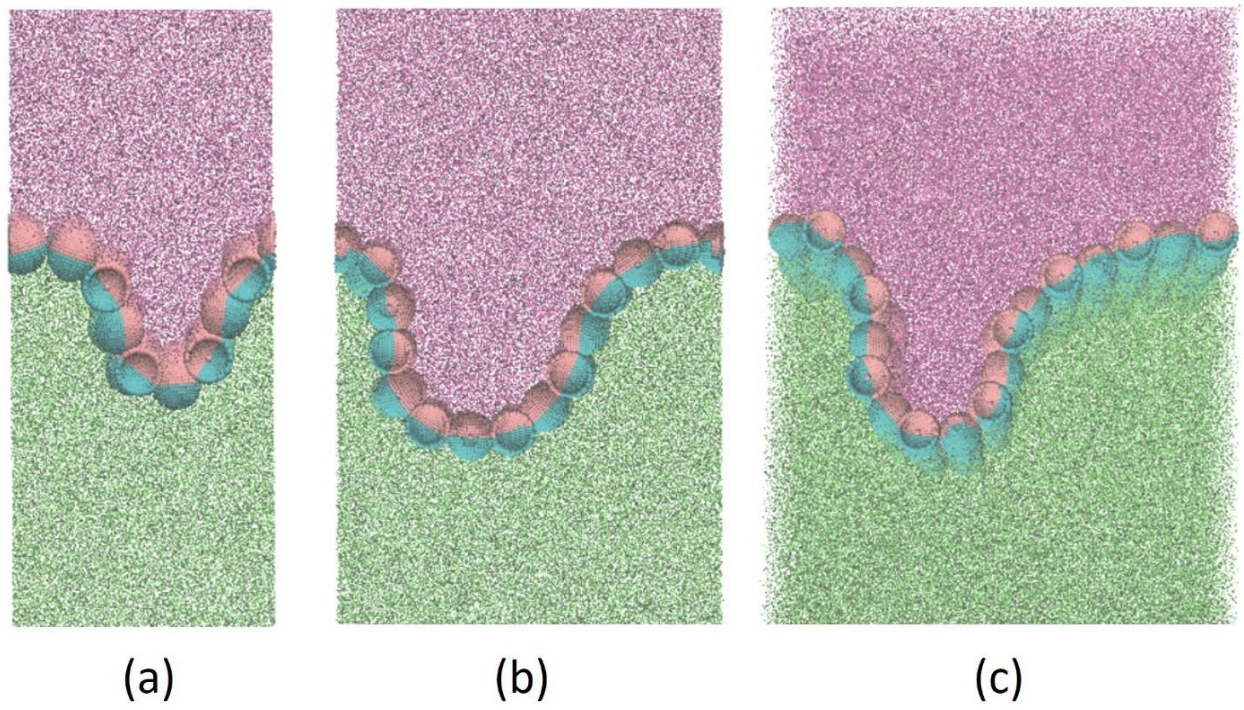

Figure A3. Final configuration of the system containing 55% initial coverage of JPs after compression to 40% of the interfacial area with the simulation box of size (a) 20×60×50, (b) 20×60×50, and (c) 20×60×50 r_c^3. Purple, green, pink, cyan are the colors of water, oil, and the Janus nanoparticle's polar and apolar beads, respectively.

The compression speed was chosen to be as high as possible for computational efficiency so that the results did not change at lower speeds. Specifically, preliminary simulations were carried out,

each with different compression speeds of 4.5×10^{-4}, 6.75×10^{-4}, 1.35×10^{-3}, 2.7×10^{-3}, 5.4×10^{-3}, 1.35×10^{-2} in reduced units (length/time). The highest speed simulation that resulted in the same final configuration as the lower speed simulations was chosen. The final speed that was employed in our study was 1.35×10^{-3}, i.e., the box was compressed along the x-direction to 40% of its original size in 2×10^{6} timesteps. One timestep (Δt) was 0.02 of the reduced DPD time unit (τ).

Density profile of surfactant at the end of the compression at different initial concentrations

Figure A4 is a depiction of the density profiles of surfactant after compression at different initial concentrations. Due to the periodic boundary conditions in the z-direction, there are two interfaces in the simulation box as seen in Fig A4. For each interface, there was one primary peak showing the position of the interface as most of the surfactant molecules were located at the interface. The other peaks represent the surfactant molecules that were partitioned into the water phase because the interfacial concentration exceeded that of the interfacial CMC as the compression proceeded. The positions and heights of the primary peaks were comparable for different initial surfactant concentrations. This result confirmed that under compression, the interfacial concentration of surfactant did not exceed the maximum concentration (i.e., the CMC). The area of the secondary peak increased by 16%, 43%, 63% when increasing the initial surfactant concentration from 60 to 65, 70, and 75% of the interfacial CMC, respectively, indicating that the excess amount of surfactant was desorbed to the water phase to keep the interfacial concentration constant.

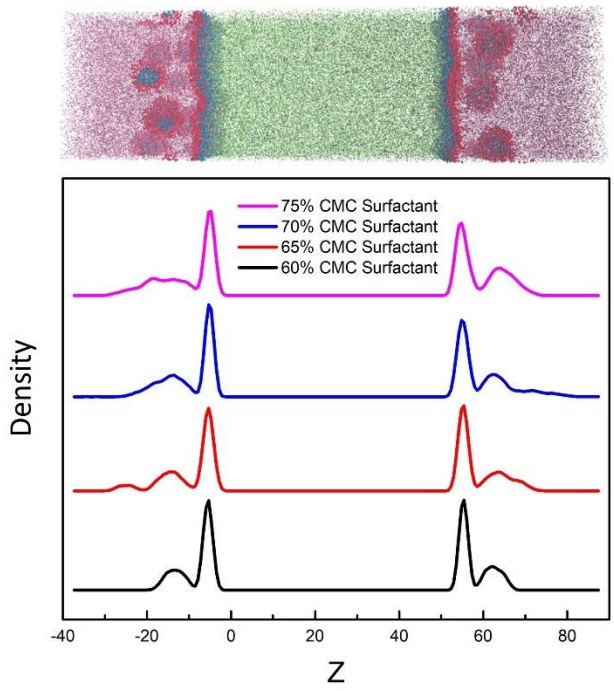

Figure A4. Density profiles of surfactant molecules added to the interface at various initial concentrations and after compression of the interface to 40% of its initial area. The snapshot on top represents the system orientation as used in the plots. Note that the baseline is at the same level for all density profiles and is presented as staggered solely for clarity.

Angle distribution of nanoparticles at the oil-water interface

Figures A5a-d illustrate the distribution of the polar angle, measured over 1×10^5 timesteps, for the case of JPs, and both hydrophobic and hydrophilic NPs. JPs showed a narrow distribution with one peak at around 0^o, confirming their cap alignment with the interface and their restricted rotational motion. The polar angles of homogeneous NPs displayed a wide distribution in the range of 0 to 180^o with mean values of 89.97^o and 89.73^o for hydrophobic and hydrophilic NPs, respectively. The shape of the distribution indicated a maximum in the middle and very low frequencies at 0 and 180^o. The mean value of the angle for a perfectly symmetric distribution is 90^o.

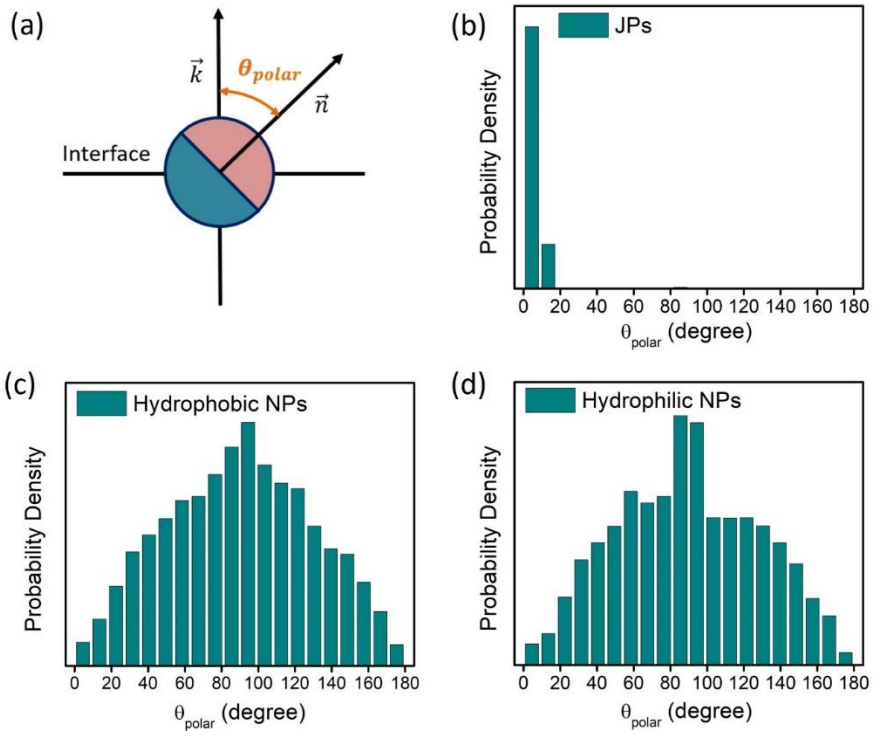

Figure A5. Distribution of the polar angle representing the orientation of the particles at the oil-water interface. (a) Schematic with the definition of the orientation angle between vectors $\vec{k}$ and $\vec{n}$. Distribution of the orientation angle for (b) JPs, (c) homogeneous hydrophobic NPs, and (d) homogeneous hydrophilic NPs.

Angle distribution of JPs at the oil-water interface and the change of order parameter

Figure A6 displays the distribution of the angle at the end of the compression with the same initial JP coverage and at different surfactant concentrations. As shown in Figure A5b, in the absence of applied compressions, the JP polar angles were in the range of 0 to 10^{o}. At the end of compression (Figure A6a), the distribution shifted to a higher angle, indicating the distortion of the interface. Adding surfactants resulted in higher angles. At high surfactant concentrations (30 and 40% interfacial CMC), the distribution did not change significantly as the interface reached saturation at these surfactant concentrations. This behavior is attributed to the fact that the excessive surfactant molecules migrated into the water phase as the interface cannot accommodate the excess molecules.

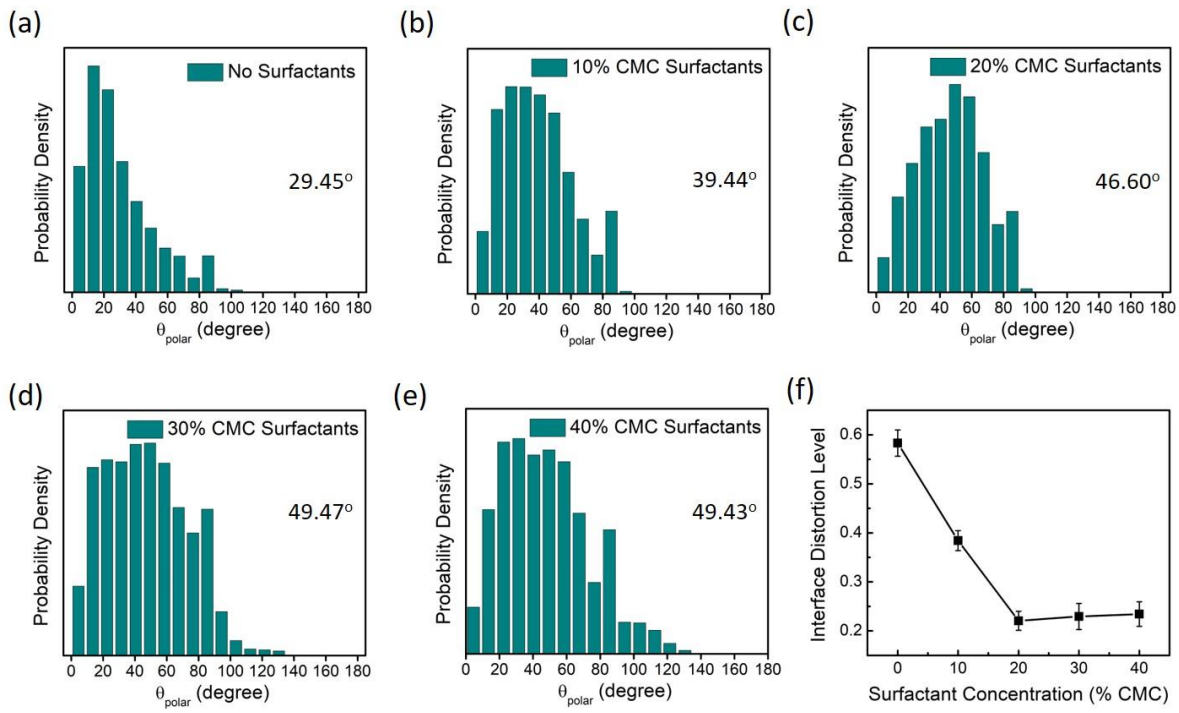

Figure A6. Distribution of angle representing orientation of JPs at the oil-water interface at different surfactant concentration: (a) 0%, (b) 10%, (c) 20%, (d) 30%, (e) 40% at the end of the compression with A/A_0 at 40%. (f) shows the change in the interface extent of distortion with the surfactant concentration. The interface distortion level was quantified using the order parameter of JPs. The number on each plot represents the mean value of the angle. The initial JPs coverage was 41% in all cases.